AFFIDAVIT

I declare that I have authored this thesis independently, that I have not used other than the declared sources/resources, and that I have explicitly indicated all material which has been quoted either literally or by content from the sources used. The text document uploaded to TUGRAZonline is identical to the present doctoral thesis.

_____
Date

_____
Signature

Abstract

To understand and optimize mechanical and printing properties (e.g. picking resistance) of coated paper, the localization of the binder after the coating process plays an important role. Recently, there is the trend to substitute petroleum-based binders, like latices, especially in precoatings by biopolymers. Examples are modified starch or newly developed biopolymers, like binders based on industrial lignins (lignosulfonates, kraft lignins).

A new method to determine binder penetration into the base paper is presented to localize the binder after the coating process. Serial sectioning is combined with fluorescence microscopy (SSFM) to obtain 3D image stacks. Image stacks are then binarized and 3D data evaluation to calculate the penetration depth is performed. This method was applied to evaluate influencing factors on binder penetration presented in the literature and to compare penetration into the base paper of water-soluble (lignosulfonate-binders, starch) and water-insoluble (latex) binders.

One important issue is the staining of the binder. For each type of binder a staining procedure needs to be developed. Regarding starch, a reactive staining procedure using 5-(4,6-Dichlorotriazinyl) Aminofluorescein (5-DTAF) was applied. Latex was stained with Rhodamine B. Lignosulfonate-binder is auto-fluorescent. The advantage of a reactive staining mechanism is the good compatibility with the resin for embedding, because of irreversible covalent bonds between dye and substrate. Rhodamine B binds to the latex due to charge differences and can be relocated by the resin in the embedding process. Therefore, samples with stained latex are not embedded and serial sectioning is performed via a sandwich method.

The idea was to investigate different influences on binder penetration found in the literature, like the influence of the binder type (water-soluble/insoluble), base paper, initial solids content, coating and drying method. Results show a different behavior of starch compared to latex binders. Penetration depth of starch into the base paper is higher compared to latex. Starch tends to follow the water into the porous structure of the base paper. Lignosulfonate-binders showed lower penetration depths into the base paper with higher degree of polymerization.

Keywords: *serial sectioning, binder penetration, fluorescence microscopy, coating layer*

Kurzfassung

Um die mechanischen und Bedruckbarkeitseigenschaften (wie zum Beispiel die Rupffestigkeit) von gestrichenen Papieren zu optimieren, spielt die Lokalisierung des Binders nach dem Streichprozess eine große Rolle. Vermehrt werden erdöl-basierte Binder, wie Latex, vor allem in Vorstrichen, durch Biopolymere ersetzt. Beispiele dafür sind modifizierte Stärken oder neu entwickelte Biopolymere, wie Binder auf Basis von industriellen Ligninen (Lignosulfonate, Kraftlignin).

Eine neue Methode zur Lokalisierung des Binders nach dem Streichprozess wird in dieser Arbeit präsentiert. Seriensschnitttechnik wird mit Fluoreszenzmikroskopie (SSFM) kombiniert, um 3D Bildstapel der untersuchten Probe zu erhalten. Die Bildstapel werden binarisiert und eine 3D-Datenauswertung wird durchgeführt. Mit dieser Methode wurden unterschiedliche Einflussfaktoren auf die Binderpenetration aus der Literatur evaluiert und ein Vergleich zwischen wasserlöslichen (Stärke und Lignosulfonat-Binder) und wasserunlöslichen Bindern (Latex) gezogen.

Ein sehr wichtiger Schritt ist die Fluoreszenzmarkierung des Binders. Jeder Bindertyp wir nach einer individuell entwickelten Strategie gefärbt. Betreffend Stärke, wurde eine Reaktivfärbung mit 5-(4,6-Dichlorotriazinyl) Aminofluorescein (5-DTAF) durchgeführt. Latex wurde mit Rhodamin B gefärbt. Lignosulfonat-Binder ist autofluoreszierend. Der Vorteil an einer Reaktivfärbung, ist die Kompatibilität mit dem Einbettmedium, weil irreversible kovalente Bindungen zwischen Farbstoff und Substrat gebildet werden. Die Bindung von Rhodamin B funktioniert mit Hilfe von Ladungsdifferenzen und der Farbstoff wird beim Einbetten heruntergelöst. Deshalb wurde für Papiere mit gefärbten Latex die Serienschnitttechnik mittels Sandwich-Methode durchgeführt.

Die Idee war, die Einflüsse auf die Binderpenetration aus der Literatur zu evaluieren. Dazu gehört zum Beispiel der Einfluss des Bindertyps (wasserlöslich/unlöslich), des Rohpapiers, initialer Feststoffgehalt, und die Streichauftrags- und Trocknungsmethode. Ergebnisse zeigen ein unterschiedliches Verhalten von Stärke und Latex hinsichtlich Penetration. Die Penetrationstiefen von Stärke ins Rohpapier sind höher als die von Latex. Unterschiedliche Feststoffgehälter führen zu unterschiedlichen Eindringtiefen. Stärke tendiert dazu der Wasserphase in das Rohpapier zu folgen. Lignosulfonat-Binder zeigt niedrigere Penetrationstiefen mit höheren Polymerisationsgraden.

Schlagwörter: *Serienschnitttechnik, Binderpenetration, Fluoreszenzmikroskopie, Strichschicht*

Acknowledgements

Life is a journey, not a destination. (Ralph Waldo Emerson).

Last but not least I want to thank all my colleges at IPZ, my friends and my family for their encouragement during my work. Thanks to my sister Alexandra, for her support and the many discussions regarding chemical tasks. Thanks to my father Georg and my mother Erika, for the possibility to go my own path. Mum, you cannot congratulate on finishing of this thesis anymore, but I know you would be proud of me.

Contents

Figures

Tables

Glossary

AA-GWR	Abo Akademi Gravimetric Water Retention
AFM	Atomic Force Microscopy
AKD	Alkyl Ketene Dimer
ATR	Attenuated Total Reflectance
CD	Cross Direction
CLSM	Confocal Laser Scanning Microscopy
CMC	Carboxymethylcellulose
CRS	Confocal Raman Spectroscopy
DMSO	Dimethylsulfoxide
DP	Degree of Polymerization
DTAF	5-(4,6-Dichlorotriazinyl) Aminofluorescein
EDX	Energy Dispersive X-ray analysis
ESCA	Electron Spectroscopy for Chemical Analysis
FCC	First Critical Concentration
FE-SEM	Field Emission – Scanning Electron Microscopy
FIB	Focused Ion Beam
FLIPPR	Future Lignin and Pulp Processing Research
FTIR	Fourier Transform Infrared Spectrometry
GCC	Ground Calcium Carbonate
IC	Internal Conversion
IR	Infrared
ISC	Inter System Crossing
LCC	Latex Coalescence Concentration
LS	Lignosulfonate
LWC	Light-weight Coated
MD	Machine Direction
MFFT	Minimum Film Forming Temperature
MIR	Multiple Internal Reflectance
MSP	Metering Size Press
MW	Molecular Weight
OBA	Optical Brightening Agent

PCC	Precipitated Calcium Carbonate
PVA	Polyvinyl Alcohol
SA	Styrene Acrylate
SB	Styrene Butadiene
SCC	Second Critical Concentration
SEM	Scanning Electron Microscopy
SSFM	Serial Sectioning in combination with Fluorescence Microscopy
ST	Starch
T_g	Glass Transition Temperature
TMP	Thermomechanical Pulp
TOF-SIMS	Time of Flight Secondary Ion Mass Spectrometry
UV	Ultraviolet
VIS	Visual
XPS	X-ray Photoelectron Spectroscopy

1 INTRODUCTION AND MOTIVATION

Optimization of paper coatings is gaining in importance because graphic paper products especially have lower prices on the market, while prices of the raw materials are increasing. The key components of a coating color are the pigment and the binder. One important issue is the control of the penetration of coating components into the base paper. If binder penetrates excessively into the base paper the degree of binding between the pigments is lowered. A higher amount of binder needs to be added resulting in unwanted additional costs.

Recently, petroleum-based binders like latex are replaced by natural binders because of cost and sustainability reasons. FLIPPR (Future Lignin and Pulp Processing Research) is an Austrian research project dealing with new application fields of side products from the paper and pulp production process. In the subproject 1.3 the focus is on the development of a new ecological coating binder, based on lignosulfonates, to substitute oil-based binders like styrene-butadiene (SB) latex in conventional coating formulations. Optimizations regarding water retention and printing properties of coating colors with this new bio-based binder were necessary, compared to reference coatings with latex as binder. The issue was to find the reason for unsatisfying coating results and understand the system of gluing the pigments and fixing them on the base paper, to enhance the bio-binder properties. So there was the need to find a fast and reliable method to localize the binder after the coating and drying process and compare the bio-binder with other conventional water-soluble binders, like starch and water-insoluble binders, like SB-latex.

There are several methods existing to investigate binder penetration. The most common method is Confocal Laser Scanning Microscopy, but the observation of penetration into the base paper is limited because of light penetration depth in z-direction. Other methods, like scanning electron microscopy, cannot be applied for a larger area of interest. Therefore, there was the need to find an appropriate method to obtain information about the binder penetration into the base paper in three dimensions with a sufficient area of interest and adequate resolution and acceptable duration.

The basic idea was to use serial sectioning and fluorescence microscopy to detect the location of binder. Prior works [Wiltsche et al. 2001] used serial sectioning in combination with a light microscope to analyze the three-dimensional coating layer formation [Wiltsche et al. 2001; Kritzinger et al. 2010] and fiber properties [Lorbach et al. 2012]. Subsequent work by Schäffner [2012] combines serial sectioning with fluorescence microscopy to facilitate the detection of fluorescently

stained fibers in paper. This method would also allow the detection of specific coating components and it leads to colored images to simplify the segmentation (transformation from RGB-image to binary image). To use fluorescence microscopy, the binder needs to be stained with fluorescent dye. Several staining mechanisms have been tested and are described in this thesis.

The method of serial sectioning in combination with fluorescence microscopy (SSFM) was established to calculate penetration depth values of binder into the base paper, based on three-dimensional data sets. The comparison of starch and bio-based binder regarding penetration depths allowed an optimization of the bio-binder and the coating color recipe. Furthermore influences of base paper and various coating additives were tested in latex-coatings. Starch-latex coatings, with both binders fluorescently labeled, were prepared to locate both binders individually after the coating and drying process.

Numerous effects potentially influence binder penetration into the base paper. The following effects were investigated in this thesis:

- Base paper: degree of refining, calendering, use of fillers
- Binder: type of binder (water soluble, water insoluble), degree of polymerization
- Coating color: solids content, water retention value
- Coating application and drying method: Manual Rod Coater with hot air dryer, SUMET Coating Unit CU5 with IR and hot air drying, Laboratory Blade Coater with IR and hot air drying

1.1 OUTLINE

This work contains three chapters dealing with basic information. It starts with the role of the binder in paper coatings and the different types of binder (Chapter 2). A chapter on the principles of fluorescence microscopy and fluorescent staining is also included (Chapter 3). Chapter 4 deals with information regarding binder migration and penetration. This chapter represents a short and simplified observation of this topic. The main part of the literature survey covers the mechanisms behind binder penetration (Chapter 4.1), available methods to determine binder penetration (Chapter 4.2) and the influential factors on binder penetration (Chapter 4.3).

The practical part includes the detailed description of the new method (Chapter 5), serial sectioning in combination with fluorescence microscopy (SSFM). This method description contains detailed information about the necessary working steps to obtain 3D-data sets and binder penetration depth into the base paper. SSFM was evaluated against confocal laser scanning microscopy (CLSM) (see Chapter 5.3).

Results are presented and discussed in Chapter 6. This section is divided into water-soluble binders and water-insoluble binders. Regarding water-soluble binders, different influential factors on binder penetration were investigated: degree of polymerization of the binder, type of binder, influence of solids contents of the coating formulation and influence of application, metering and drying method. For water-insoluble binders, the influence of base paper properties and the influence of different coating formulations and additives were investigated.

Chapter 7 discusses further application fields of the established SSFM method. This chapter includes the staining of fibers and paper to characterize sheet properties. Furthermore, optical brightening agents are localized via SSFM.

1.2 PUBLICATIONS

Papers

- Hofer K., Seidl B., Ortner A., Nyanhongo G.S., Winter H., Kozich M., Gübitz G., Bauer W., **Serial Sectioning of Coated Paper as a Novel Method to analyze Binder Penetration,** *Papir,* Vol. 13, June 2015, pp. 45 – 47

- Ortner A., Huber D., Haske-Cornelius O., Weber H. K., Hofer K., Bauer W., Nyanhongo G.S., Gübitz G.M., **Laccase mediated oxidation of industrial lignins: Is oxygen limiting?**, *Progress Biochemistry*, Vol. 59, Iss. 8, May 2015, pp. 1277 – 1283

Conference Proceedings

- Hofer K., Ortner A., Nyanhongo G.S., Winter H., Gübitz G., Bauer W.; **Serial Sectioning of Fluorescent Coating Layers as a Tool to Analyze Binder Penetration**; *Tappi Advanced Coating Fundamentals Symposium*, Minneapolis – USA, 10/2014, pp. 43 – 46

- Hofer K., Seidl B., Ortner A., Nyanhongo G.S., Winter H., Kozich M., Gübitz G., Bauer W., **Serial Sectioning of Coated Paper to investigate the Influences on Binder Penetration via Fluorescence Microscopy**, *PTS – Coating Symposium*, Munich, 15 – 16.09.2015, pp. 68 – 71

Oral Presentations

- Hofer K., Bauer W.; **Serial Sectioning of Fluorescent labeled Paper**; *Materials Day TU Graz*, 10/2013

- Hofer K., Ortner A., Nyanhongo G.S., Winter H., Gübitz G., Bauer W.; **Serial Sectioning of Fluorescent Coating Layers as a Tool to Analyze Binder Penetration**; *10. Minisymposium der Verfahrenstechnik*, Vienna – Austria, 06/2014

- Hofer K., Ortner A., Nyanhongo G.S., Winter H., Gübitz G., Bauer W.; **Serial Sectioning of Fluorescent Coating Layers as a Tool to Analyze Binder Penetration**; *Tappi Advanced Coating Fundamentals Symposium*, Minneapolis – USA, 10/2014

- Hofer K., Ortner A., Nyanhongo G.S., Winter H., Gübitz G., Bauer W.; **Serial Sectioning of Fluorescent Coated Paper as a Novel Method to Analyze Binder Penetration**; *41th international annual symposium DITP*, Bled – Slovenia, 11/2014

- Hofer K., Seidl B., Ortner A., Nyanhongo G.S., Winter H., Kozich M., Gübitz G., Bauer W., **Serial Sectioning of Coated Paper to analyze Binder Penetration via Fluorescence Microscopy**, *Zukunft.Forum Papier – Die österreichische Papierfachtagung*, Graz, 05/2015
- Hofer K., Seidl B., Ortner A., Nyanhongo G.S., Winter H., Kozich M., Gübitz G., Bauer W., **Serial Sectioning of Coated Paper to investigate the Influences on Binder Penetration via Fluorescence Microscopy**, *PTS – Coating Symposium*, Munich, 15 – 16.09.2015
- Hofer K., Seidl B., Kozich M., Bauer W., **Investigation of Binder Penetration via Serial Sectioning of Fluorescently Labeled Coating Binders**, *9th International Paper and Coating Chemistry Symposium*, Tokio – Japan, 29.10. – 01.11.2015
- Hofer K., Seidl B., Kozich M., Bauer W., **Determination of Latex and Starch Penetration via Serial Sectioning in Combination with Fluorescence Microscopy**, *EFPRO – Early Stage Researchers Workshop at European Paper Week*, Brussels, 17.11 – 19.11.2015

Poster Presentations

- Hofer K., Nyanhongo G.S., Gübitz G., Bauer W.; **Future Lignin and Pulp Processing Research – Presentation of a new Austrian Research Project**, *COST Meeting FP1105*, Trabzon – Turkey, 10/2013

2 PAPER COATING AND THE ROLE OF THE BINDER

Paper coating is applied to optimize the surface and printing properties of a paper sheet [Huang and Lepoutre 1998]. A typical coating color consists of several components having different functions. Pigments, binders and additives are the three distinctive groups of materials besides water [Walter 1993]. Figure 1 shows a schematic drawing of part of the coating layer on a base paper after drying including the two most important components – pigments and binder [Lepoutre 1989]. The pigments could be either plate-like (clay) or spherical (CaCO$_3$).
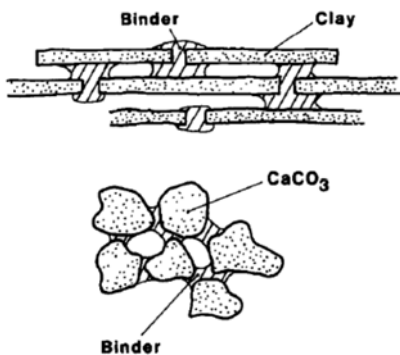
Figure 1: Binder gluing the pigments (Calcium Carbonate and Clay) [Lepoutre 1989]

Pigments are inorganic particles and account for 80-95% of the coating by weight. The selection of the pigment or pigment mixture depends on certain coating paper properties to be realized. Different types of calcium carbonate and clay are used as the main coating pigments [Paltakari 2009].

The second most abundant component in a coating color is the binder. In the following parts of this thesis the focus will be on different coating binders and their localization after the coating process.

The rheological behavior of a coating formulation is controlled by usage of so-called co-binders or thickeners. Optical properties are optimized by the addition of optical brightening agents in combination with a carrier. Further additives are e.g. dispersants, biocides, pH controllers, dyes and foam controllers. The target solid content is set by adding water [Walter 1993].

In this work, the focus is on binders and their behavior in the coating application. Therefore, theoretical background including types of binders, mechanisms of binder penetration and the influencing factors on binder penetration are described.

2.1 TYPES OF COATING BINDERS

Two types of coating binders are used in the paper coating process: natural polymers and synthetic polymers. Natural polymers include starch, soy protein and casein. The group of synthetic polymers consists of styrene-butadiene latices (SB), styrene-acrylic latices (SA), polyvinyl acetate latices (PVAc), vinyl acrylic latices and polyvinyl alcohol (PVOH) [Walter 1993].

The coating binder has four different functions [Paltakari 2009]:

- Glue the pigment particles together
- Fix the coating layer to the paper substrate
- Fill voids between pigment particles
- Control viscosity/rheology and water retention (mainly for natural polymers)

Binders for coating application can also be divided into groups of water soluble and insoluble binders. One sample of each type is here further described.

2.1.1 Latex

Latex is the most common water insoluble binder. Latex consists of monomers and in general, these monomers are styrene and butadiene or acrylate. The more styrene is used the harder and more brittle the latex gets but the binding power decreases. These properties can be observed by the measurement of glass transition temperature (T_g) [Walter 1993]. The monomers are polymerized by emulsion polymerization and groups of unsaturated carboxylic groups are incorporated to stabilize the latex [Proctor and Hoover 1990]. Emulsion polymerization is based on free radical polymerization. To avoid latex coagulation, surfactant is added and latex spheres with a typical size of approximately 150nm are formed [Chern 2008]. Typically, latex particles vary between the size of 80 and 300nm and small particles have a higher binding strength than larger particles [Walter 1993].

Latex particles undergo a transformation during drying. In Figure 2 the different stages of drying are shown. Vanderhoff and Bradford [1963] describe the process of latex film formation. The initial volume fraction of latex in the polymer-water dispersion is 0.5. Water evaporates, until a volume fraction of $0.70 - 0.75$ is reached. Then the transformation from individual particles to a continuous film takes place. This film forming state is characterized by the minimum film forming temperature (MFFT) [Hendershot and Klun 1990]. This property is specific for each type of latex.
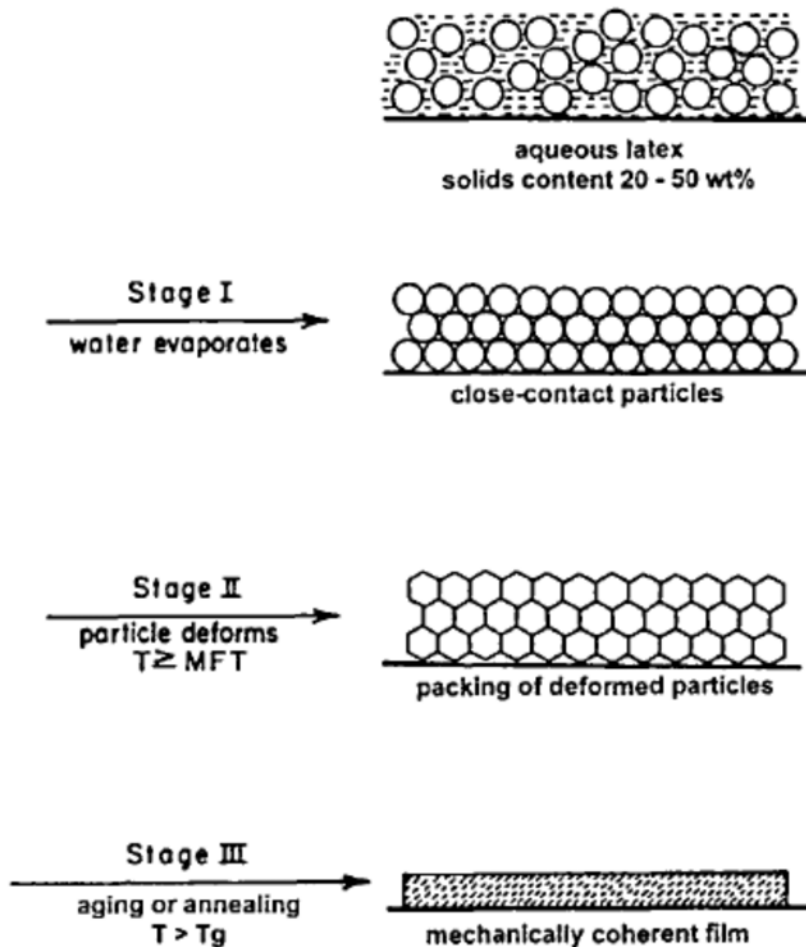
Figure 2: Latex film formation process [Winnik 1997]

In Figure 2 three stages from an aqueous latex dispersion to a latex film are shown [Winnik 1997]. The first stage takes place when water evaporates and polymer particles become concentrated. The starting concentration of latex dispersions usually is around 50%. In the second stage, the latex particles deform because the temperature exceeds the MFFT. There a honeycomb structure is formed. This structure is then modified to a mechanically coherent film, when the temperature is above the glass transition temperature (T_g). MFFT and T_g are important for the coating process and the properties of the coated paper.

2.1.2 Starch

Starch is one of the most common water soluble binders and consists of anhydroglucose units ($C_6H_{10}O_5$). Starch as a high-molecular weight molecule consists of two different units: amylose and amylopectin. Amylose (see Figure 3) has a linear structure compared to amylopectin (see Figure 4) with its branched structure.
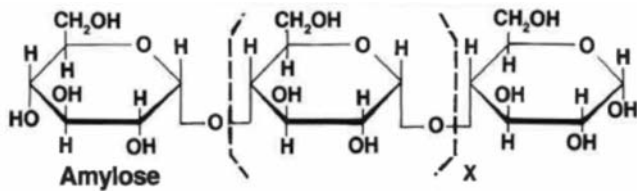
Figure 3: Amylose – one component of the starch molecule [Kearney and Maurer 1990]
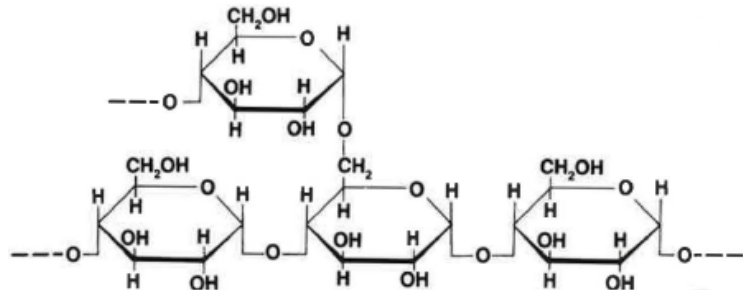
Figure 4: Amylopectin – the second component of the starch molecule [Kearney and Maurer 1990]

Amylose consists of anhydroglucose units bound by alpha-1,4 linkages. The molecular weight of starch depends on the type of plant it originates from [Kearney and Maurer 1990].

Kearney and Maurer [1990] point out that for coating application starches need to be modified. Unmodified starches tend to gelatinize. Therefore, starches applied in paper coatings are modified by:

- Hydroxyethylation and acid thinning (performed by the manufacturer)
- Oxidation (performed by the manufacturer)
- Enzymatic treatment (performed by the user)
- Thermal-chemical treatment (performed by the user)

Recently, latex is replaced by natural binders like starch in paper coatings because of rising oil-prices and environmental reasons [Du et al. 2011].

3 FLUORESCENCE MICROSCOPY

3.1 DEFINITION OF FLUORESCENCE

Luminescence can be divided into two effects: fluorescence and phosphorescence. A molecule gets electronically excited and light called luminescence is emitted [Lakowicz 2006].

Fluorescence appears when the electron in the excited orbital from the first singlet state returns to the ground state. Phosphorescence appears when light is emitted from the triplet excited state. In Figure 5 the three different states are illustrated: the ground state, the singlet excited state and the triplet excited state. Intersystem crossing causes the turn of the spin of the electron and this leads to the triplet excited state [Lakowicz 2006].
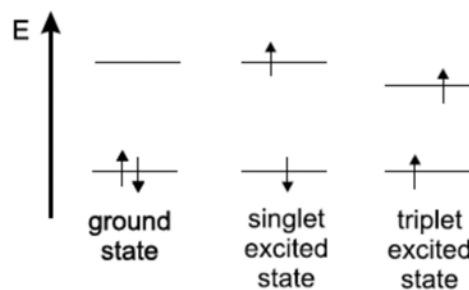
Figure 5: Three different states in an orbital [Valeur 2002]

The Perrin - Jablonski – diagram illustrates the two different types of luminescence and their mechanisms (see Figure 6). A molecule absorbs light and the energy level rises from the ground state (S_0) to the singlet state (S_1 or S_2). The horizontal lines at the energy states show the different vibrational energy levels. Internal conversion (IC) indicates the vibrational relaxation. The return from the first singlet state to the ground state results in emission of photons (fluorescence). Spin conversion can also appear and the molecule is transferred to the triplet state (T_1 or T_2). This process is called intersystem crossing (ISC) and leads to emission of photons (phosphorescence).
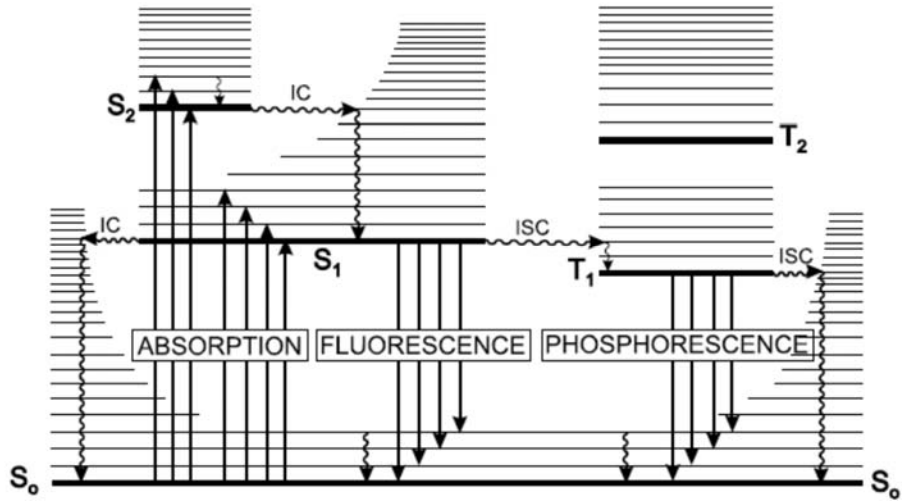
Figure 6: Perrin - Jablonski – diagram [Valeur 2002]

The energy of the emission is lower than those of absorption. As a consequence, fluorescence occurs at longer wavelengths with less energy. Sir George Gabriel Stokes found out this effect in 1852. The Planck-Einstein relationship (see Eq. 1) defines the correlation of wavelength (λ) and the energy (E) applied [Sauer et al. 2011].

Eq. 1

$$E = \text{h} \cdot \nu = \frac{hc}{\lambda}$$

E … energy

h … Planck's constant ($6{,}626 * 10^{-27}$ Js)

ν … frequency

c … speed of light

λ … wavelength

A loss of energy is observed between excitation and emission and regarding to the Planck-Einstein equation lower energy results in higher wavelength [Lankowiz 2006]. The distance between the maximum of the excitation spectrum and the maximum of emission spectrum is called the Stokes shift [Valeur 2002]. This phenomena is shown in Figure 7 with 5-DTAF as an example which has been used for starch labeling in this work.
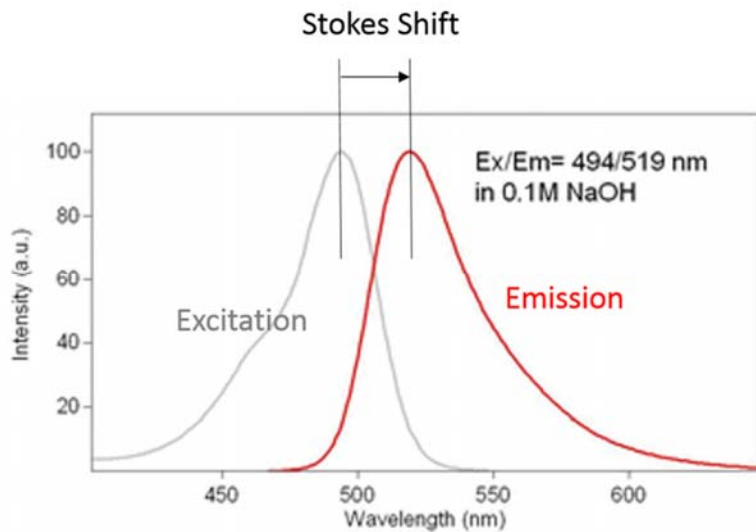
Figure 7: Stokes Shift of 5-DTAF adapted from [AAT Bioquest 2014]

3.2 FLUOROPHORES

One major issue in this work was the establishment of a suitable staining procedure for each type of binder. Therefore, various labeling techniques and fluorophores have been evaluated.

Fluorophores can be separated into two groups [Lakowicz 2006]:

– Intrinsic or natural fluorophores (auto-fluorescence)
  The molecule is fluorescent. No stain is necessary for the absorption of UV- and emission of fluorescent light.
  Examples: aromatic amino acids, flavins, lignins and chlorophyll
– Extrinsic fluorophores
  The molecule does not absorb UV-light. It needs to be stained with a fluorescent dye.
  Examples: fluorescein, rhodamine…

3.2.1 Intrinsic fluorophores

Intrinsic fluorophores are also named natural fluorophores. There are parts of the molecular structure, which absorb UV- and emit fluorescent light. In this work, we used the ability of lignins to absorb UV-light, to locate the lignosulfonate based bio-binder after the coating and drying process.

3.2.1.1 Lignin

Cellulose, hemicellulose and lignin are the principal components of plants. Lignin as a polymer consists of different units, depending on the type of wood (see Figure 8). The three basic monomers are [Heitner et al. 2010]

- p-coumaryl alcohol
- coniferyl alcohol
- sinapyl alcohol
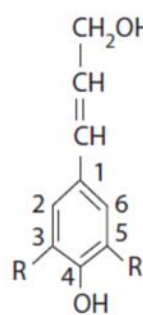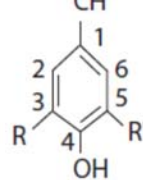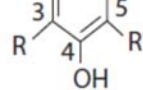
Figure 8: Lignin monomer types [Heitner et al. 2010]

The different positions of side chains (functional groups) of the aromatic ring get numbers from C-1 to C-6 (see Figure 8). Further functional groups appear at the side-chain carbons. They are named α, β and γ (see Figure 9).
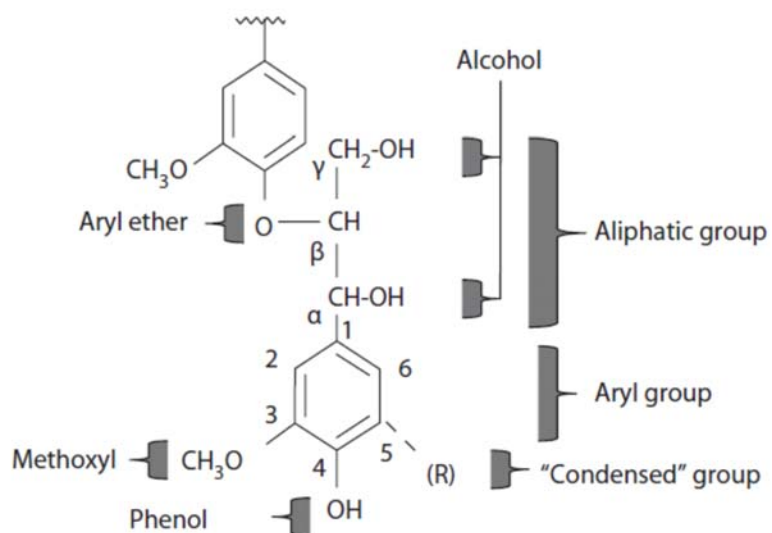
Figure 9: Functional groups of lignin [Heitner et al. 2010]

The aromatic structure of lignins absorbs UV-light. As there are different types of lignin depending on the origin, also UV spectra differ. The Beer – Lambert Law (see Eq. 2) forms the base of quantitative measurement of lignin concentration via UV microscopy [Lin and Dence 1992].

Eq. 2

$$A = D \cdot c \cdot d$$

A … UV absorbance

D … extinction (absorption) coefficient $[lg^{-1}cm^{-1}]$

c … concentration $[gl^{-1}]$

d … section thickness [cm]
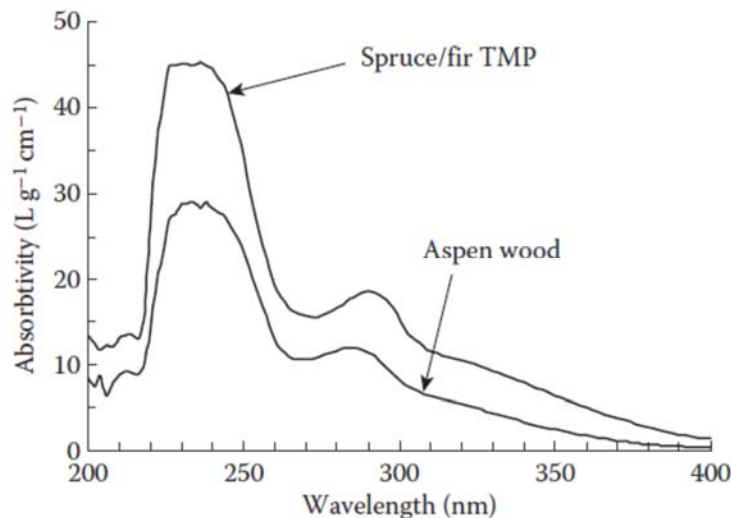
Figure 10: UV absorption spectra of lignin solutions [Heitner et al. 2010]

Heitner et al. [2010] show typical UV absorption spectra of lignin solutions depicted in Figure 10. The lignin originates from softwood TMP and from aspen wood. Albinsson et al. [1999] investigated the origin of lignin fluorescence. In Figure 11 the emission spectra of different lignins and model compounds are shown. The untreated spruce lignin is highlighted. The emission maximum of untreated spruce lignin is at 370nm.
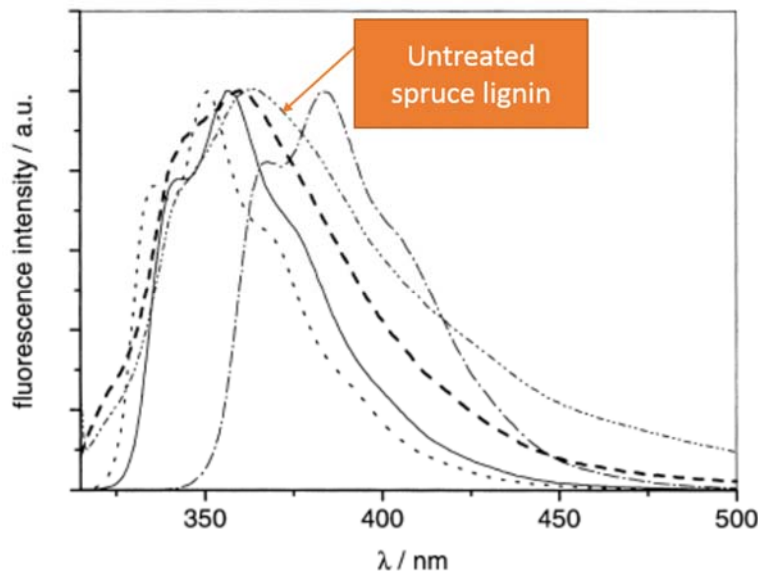
Figure 11: The emission spectra of different lignins and model compounds (adapted from [Albinsson et al. 1999])

3.2.2   Extrinsic fluorophores

Extrinsic fluorophores represent the group of fluorescent dyes. They can be divided into different types, based on the bonding mechanism. Mulisch and Welsch [2010] define three different types as following:

3.2.2.1   Chemical staining

There is a chemical reaction ongoing during the staining process. A covalent bond between the dye molecule and the substrate is formed.

As the focus in this work is on chemical staining, the underlying mechanism, will be further described:

The mechanism of chemical staining was first investigated in dyeing of cotton fabrics. Stead [1982], Tam et al. [1997] and Rosenau et al. [2005, 2009] presented the reaction of dichloro-triazinyl-group with cellulose. The working principle is presented in Figure 12. The reactive group is linked to a dye molecule (chromophore). In dyeing of cotton fabrics the dichloro-trianzinyl group was attached to non-fluorescent dyes. This dichloro-triazinyl-group forms then a covalent bond with the dissociated OH-groups of the cotton fabric (see Figure 12).
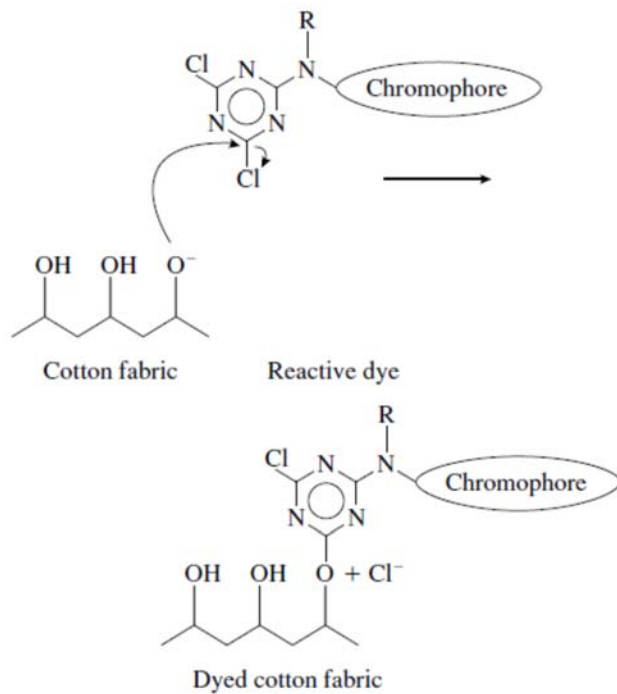
Figure 12: The principle of chemical staining [Tam et al. 1997]

Regarding this thesis a literature survey was performed to find fluorescent dyes linked to the reactive dichloro-triazinyl-group, to apply fluorescence microscopy and to locate the binder after the coating process. The literature study was expanded on dyeing strategies of proteins and plant cells [Harapanhalli et al. 1995; Ahmed et al. 2011; Helbert et al. 2003; Siegler et al. 1989], because fluorescent staining is more common in the field of biotechnology. The idea was to apply the same system to paper and coating ingredients based on the literature survey.

Rate of fixation $= k_1$ [Dye] [Cellulose—O$^-$]
Rate of hydrolysis $= k_2$ [Dye] [OH$^-$]
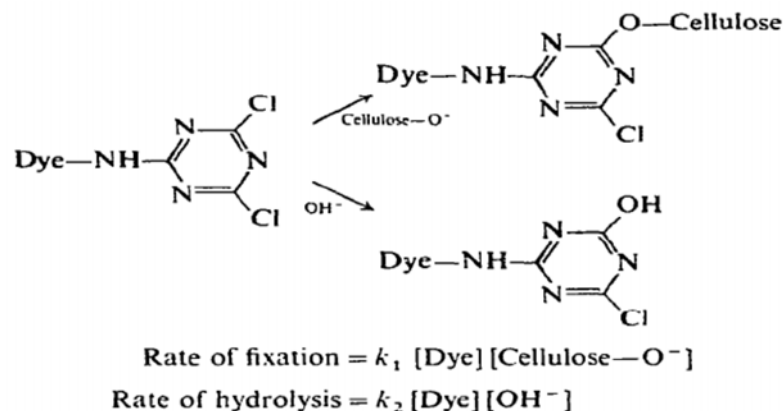
Figure 13: Two reactions of the triazine-group [Stead 1982]

Beside the chemical staining reaction, unwanted hydrolysis appears. The triazine groups reacts with the OH-groups of the aqueous solution and inhibits a further reaction with the OH-groups of the substrate to be stained. In Figure 13 the two reactions of the triazine-group are shown. On the one hand there is a bond formed with cellulose (see Figure 13 top) and on the other hand hydrolysis appears (see Figure 13 bottom). So the amount of dye to get a sufficient staining result needs to be investigated and the fact of hydrolysis needs to be kept in mind.

3.2.2.2 Physical staining

This staining mechanism focuses on physical properties which affect the staining process. For example density variations, size of pores, or solubility of the substrate define the location of the dye after staining.

3.2.2.3 Physio-chemical staining

Physio-chemical staining is based on electrostatic interaction of the dye molecule and the substrate. Mulisch and Welsch [2010] and Drnovšek and Perdih [2005] define two types of dyes adsorbed to a substrate: dye base (positively charged ion) and dye acid (negatively charged ion).

- Acid dyes (anionic dyes)
  Acid dyes are negatively charged and mainly used for protein staining. These types of dyes cannot be used for fiber staining, because fibers are negatively charged too [Drnovšek and Perdih 2005]. Cationic fixing agents are needed to stain the fibers [Roberts 1991].
- Basic dyes (cationic dyes)
  Basic dyes are positively charged and mainly used to stain cellulosic material [Drnovšek and Perdih 2005]. These type of dyes are applied to negatively charged material [Roberts 1991].

4 BINDER PENETRATION/MIGRATION

This chapter deals with basic information about binder movement during application and drying of coatings on a paper substrate. A short summary of the literature survey is presented as background for the interpretation of data obtained by SSFM. Therefore, a simplified view of mechanisms behind binder penetration into the base paper is presented. Furthermore, also methods to determine binder penetration are discussed and an overview of influencing factors on binder movement is illustrated.

The mechanism of binder penetration/migration occurs during the wet state of the coating process. On the one hand the binder is transported into the porous system of the base paper. The binder follows the water into the paper substrate. This is called *binder penetration* (see Figure 14 – 2). On the other hand the binder moves to the coating surface during the drying process. The binder follows the evaporated water phase to the coating surface. This is called *binder migration* (see Figure 14 – 1). These two mechanisms lead to uneven binder distribution in Z-direction within the coating layer, near the interface between coating layer and base paper, and on the coating layer surface [Whalen-Shaw 1993].
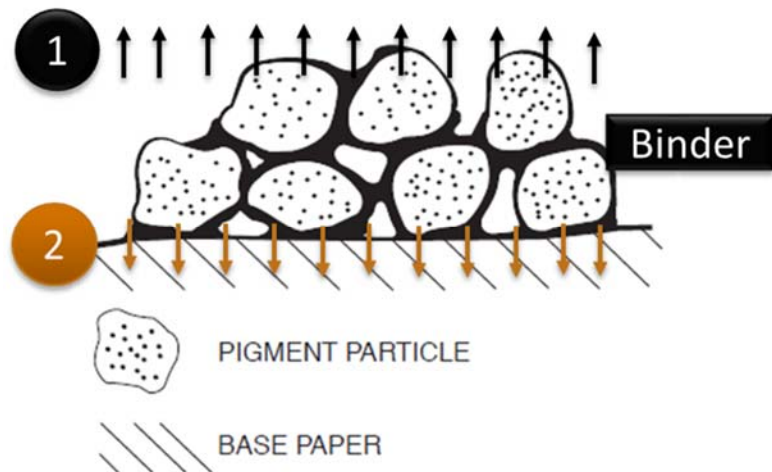
Figure 14: Principle of binder migration and penetration (adapted from [Paltakari 2009])

There are various factors influencing binder penetration and these effects can be explained by different mechanisms.

4.1   MECHANISMS BEHIND BINDER PENETRATION

To understand the mechanisms behind binder penetration, the consolidation of a coating layer needs to be discussed. The transport towards the base paper and the coating surface underlies some physical principles presented below.

4.1.1   Coating layer consolidation

First of all, the formation of a coating layer on a paper substrate needs to be discussed [Whalen-Shaw 1993]. Watanabe and Lepoutre [1982] and Lepoutre [1989] divide the consolidation of a coating layer into three phases. These phases are separated by two specific points: FCC (first critical concentration) and SCC (second critical concentration). The two concentrations are determined by significant changes in gloss and opacity of the coating layer (see Figure 15).
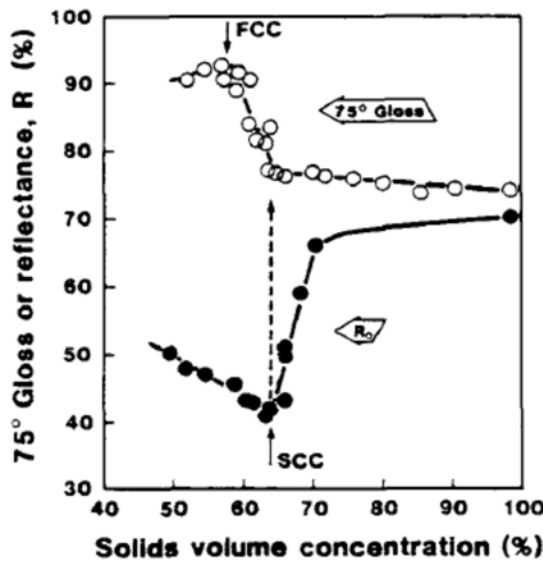
Figure 15: Consolidation of a coating layer with nonfilming latex [Watanabe and Lepoutre 1982]

Gloss depends on the properties of the surface, for example the roughness [Watanabe and Lepoutre 1982]. When water gets sucked into the base paper and the coating layer is immobilized, the gloss of the coating layer decreases, because the surface roughness increases. This point is called the FCC. In Figure 15, the gloss of a coating color, containing a nonfilming latex, is illustrated. Regarding filmforming lattices, the gloss would stay longer at a high level. Watanabe and Lepoutre [1982] point out that in this case the continuous water film on the surface stays longer and this leads to higher gloss compared to nonfilming latices.

Opacity depends mainly on the void volume of the coating layer. This void volume develops during drying and evaporation of the water phase. Then more light is refracted because of the larger amount of phase transition areas between solids and air. Therefore, opacity is increasing.

Zang et al. [2010b] introduce the LCC (Latex Coalescence Concentration) additionally to the theory of Watanabe and Lepoutre [1982], which appears between FCC and SCC. They divide the coating layer consolidation into four stages (see Table 1).

Table 1: The four stages of coating layer formation [Zang et al. 2010b]

Stage	Process	Time
1	Filter cake formation	Liquid till FCC
2	Cake growth	FCC till LCC
3	Latex coalescence	LCC till SCC
4	Solid	After SCC

Zang et al. [2014] summarizes in his review the most important mechanisms causing binder penetration and migration during drying. He points out that the transport mechanisms of the binders vary because of the constitution of the binders – whether they are water-soluble like starch or insoluble like latex. Also Whalen-Shaw [1993] distinguishes between those two groups of binder. While water-soluble binders are transported with the aqueous flow, latex particles are carried by viscous drag.

Clark et al. [1969] and Whalen-Shaw [1993] divide the coating layer consolidation in four sections based on the application, metering and drying (see Table 1):

- First capillary section

The coating color is applied onto the porous paper sample. The dewatering process of the coating color starts. This process is driven by the water absorption through the fiber walls and the capillary penetration into the porous system. As a consequence, the solids content of the coating color near the base paper increases significantly. Whalen-Shaw [1993] and Clark et al. [1969] define this as the first step of binder penetration.

- Pressure section

The metering element (blade, rod etc.) applies a force onto the coating layer. Binder will penetrate into the base paper, driven by hydrodynamic pressure. Water and binder will be sucked into the

porous system of the base paper until the capillary forces of the coating are higher, compared to those of the base paper.

- Second capillary section

This section describes the time frame between the pressure section (metering element) and the first drying stage [Clark et al. 1969]. In this section filtration processes play an important role.

- Drying section

The evaporating point at the coating layer surface is reached by applying heat during the drying process. The evaporation process is started and binder migration towards the paper surface occurs.

The focus in this work is on the first capillary section, the pressure section and the second capillary section, as these are the zones, where binder penetration takes place [Whalen-Shaw 1993]. The drying section is more important with regard to binder migration [Engström et al. 1991].

4.1.2 Physical principles

Water and binder transport into the base paper underlies some physical principles [Whalen-Shaw 1993], which are discussed in the following section.

The pressure drop (Δp_f), due to the flow of a fluid, is consisting of the drop of external pressure, like gravity, (Δp_a) and the capillary pressure drop (Δp_y) as presented in Eq. 3 [Whalen-Shaw 1993].

Eq. 3

$$\Delta p_a + \Delta p_y = \Delta p_f$$

Δp_f is based on the Hagen-Poiseuille equation (see Eq. 4) for a laminar flow through a capillary. The capillary and the flow are shown in Figure 16. The fluid, having a dynamic viscosity (η), flows through a capillary (length l and inner radius r) and the volume stream per unit is Q.
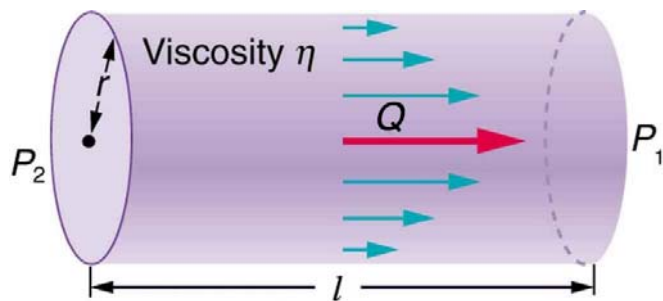
Figure 16: Principle of Hagen-Poiseuille [Openstax CNX 1999]

Eq. 4

$$\frac{dV}{dt} = \frac{\pi \cdot r^4}{8 \cdot \eta} \cdot \frac{\Delta p_f}{l}$$

The volume stream per unit ($\dot{Q}$) is expressed by dV/dt in Eq. 4 and V can be calculated as shown in Eq. 5.

Eq. 5

$$V = r^2 \pi \cdot l$$

This leads to the final equation of Δp_f shown in Eq. 6.

Eq. 6

$$\Delta p_f = \frac{8\eta}{r^2} \cdot l \frac{dl}{dt}$$

The capillary pressure drop (Δp_y) can be described by the Young-Laplace Equation (see Eq. 7 and Figure 17). The surface tension of the liquid is named γ.

Eq. 7

$$\Delta p_y = \frac{2\gamma \cos \theta}{r}$$
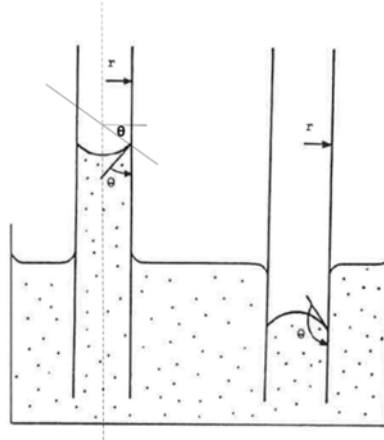
Figure 17: Liquid surfaces in capillaries with different surface tension (adapted from Whalen-Shaw [1993])

Eq. 6 and Eq. 7 are inserted into Eq. 3 and after transformations and integration the result is presented in Eq. 8.

Eq. 8

$$l = \left[\frac{2r \cdot \gamma \cdot \cos\theta + \Delta p_a \cdot r^2}{4\eta}\right]^{(1/2)} \cdot t^{(1/2)}$$

In the first case, the Δp_a is zero and this will lead to Lucas-Washburn equation (see Eq. 9). This represents the capillary penetration mentioned above.

Eq. 9

$$l = \left(\frac{r \cdot \gamma \cdot \cos\theta}{2\eta}\right)^{1/2} \cdot t^{1/2}$$

The second case represents the pressure penetration through a capillary. This appears when Δp_a is much greater than Δp_y.

Schölkopf et al. [2000] point out that there are drawbacks of the application of the Lucas-Washburn equation (Eq. 9). Inertial terms are neglected in the Lucas-Washburn equation [Schölkopf et al. 2004]. They observed the phenomena that a fluid flow into a smaller pore is accelerated in contrast to larger pores. Due to the inertial delay, the fluid resists the acceleration, caused by capillary forces. This especially happens at short contact times and large pores. In contrast to that, the fluid is accelerated in small pores. These observations cannot be explained by Lucas-Washburn equation, where the pore radius r and the penetration length l are directly proportional. In the work of Schölkopf et al. [2000, 2004] and Matthews [2000] the Bosanquet equation (see Eq. 10) is presented. In this equation the inertial flow is not neglected and it explains the retarded flow of fluid in large pores at short contact times.

Eq. 10

$$\frac{d}{dt}\left(\pi r^2 \rho x \frac{dx}{dt}\right) + 8\pi\eta x \frac{dx}{dt} = P_e \cdot \pi r^2 + 2\pi r \gamma \cos\theta$$

P_e is the applied external pressure and ρ is the density of the fluid. All the other terms have already been explained. Schölkopf et al. [2000] integrates and simplifies Eq. 10 (see Eq. 11). In his work the Bosanquet equation was used to describe the absorption of printing ink into a coated paper. Therefore, the external pressure is set to 0 because no pressure is applied in the printing process. This simplification is not valid for coating color and binder absorption into the base paper.

Eq. 11

$$x^2 = \frac{2\gamma t^2 \cos\theta}{r \cdot \rho}$$

In Eq. 11 the explanation of the retarded flow into large pores can be identified. The inertial flow is inversely related to the pore radius r in contrast to Lucas-Washburn.

Ridgway et al. [2013] observed that a continuous flow of a fluid through a porous sample follows the Darcy's law (see Eq. 12). Furthermore, external pressure under the metering element occurs and pressure is not considered in the Lucas-Washburn equation (Eq. 9) and in the simplification of the Bosanquet equation (Eq. 11). The Bosanquet equation is valid for short contact times [Schölkopf et al. 2000] after the coating color is applied. When the coating color is immobilized in the regions near the base paper, Darcy's law plays an important role. In his study Darcy investigates the flow through a bed of sand (see Figure 18). Darcy's law is valid for laminar flow.

Eq. 12

$$\frac{dV}{dt} = \frac{K \cdot \Delta p \cdot A}{\eta \cdot L} = \dot{Q}$$

Δp can now be either Δp_a or Δp_y. K is the permeability of the bed and can be determined via the Kozeny-Carman equation (see Eq. 13).
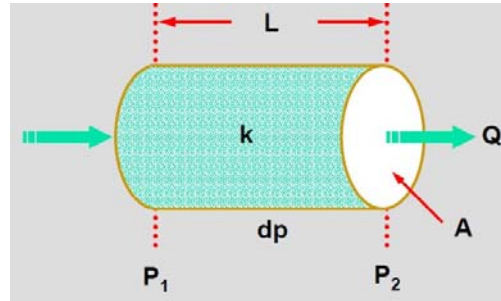
Figure 18: Principle of Darcy's equation (adapted from [Crain 2015])

Eq. 13

$$K = \frac{\varepsilon^3}{k_0 \cdot (1-\varepsilon)^2 \cdot S_p^2}$$

In Eq. 13 ε is the porosity of the bed, S_p is the specific surface area of the particles and k_0 is the Kozeny constant. This constant can be determined experimentally and is dependent on the structure of the bed.

4.2 METHODS TO DETERMINE BINDER PENETRATION PRESENTED IN THE LITERATURE

This chapter shows an overview of the most common available methods to localize the binder during or after the coating process. Several methods to determine binder penetration and binder migration are described in the literature. Vyörykkä et al. [2006] published a review of different methods to characterize paper coatings including binder penetration. He divides them into groups of determination of chemical and structural composition (see Figure 19).
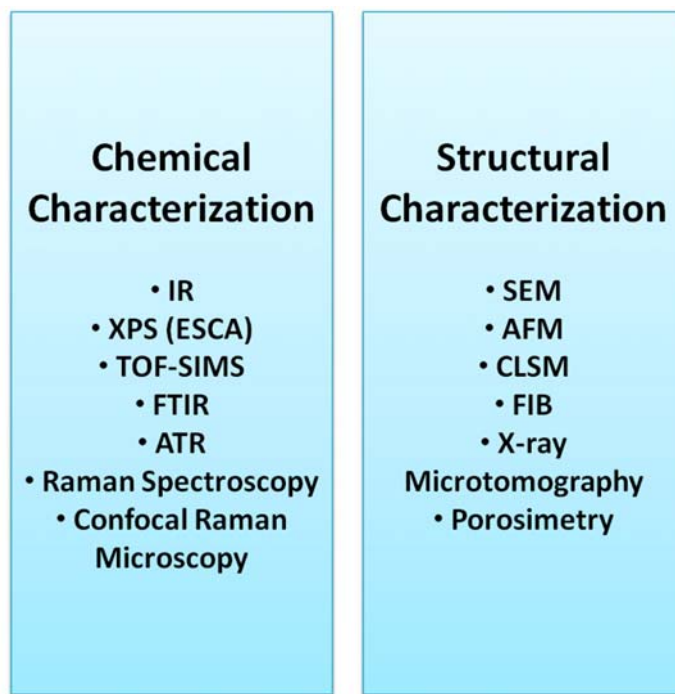
Figure 19: Methods presented in the review of Vyörykkä et al. [2006]

In this thesis, all the methods were divided into two different groups:

- Surface analysis to investigate binder migration
- Cross-section analysis to investigate binder penetration and binder distribution within the coating layer

The focus in this thesis is on the cross-section methods because SSFM can be categorized in this section. These methods are presented more in detail in contrast to surface analysis methods, which are described shortly just for the sake of completeness.

A list of available methods is presented in Figure 20.
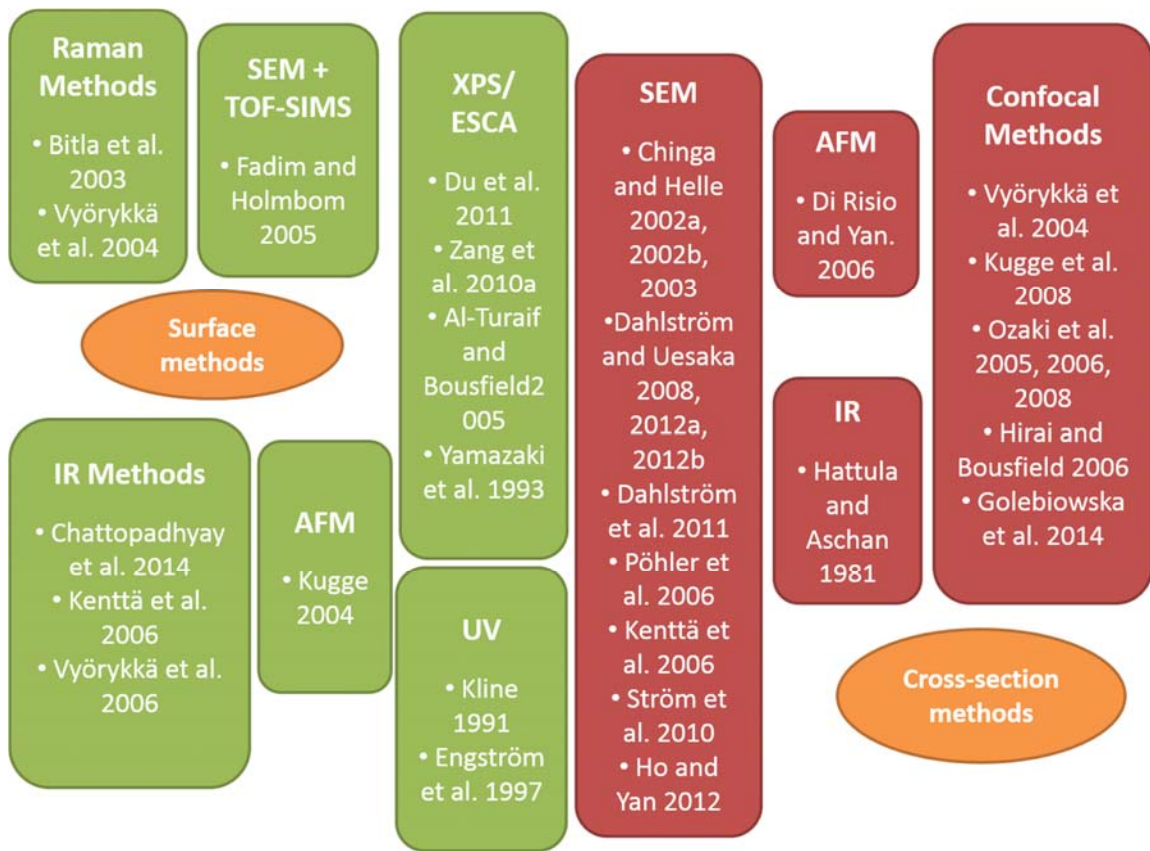
Figure 20: Methods to determine binder migration/penetration

4.2.1 Surface analysis to determine binder migration

In general, surface methods were established to characterize the coating surface and binder migration. But binder migration directly correlates to binder penetration. If there is a depletion of binder at the surface it may have penetrated into the base paper.

4.2.1.1 Infrared (IR) methods

IR methods have the longest history in coating characterization [Vyörykkä et al. 2006]. IR methods determine the functional groups via molecule vibrations. These methods include Attenuated Total Reflectance (ATR) and Fourier Transform Infrared Spectrometry (FTIR).

Kenttä et al. [2006] present the ATR-IR method to control print mottling. They point out that the binder distribution and coating ingredients uniformity at the surface have an important impact on print quality. Latex content and uniformity was measured on the surface up to a penetration depth of 1-2μm.

Chattopadhyay et al. [2014] studied dynamic binder migration via ATR. They applied the coatings on an ATR crystal and dried it. No sample preparation is necessary and the penetration depth of the waves reaches from 1 to 5 μm.

4.2.1.2   Raman methods

Raman spectroscopy is applied to determine latex and pigment concentrations in lateral direction [Bitla et al. 2003]. Raman spectroscopy is a non-destructive method and no sample preparation is necessary. It is limited to 1 μm of lateral resolution [Vyörykkä et al. 2004]. Raman spectra are quenched by fluorescent emission.

Bitla et al. [2003] investigated the surface binder concentration via Raman spectroscopy. Vyörykkä et al. [2004] applied Confocal Raman Microscopy in x-y plane for the determination of chemical surface composition. By using the confocal principle the area of interest being observed is larger compared to the work of Bitla et al. [2003]. Intensity maps of $CaCO_3$ and SB-Latex were created. For an area of interest of 1,16 x 0,92 mm (40 μm step size) analysis time was approximately 4,5 hours.

4.2.1.3   Scanning electron microscopy (SEM)

Fardim and Holmbom [2005] applied field emission SEM (FE-SEM) to study the surface morphology of coated paper. Samples were coated with an Au-Pd layer first to increase the image quality. Coupled with an x-ray spectrometer, chemical information of the analyzed surface was obtained.

4.2.1.4   X-ray photoelectron spectroscopy (XPS)

XPS is also known as Electron Spectroscopy for Chemical Analysis (ESCA). It is a technique to quantify the chemical composition, except the molecules hydrogen and helium. Du et al. [2011] investigated the elemental composition of the coating surface via XPS. They correlated the surface carbon content with the latex content of coating colors, applied on a non-porous polyester film (Mylar). A depth in z-direction up to 5 nm can be realized. A similar investigation was performed by Zang et al. [2010a], Yamazaki et al. [1993] and Al-Turaif and Bousfield [2005]. In their work, also XPS was used to determine latex particles migrating to the surface during drying. Zang et al. [2010a] analyzed a scan area of 300 x 700 μm^2.

4.2.1.5   Time of flight secondary ion mass spectrometry (TOF-SIMS)

Fardim and Holmbom [2005] compare TOF-SIMS to FE-SEM, EDX and XPS. With TOF-SIMS chemical information of the surface is determined via mass spectra at depth lower than 1nm. The

lateral resolution is about 200 nm. This method is very sensitive to surface topographic effects which cause artifacts. Coated and uncoated papers were investigated.

4.2.1.6   Atomic force microscopy (AFM)

AFM to investigate binder migration has been applied by Kugge [2004]. Different coating colors on non-porous substrates (Mylar) were analyzed. The sample size using the AFM is limited to 100 μm x 100 μm.

4.2.1.7   Ultraviolet (UV) methods

Via UV light shining onto a paper sample the surface content of styrene is detected [Kline 1991]. Kline [1991] studied the effect of drying of coatings on Mylar on the latex surface content. Engström et al. [1997] used the same method to correlate print mottle to surface latex content.

4.2.2   Cross-section methods to determine binder penetration

In this chapter, the cross-section methods for the determination of binder penetration are presented. Binder distribution within the coating layer has also been investigated using these methods.

4.2.2.1   Scanning electron microscopy (SEM)

One of the most common 3D methods to investigate binder penetration is based on SEM in combination with staining of the coated paper with osmium tetroxide (OsO_4). Chinga and Helle [2002a, 2002b, 2003] developed the staining mechanism of coated paper to determine the structure of coated paper. Beside latex, also the lignin of the fibers reacts with OsO_4. OsO_4 forms covalent bonds with the carbon double bonds of the latex binder [Ho and Yan, 2012]. After staining, paper samples are embedded in epoxy resin and blocks were then grinded and polished to obtain a cross-section for SEM analysis [Chinga and Helle 2003]. Chinga and Helle [2002a, 2002b] developed a method to calculate the pore volume within a coating layer. Image analytical segmentation routines were used to separate areas of stained coating binder from void areas. They correlated the pore volume calculations with print gloss. Chinga and Helle [2003] determined the latex volume fraction by analyzing the pore volume before and after the staining procedure. They did not focus on the depth of penetration of binder into the base paper.

Kenttä et al. [2006] and Pöhler et al. [2006] used SEM to determine the latex distribution of coating layers in z-direction. They analyzed 5 layers (each 1μm thick) of coated paper samples, after being stained with osmium tetroxide, embedded and grinded. Ho and Yan [2012] applied EDX (energy

dispersive x-ray analysis) additionally to SEM image analysis to specify the latex distribution in z-direction.

Ström et al. [2010] presented a method, where the embedding step was unnecessary. They performed cross-sectioning, using a polisher with an ionized argon beam. The paper is protected with a nickel plate from the ion beam. Afterwards they used SEM to determine the latex volume and this sectioning technique led to better image quality. They did not focus on penetration of latex into the base paper. Also Dahlström and Uesaka [2008] used SEM of coated paper cross-sections to analyze the base paper and the coating layer distribution. They compared between leveling and contour coatings applied on different base papers. In their work, they did not focus on binder distribution or penetration/migration. Further work of Dahlström and Uesaka [2012a, 2012b] deals with coating microstructure and the distribution of OsO_4-stained binder within the coating layer. They apply the argon ion beam milling sectioning technique in combination with field emission scanning electron microscopy (FESEM). This leads to better image quality. Compared to Ström et al. [2010], Dahlström et al. [2011] used a copper tape to protect the sample from the beam and to support the sample (see Figure 21).
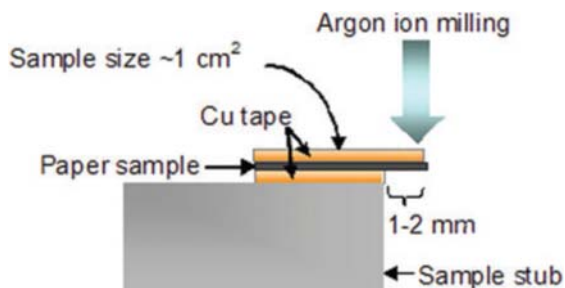
Figure 21: Argon ion beam milling [Dahlström and Uesaka 2011]

The amount of latex in different layers near the surface and also near the base paper was investigated [Dahlström et al. 2011; Dahlström and Uesaka 2012a, 2012b]. This method has a resolution down to the size of latex particles (around 100 nm). The penetration depth of binder into the base paper was not determined and no chemical information can be obtained.

4.2.2.2 Infrared methods

Regarding 3D observations, infrared methods also are applied. Hattula and Aschan [1981] used multiple internal reflectance (MIR) infrared spectroscopy of surface-grinded samples to determine the binder distribution in clay coatings.

4.2.2.3   Confocal methods

There are two different types of confocal methods applied for the characterization of paper coatings: Confocal Raman Spectroscopy (CRS) and Confocal Laser Scanning Microscopy (CLSM).

First, CRS is used to identify the different components in coating colors in z-direction [Kugge et al. 2008]. No staining compared to SEM is necessary. The area analyzed is relatively small, but a characterization in lateral and depth direction is possible. In both directions this method works well within 10-30 µm in z-direction. Kugge et al. [2008] analyzed all raw materials in solid or liquid form via Raman Spectroscopy. Paperboard samples were microtomed and placed in a sample holder and analyzed at different cross-sectional points (see Figure 22). Different types of pigments and latices can be identified by the location of the peak in the Raman spectra as illustrated in Figure 22.
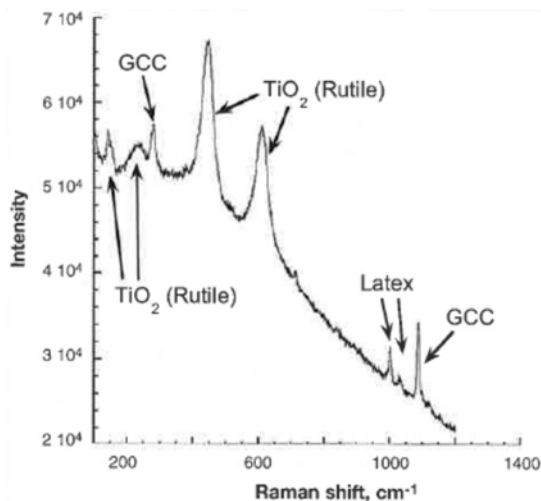
Figure 22: Raman spectra of a paperboard cross-section [Kugge et al. 2008]

Different types of latices and SB-latices with various T_g show different Raman spectra. This fact enables a localization of the binders after the coating process.

Regarding starch, the Raman peak cannot be detected because of the similarity in structure compared to cellulose.

Vyörykkä et al. [2004] analyzed double-layered coatings with different pigment types and SB-latex as binder. They determined the base paper – coating interface via the cellulose peak of the Raman spectrum. Vyörykkä et al. [2004] did not use sectioned samples but depth mode of CRS. Disadvantages of the method presented by Vyörykkä et al. [2004] were the limited penetration depth in z-direction and the small analyzed areas. A large number of single measurements would be necessary to analyze a significant area of interest.

Second, CLSM was used to characterize the coating layer properties. Ozaki et al. [2005, 2006 and 2008] investigated the penetration of printing colors and of stained latex into the base paper. Ozaki et al. [2006] developed a staining mechanism for latex with Rhodamine B to localize the binder afterwards with CLSM. Surface was observed, but also cross-sections by rapid scanning in z-direction were analyzed. The major advantage is the non-destructive method.

Hirai and Bousfield [2006] used the same method to determine the coating layer thickness and the amount of liquid penetrating into the base paper. They used the paper staining method with Rhodamine B dissolved in ethanol presented by Ozaki et al. [2003]. Paper staining means that the paper with the dry coating layer on it has been stained, in contrast to previous staining of different components. They applied different coat weights on paper samples and determined the coating layer thicknesses and compared the results to SEM results. Using double staining – paper was stained with Nile Blue A and latex were stained with Rhodamine B – Hirai and Bousfield [2006] investigated the surface coating layer, the surface of the base paper and the bottom line of the coating layer.

4.2.2.4 Atomic force microscopy (AFM)

AFM was also applied in 3-dimensional methods to determine the binder distribution of a coating layer on plastic film and paper substrate by Di Risio and Yan [2006]. Binder can be discriminated from pigments, because of the appearance of different adhesion forces of the AFM tip. Samples were embedded in an epoxy type resin and sectioned with an Ultramicrotome. Time factor for an adhesion map of 10x10µm limits this method. Adhesion maps are then segmented to determine a z-direction profile of the binder.

4.3 INFLUENCING FACTORS ON BINDER PENETRATION

There are several effects influencing binder penetration. In Figure 23, the influences found in the literature are illustrated and will be further described in this section.
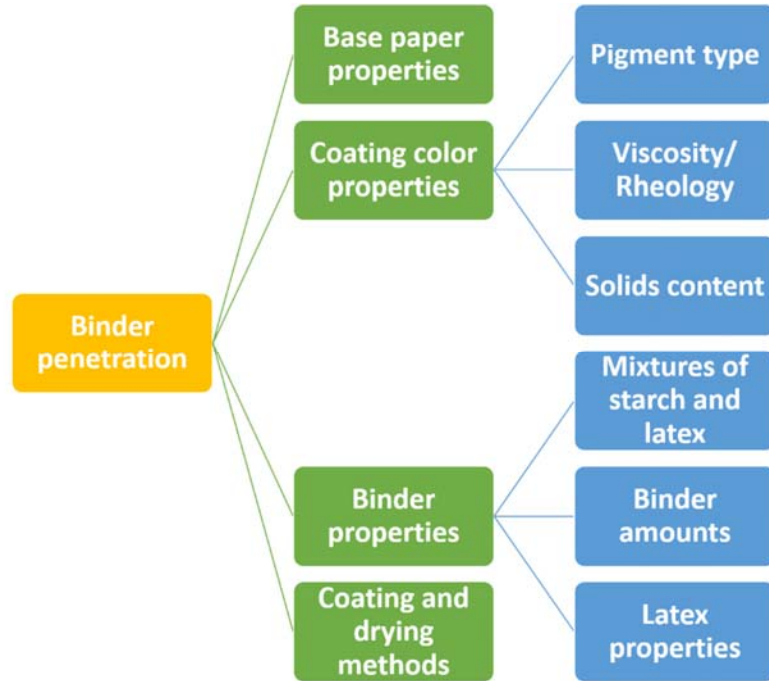
Figure 23: Influences on binder penetration

4.3.1 Base paper properties

Huang and Lepoutre [1998] investigated the influences of the base paper on coated paper properties. They focused on the capillary absorption, based on the effect of sizing (AKD) and sheet density and watched coating uptake, coated paper gloss, roughness and coat weight distribution. In their work, they investigated the coating "holdout" which means the resistance of the base paper to coating penetration. They found out that unsized porous sheets had a higher coating uptake. Also Clark et al. [1969] and Kim and Bousfield [2003] confirm this statement. Clark et al. [1969] differentiate between capillary and pressure penetration. While sizing reduces the capillary penetration, it has no influence on pressure penetration. Regarding sized sheets, dense ones showed a higher penetration into the base paper and a higher gloss, due to the fact that slower water absorption led to reorientation of the clay particles [Huang and Lepoutre 1998]. Kim and Bousfield [2003] observed surface sizing to be more effective regarding coating holdout than internal sizing. Al-Turaif and Bousfield [2005] found out that the substrate the coating is applied to has an influence on latex penetration and migration.

Coatings on a plastic film (non-absorbent substrate) showed a higher latex surface content, compared to coatings applied on a paper (absorbent substrate). In the case of the coatings on a paper, the latex particles are removed from the surface layers and transported into the porous system.

Engström et al. [1991] pointed out that the base paper properties are the main influence on binder penetration. They tested two different types of fibers (chemical pulp and mechanical pulp) and watched the surface SB-latex content during drying. Engström et al. [1991] found out that the SB-latex content on the coating surface is higher for samples made of chemical pulp. If the water is transported by diffusion and not by capillary forces into the base paper, the latex remains within the coating layer and migrates to the surface areas. Engström et al. [1991] pointed out that water transport by diffusion is more pronounced in chemical fibers than in mechanical fibers. Also Skowronski and Lepoutre [1985] and Kim and Bousfield [2003] confirm this observation.

Engström et al. [1991] determined latex distribution on the surface of coatings on three different base papers. Unsized sheets showed an uneven binder distribution compared to LWC paper. Sized sheets had the most even binder surface distribution of all the paper grades. Depending on the type of base paper, correlation between offset mottling and latex surface content differed. They found a correlation of mottling and the standard deviation in coat weight.
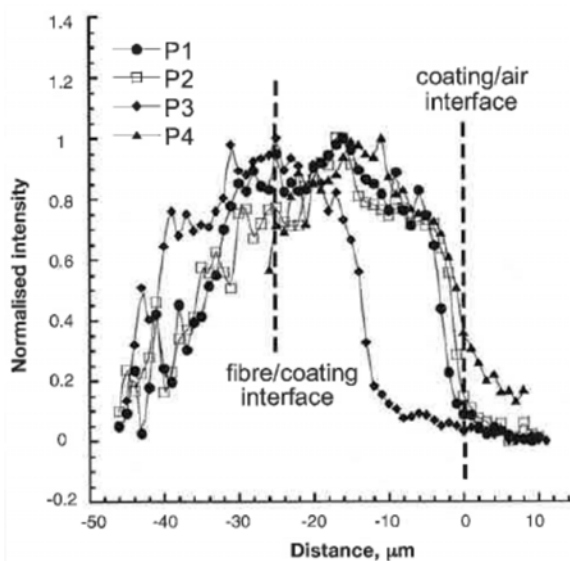
Figure 24: Latex distribution in a cross section [Kugge et al. 2008]

Kugge et al. [2008] compared two different paperboards regarding latex distribution and found significant differences in the line scans. In Figure 24 the latex distribution of one paperboard sample (cross-section) is illustrated. This figure shows the coating/air interface (right) and the fiber/coating

interface (left). P1 – P4 name four different positions. Figure 24 shows a high concentration of latex near the fiber/coating interface and in the first layers of the base paper. This indicates that binder penetration into the base paper plays an important role.

Ozaki et al. [2006] observed differences in penetration of latex into the base paper for different LWC paper grades via CLSM. Bitla et al. [2003] tested LWC paper and sized wood-free paper, compared to a non-absorbent plastic film and observed the latex/$CaCO_3$ ratio at the coating surface. The coating formulation using coarse $CaCO_3$ led to highest latex surface contents of coatings on plastic film, whereas sized base paper and LWC paper showed the lowest latex surface contents.

Dappen [1951] investigated another base paper influence on binder penetration. He observed starch penetration of clay-starch coatings applied on base papers with different moisture contents. Higher moisture content causes a change in capillary structure. The higher the moisture content is, the smaller the penetration losses of starch into the base paper.

4.3.2 Coating color properties

The initial solids content of a coating color and the coating formulation itself, but also the wet coating properties including rheology and water retention can be allocated to coating color properties.

4.3.2.1 Pigment type

One important issue is the type of pigment used. Kenttä et al. [2006] investigated the influence of clay in calcium carbonate based coating formulations regarding latex penetration and migration. A mixture of carbonate and clay (70/30) led to higher water retention and therefore binder penetration into the base paper decreased.

Al-Turaif and Bousfield [2005] and Bitla et al. [2003] observed the effect of particle size distribution on latex migration/penetration. They determined the surface latex content of the dry coating and found out that narrower particle size distributions lead to more latex penetration into the substrate and a decrease in surface latex content. The effect is illustrated in Figure 25. A narrow particle size distribution (left image in Figure 25) leads to larger pores, compared to a broad particle size distribution (right image in Figure 25). Larger pores cause a higher amount of water and latex being transported into the porous substrate. Bitla et al. [2003] emphasizes that latex motion just occurs when the void volume between the pigments is larger than the latex particle size. Chattopadhyay et al. [2014] observed an increased starch movement in coatings with coarse precipitated calcium carbonate (PCC), compared to fine PCC. The same trend could be observed using latex and starch mixtures.
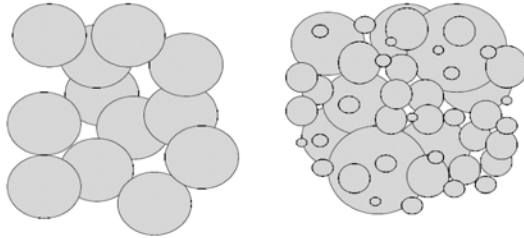
Figure 25: Influence on particle size distribution on a porous system [Al-Turaif and Bousfield 2005]

Also Chinga and Helle [2002b] studied the influence of pigment distribution on pore structure within the coating layer to control coating quality and uniformity. They focused on the determination of pore geometry to get the best print quality. Pore structure is also dependent on the binder distribution and penetration during the coating process. Chinga and Helle [2002b] analyzed several LWC paper grades with different pigment mixtures including clay and calcium carbonate. They observed a reduction in pores with increasing clay contents compared to GCC based coatings. Di Risio and Yan [2006] analyzed model coatings on plastic films regarding binder migration and binder distribution. The pigments were varied in size and distribution, but binder level was kept constant. Pigments with coarser particles and broader particle size distribution showed more uneven binder distributions in z-direction. No binder movement towards the surface was identified by Di Risio and Yan [2006]. Ho and Yan [2012] observed higher surface latex contents of coating formulations with larger particle size.

4.3.2.2 Rheology and water retention

The behavior of a coating color in wet state has an influence on binder movement towards the base paper and towards the coating surface.
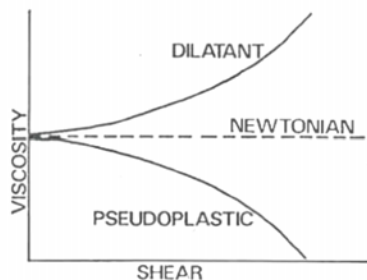
Figure 26: Types of fluids [Bartell 1976]

Bartell [1976] shows the theoretical model of coating color viscosity over shear rate (see Figure 26). There are two types of fluids: Newtonian fluids and non-newtonian fluids including dilatant and

35

pseudoplastic fluids. Dilatant means shear thickening and pseudoplastic means shear thinning, as is illustrated in Figure 26. Coating colors are non-Newtonian fluids.

The coating color rheology can be influenced by various additives which modify the water phase of a coating. Bartell [1976] describes the coating color viscosity under shear and the influence of different additives. He observes the effect of hydrocolloids like carboxymethylcellulose (CMC), sodium alginate or hydroxymethylcellulose on coating rheology. These additives control the dewatering and decrease binder penetration.

Kenttä et al. [2006], Pöhler et al. [2006] and Bitla et al. [2003] support the theory of Bartell [1976] that CMC lowers binder penetration. The addition of CMC to a coating formulation resulted in a higher water retention and retarded transport of latex towards the base paper. Furthermore, the latex distribution on the surface was more uniform.
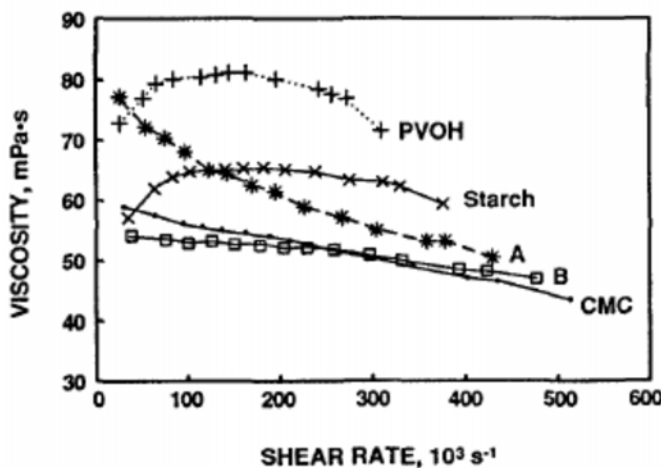
Figure 27: Co-binders and their influence on viscosity at different shear rates [Sandas and Salminen 1991]

The effect of CMC and other Co-Binders in clay/latex-Coatings on viscosity at different shear rates is shown in Figure 27, in the work of Sandas and Salminen [1991]. Cold-soluble starch, PVOH (=PVA), CMC, and two synthetic thickeners (A, B) were tested. As illustrated in Figure 27, PVOH showed the highest viscosity at high shear rates. Sandas and Salminen [1991] found out, that a higher viscosity leads to a better water retention.

Bushhouse [1992] compared three types of polymers (CMC, PVA and alginate) regarding the ability to lower binder migration. CMC and especially alginate showed better results than PVA.

Bitla et al. [2003] emphasize that CMC bridges and agglomerates the pigments into a network and lowers binder penetration. Chattopadhyay et al. [2014] investigated the coating structure on a crystal

via ATR-IR during drying. Their observations, when adding CMC to the coating formulation showed the same results as the work of Bitla et al. [2003]. The motion of latex is hindered with the addition of CMC and a structure of coating in the wet state seems to exist.

Kugge [2004] observed a lower surface latex content with the addition of CMC (Finnfix 10) to a coating color, containing $CaCO_3$ and latex, applied on a non-absorbent plastic film. Usage of a CMC having a higher molecular weight (Finnfix 30) led to higher viscosity of the coating color. Because of this fact, the film formation should be prolonged and the evaporation rate reduced. A difference in amount of latex in the surface regions compared to low MW-CMC could not be detected. Zang et al. [2010a] determined a reduction in surface carbon content, which is associated with the SB-latex content, when adding CMC (0,25 pph and 0,5 pph) to a coating applied on a plastic film.

Regarding the effect of viscosity and water retention of the coating formulation on binder penetration into the base paper, the observations found in the literature differ. There was no clear evidence that a higher viscosity by adding CMC, led to less binder movement, both towards the surface and into the base paper. The addition of CMC and therefore the increase of viscosity led to higher water retention of the coating color. Different studies were published with coatings on absorbent and non-absorbent substrates. A non-absorbent substrate cannot be compared with a coating on a paper sample regarding binder movement and distribution.

4.3.2.3 Solids content

The influence of solids content on the penetration of binder was investigated by Lepoutre [1978] and Clark et al. [1969].

Lepoutre [1978] investigated the influence of solids content of the coating color on coating behavior, coat weight and surface composition. He compared coatings having 60% solids content to coatings with 40%. A fast dewatering appears especially at low solids and coat weights of coatings on different papers were lower.

Clark et al. [1969] developed an apparatus to determine the capillary and pressure penetration into a base paper. Reflectance of the coating color on the surface was measured after staining the coating color with nigrosine black. The results of the realization of different solids contents showed that penetration into the base paper increases with lower solids, especially the capillary penetration.

Zang et al. [2010a] applied coatings with different solids contents on a plastic film and observed lower surface carbon concentrations with higher solids contents via XPS (see Figure 28). Surface

carbon content represents the surface latex content. Coatings were applied to a non-porous substrate and dried immediately after coating with a hot air dryer at 50°C.
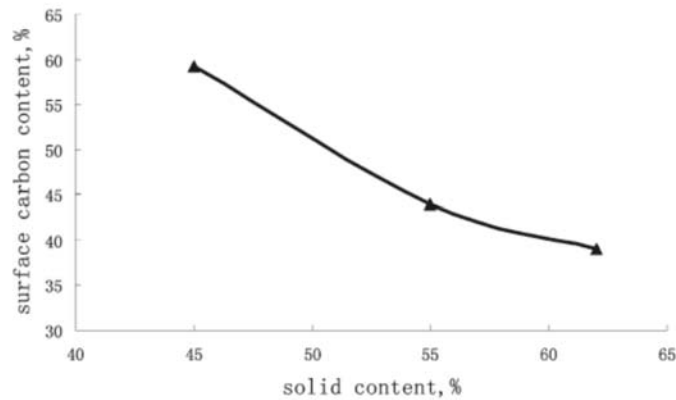
Figure 28: Influence of the solids content of a coating on the surface carbon content [Zang et al. 2010a]

4.3.3 Binder properties

In this chapter the influences of the type of binder and the chemical composition is discussed. Water-soluble and water-insoluble binders are compared. Furthermore the influence of addition level of binder in the coating formulation is observed.

4.3.3.1 Mixtures of starch and latex

Du et al. [2011] investigated the effects of starch level in a mixture of latex and starch as binder. They used a non-porous plastic film and analyzed the coating layer on it via XPS. Results showed decreasing latex level at the coating surface with increasing starch level. Both latex and starch level decreased leading to a depletion of starch at the coating surface. This indicates lower latex migration ability, when more starch is added. Also Chattopadhyay et al. [2014] found less starch at the coating surface, when latex is present in the formulation. The coating was applied on a paper substrate and surface was analyzed via ATR-IR. Figure 29 illustrates the effect of latex and starch penetration and migration presented by Chattopadhyay et al. [2014]. When the coating is applied onto a paper substrate, starch and also some latex moves into the pores of the base paper. During drying, latex forms a barrier on the surface (see Figure 29 middle) and starch cannot migrate back towards the surface.
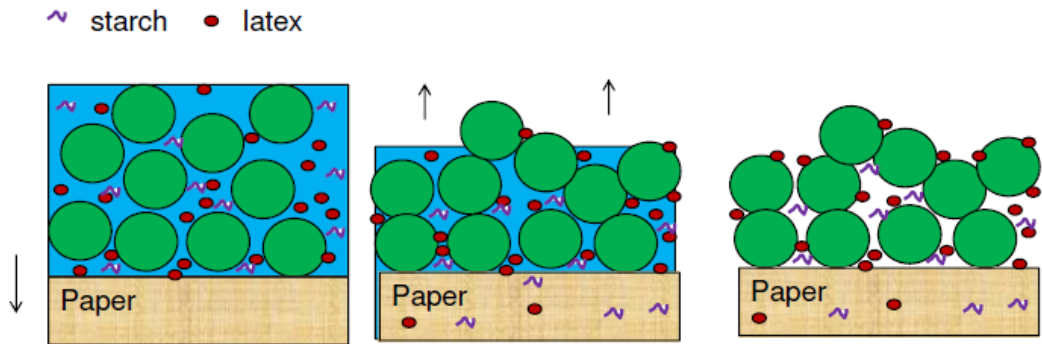
Figure 29: Effect of penetration and migration in mixed starch and latex coatings [Chattopadhyay et al. 2014]

Engström et al. [1991] observed the same effect. Although the starch concentration in the formulation was higher than the latex concentration (starch/latex = 7/5), a higher latex content at the coating surface was present, when applying the coating on different base papers. Yamazaki et al. [1993] investigated the surface latex and starch concentration via a surface scraping method (0,3 µm scraped off) and characterization with ESCA. They found out that the surface latex content and migration behavior is different between starch and latex. Surface starch content decreased with longer time period between application and drying which indicates binder penetration into the base paper.
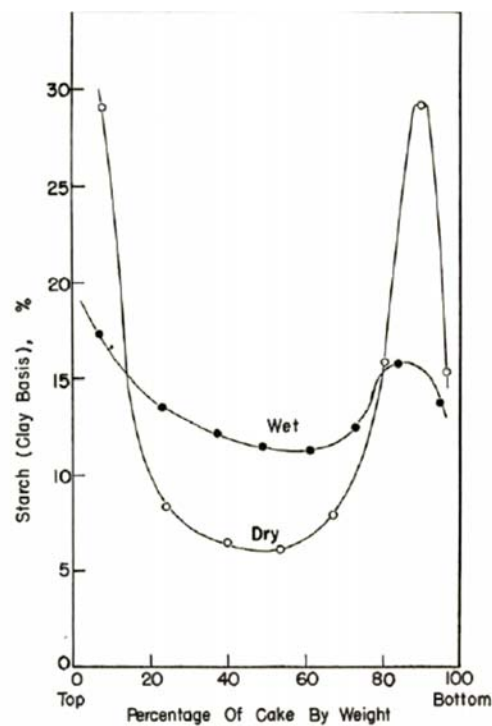
Figure 30: Distribution of starch in a filter cake [Dappen 1951]

In the work of Dappen [1951], the ability of clay-starch coatings to penetrate into the base paper was investigated. The same coating was applied on a glass plate and on a paper substrate. Wet coating was removed and the loss of the starch was determined. Dappen [1951] observed a loss of starch of 3 to 4% after 4 minutes contact with the base paper. The biggest change in starch content in the wet state appeared within 15 seconds. Approximately 28 to 33% of total water and 3 to 4% of starch were lost after 2 to 4 minutes by penetration into the base paper. The loss of starch is supposed to decrease with increasing amount of binders, because of the higher viscosity of the coatings. In Figure 30 the distribution of starch in a filter cake is shown in the dry and wet state. Coating formulations having a solids content of 48,5% and a starch content of 20% were used to form a filter cake. The coating layers were dried in the oven at 105°C and sectioned (parallel to surface) to analyze the single layers. The starch concentration in the dry coating increased in the top and bottom layers. The higher starch contents in the top layers indicate binder migration during evaporation of water from the sample. Coatings were also applied on glass plates and oven dried. Starch migration towards the air interface was observed. Groves et al. [2001] also saw an enrichment of starch at the surface, when applying thick coating layers on a plastic film. Regarding latex formulations they found no evidence for latex migration towards the coating/air interface independently whether with drying period interval, latex level or pigment properties.

4.3.3.2 Binder amounts

Al-Turaif and Bousfield [2005] investigated the influence of the amount of latex used in clay coatings. They found a higher surface latex content when more latex was used. In contradiction to that, Bitla et al. [2003] observed no influence of binder level on binder motion in formulations with large pigment sizes. But solids content was set to 65%, compared to 55%, in the work of Al-Turaif and Bousfield [2005]. Bitla et al. [2003] used $CaCO_3$ as pigment, which is different in shape, compared to clays used by Al-Turaif and Bousfield [2005]. Ström et al. [2010] focused on the determination of pore volume after coating with 10, 20 and 30 pph of latex as binder. Higher latex contents (30 pph) led to a structure almost free of pores. They correlated their SEM technique with mercury porosimetry and voids were significantly lower than values of porosimetry. Therefore the smaller amount of voids does not lead to a higher latex content, as predicted from mercury porosimetry.

4.3.3.3 Latex properties

Kugge et al. [2008] used CRS of microtomed cross-sections to characterize different types of binders in coating layers. They distinguish between latices varying in their structure (SA, SB, PVA-latex) and T_g. Starch cannot be detected because of the similarity to cellulose. Kugge et al. [2008] compared

two coated paperboards, having different picking resistance. As reference they used a latex coated aluminum plate (see Figure 31).
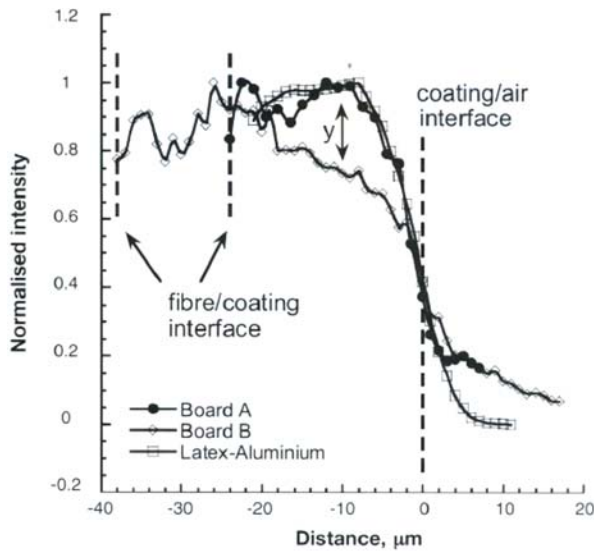
Figure 31: Binder migration and penetration of two different boards [Kugge et al. 2008]

The board with the higher picking resistance showed higher amounts of latex in the surface regions (see Board A in Figure 31). Board A correlates well to the reference coated aluminum. Kugge et al. [2008] point out that latex acts as glue between the pigments. If the latex penetrates into the base paper, there will be less latex in the surface layers leading to insufficient picking resistance. In Figure 31 the differences in location of the fiber/coating interface indicates the higher latex penetration into the base paper of Board B.

In the work of Kugge [2004], latices having different glass transition temperatures were used to observe the differences in binder migration. Latex with high T_g, added to a coating color, is concentrated in the surface regions of a coating applied on a plastic film. Kugge [2004] assumes that a latex having a higher T_g migrates more easily, because it is less tacky. Yamazaki et al. [1993] observed the same effect.

4.3.4   Coating and Drying methods

Regarding binder migration towards the coating surface, drying methods play an important role. The delay time between the application and drying of coating has an impact on binder penetration. During the wet state of the coating, capillary penetration and filtration processes take place. Regarding the effect of pressure penetration, the application and metering method of the wet coating should be discussed.

Kline [1991] studied the effect of drying on binder migration via UV surface analysis. He compared hot air, cold air and IR drying. All those drying procedures showed a small amount of binder migration. He demonstrated one case, where the binder penetrated more into the base paper than migrated to the coating surface. This appeared with hot air drying, which indicates that the porous coating structure was more open and pigment structure was set rapidly. Zang et al. [2010] add the importance of delay time before drying to the theory of Kline [1991]. Investigations with increasing delay times of coating layers on a plastic film (22 g/m^2) showed a decreasing surface carbon content. Surface carbon content of XPS is associated with SB-latex level. Yamazaki et al. [1993] investigated the surface starch and latex contents on a paper substrate. In their trials, they realized different time periods between coating application and drying. Surface latex content was constant over different drying intervals, while surface starch content decreased with increasing drying interval. Starch is penetrating into the base paper. They tested two different application methods (blade and rod) with 8 g/m^2 (blade) and 17 g/m^2 (rod) on a base paper (wood-free) with a grammage of 46 g/m^2. Yamazaki et al. [1993] observed the same trend regarding surface latex and starch content. Starch content decreased with increasing drying interval period. They correlated the laboratory coating results to pilot coating results (pilot SDTA coater with five air flotation dryers) and applied 10 g/m^2 of coating. Both starch and latex surface contents were lower at pilot coating, compared to laboratory coatings. This indicates a higher amount of binder penetrating into the base paper for pilot coating. Also Dappen [1951] found lower starch surface concentrations at paper samples with starch-clay coatings dried at room temperature in comparison to samples dried with hot air blast. There starch concentration increased from the fiber to the air interface.

Engström et al. [1991] investigated the influence of drying (hot air and IR) on surface binder content of different coatings. Results showed, that the evaporation rate of the hot-air dryer only had a marginal effect on binder migration, compared to the influence of base paper. Regarding the sized base paper an influence of the drying strategy on surface SB-latex content was observed, when evaporation rates increased. They also noted a higher surface latex content when applying IR dryers.

Vyörykkä et al. [2004] investigated the differences in drying conditions of two double coated papers. Coating colors contained 100% calcium carbonate, 12% SB-latex and 1% CMC as thickener. 9 g/m^2 was applied on each side. Paper A had no visible backtrap mottle compared to Paper B. Vyörykkä et al. [2004] calculated the coating layer thicknesses and the SB-latex/calcium carbonate ratio at the surface (first 2 μm in z-direction). They found out that Paper A had larger SB-latex surface contents, which indicate higher binder migration. There was no significant difference in latex content for points

of even and uneven print density of both papers. Engström et al. [1997] observed no link between surface latex content and print mottle and proposed porosity distribution of the coating to be the governing effect. Dahlström and Uesaka [2012] and Yamazaki et al. [1993] also found no correlation of print mottle and latex surface distribution. Another interesting fact regarding the work of Vyörykkä et al. [2004] was the localization of the SB-latex (highlighted red in Figure 32) after the coating process within the coating layers and the first layers of the base paper. Cellulose can also be detected via CRS (see Figure 32 – highlighted green). So the interface between coating and base paper can be determined. One interesting fact is the second peak in latex spectrum within the base paper region (see number 2 in Figure 32). This indicates latex penetration into the base paper during coating application and drying.
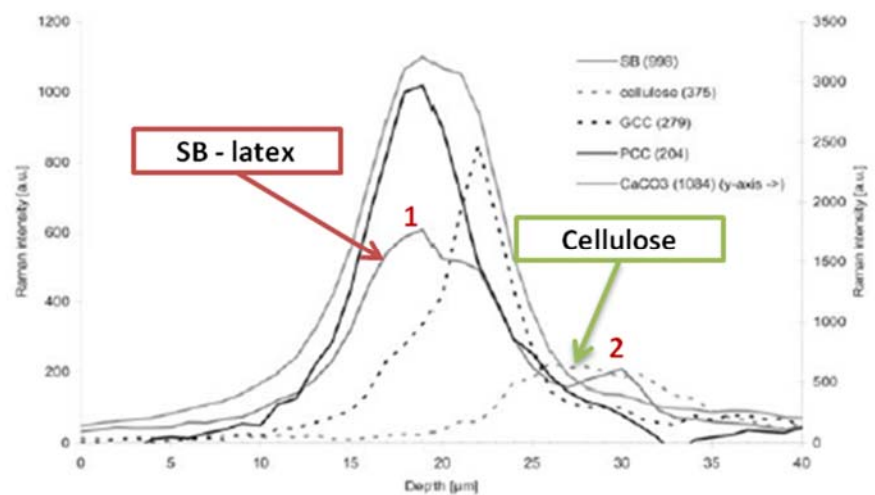
Figure 32: Depth profiles of the coating ingredients (adapted from [Vyörykkä et al. 2004])

Ozaki et al. [2008] investigated the thickness of a fluorescently stained coating layer on four paper samples using CLSM. The samples just differed in drying method of the coating layer. Base paper, coating color and coat weight were the same. Samples A and B showed a good print quality and for samples C and D backtrap mottling appeared. As illustrated in Figure 33 the samples C and D (bottom) showed an uneven coating layer.

Average stained coating layer thicknesses showed similar values of the four samples. The higher standard deviation of the samples C and D indicate the uneven coating layer (see Figure 34). As 22 g/m^2 were applied on each side, a coating layer thicknesses of around 10 µm seems to be low.

43
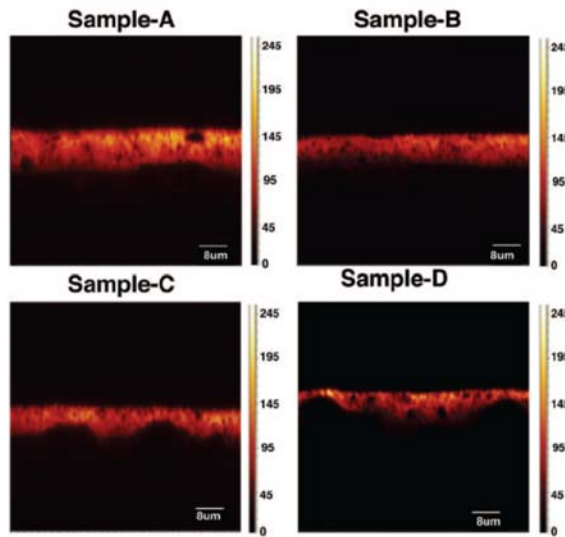
Figure 33: Coating layer stained with Rhodamine B (sample A, B top, sample C, D bottom) [Ozaki et al. 2008]

	Average thickness (um)	Standard deviation
Sample-A	10.1	1.6
Sample-B	9.5	1.3
Sample-C	9.8	4.6
Sample-D	9.3	4.7
		n=125

Figure 34: Average stained coating thickness of the four samples [Ozaki et al. 2008]

Ho and Yan [2012] compared two different coating methods to analyze binder penetration and binder distribution in z-direction. They compared coatings of a metering size press (MSP) with coatings applied with a spray coater. The MSP showed a higher amount of latex penetrated into the base paper. There is no hydrodynamic pressure applied in spray coatings. Unfortunately, the coating formulations in spray coating and MSP did not have the same solids content and the same level of latex.

4.4 CONCLUSIONS

Different aspects regarding binder penetration have been discussed in Chapter 4.

The first section (4.1) was about the mechanisms behind binder penetration. Coating application on a paper substrate is a complex topic and different mechanisms have to be considered. The theoretical background presented in chapter 4.1 was just a brief overview to introduce the penetration mechanisms. The coating process can be divided into four sections: first capillary, pressure, second capillary and drying section. Capillary penetration is described via Lucas-Washburn and Bosanquet equation. The difference between those two equations is observation of fluid flow into large pores. The proportionality of pore radius and penetration length is different. Also Darcy's law needs to be considered because of the appearance of a filter cake during coating application.

Different methods to determine binder penetration were discussed in section 4.2. This section was divided into the surface analysis and cross-section methods to determine binder penetration. The focus was on the cross-section methods, because the new established method called SSFM can be classified into this category. There was the need to develop a newly method, because the methods presented in the literature did not fulfill the requirements well. The requirements were the investigation of binder penetration of a significantly large region of interest (several mm^2) in three dimensions and the ability to detect the most common coating binders, like starch and latex.

Most of the techniques to characterize the coating layer work on single cross-sections concentrating on one location area [Vyörykkä et al. 2004; Kugge et al. 2008, Ozaki et al. 2006, 2008]. The output is a 2D cross-section image. Other methods observe the surface layer (see Chapter 4.2.1) or apply grinding techniques to characterize several layers of the coating [Hattula and Aschan 1981; Yamazaki et al. 1993; Groves et al. 2001]. Dappen [1951] removed and analyzed the wet surface layers during consolidation.

Table 2 shows the comparison of the common cross-section methods to determine binder penetration. The limiting factor regarding SEM [Dahlström et al. 2011] methods is the relative small sample size that can be analyzed and the elaborate sample preparation.

Confocal methods like CRS [Vyörykkä et al. 2004; Kugge et al. 2008] or CLSM are non-destructive methods. No sample preparation steps are necessary regarding CLSM [Ozaki et al. 2008]. CLSM [Ozaki et al. 2008] is limited in light penetration depth in z-direction. Hiari and Bousfield [2006] reported troubles with high coat weights using XZY mode with CLSM. CRS is limited in the

determination of starch penetration into the base paper, because of the similar structure of cellulose and starch.

Table 2: Comparison of the common cross-section methods to determine binder penetration in the literature

Method	Resolution	Region of interest (surface/depth)	Destruction	Sample preparation	Chemical characterization
SEM	++	--	Yes	Staining, embedding (microtome) or argon ion milling	No
CLSM	+	-	No	staining	No
CRS	+	-	Yes	Embedding, microtome	Yes
AFM	+	-	Yes	Embedding, microtome	No

Section 4.3 summed up the influencing factors on binder penetration. Four big issues were discussed: the base paper properties, the coating color properties, the binder properties and the coating and drying method. Several publications indicated the base paper, coating is applied to, as the main influential factor regarding binder penetration.

5 ESTABLISHMENT OF A NEW METHOD TO ANALYZE BINDER PENETRATION

In this chapter the new method to determine binder penetration is presented. Some technical details of the instrument (µSTRUSCOP) are described. Furthermore, the necessary working steps to obtain a binder penetration depth into the base paper are listed and explained in detail. This chapter also includes the evaluation of the newly established method (SSFM) with confocal laser scanning microscopy (CLSM).

The presented method is based on a serial sectioning technique combined with a fluorescence microscope (SSFM).

Prior works combined visual light microscopy with serial sectioning (first prototype). So coating layer thickness [Kritzinger and Bauer 2012; Kritzinger et al. 2008], penetration of coating pigments into the base paper [Kritzinger et al. 2011], calendaring influences on coating layer formation [Wiltsche et al. 2006] and also fiber properties [Lorbach et al. 2012; Kontschieder et al. 2010; Donoser et al. 2008] were determined. Another application field of this method was the calculation of bonded area of individual fiber bonds (Kappel et al. 2009; Kappel et al. 2010a; Kappel et al. 2010b].

A second generation prototype (µSTRUCSCOP – see Figure 35) was developed by Schäffner [2012]. This prototype consists of two units: The microtome (see Figure 35 – right part) and the microscope unit (see Figure 35 – left part). New tools compared to the first prototype are the possibility to switch between a visual light source and a UV-light source, the filter cube section and the software regarding stitching and aligning.

Two different sample holders can be used. The one illustrated in Figure 35 in combination with a diamond knife as sectioning tool is used for embedded samples. The one in Figure 36 in combination with a steel knife as sectioning tool is used for the sandwich method. The sandwich method is presented in the work of Voura [2008]. The paper sample is fixed between two plastic strips and no previous embedding is necessary, but the image quality is worse.
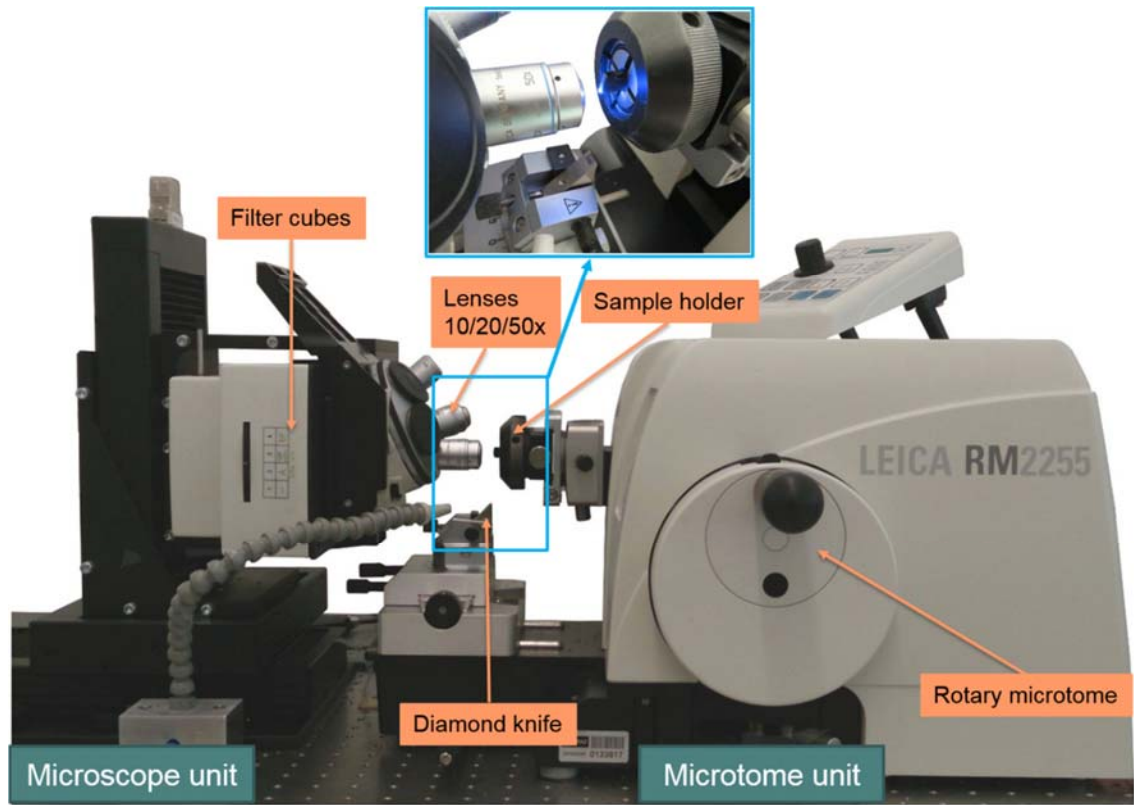
Figure 35: Working device (µSTRUCSCOP) for SSFM
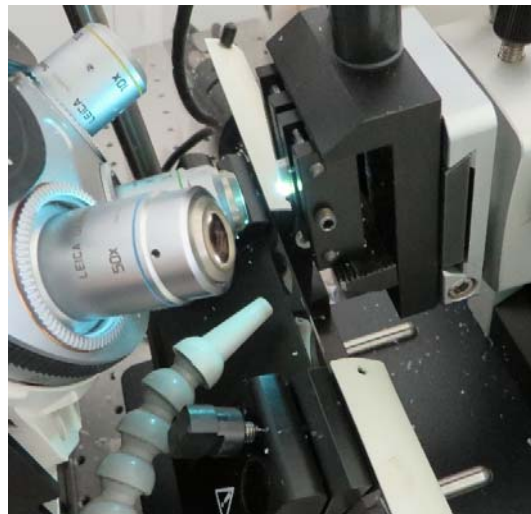
Figure 36: Sandwich method with steel knife

5.1 TECHNICAL DETAILS OF µSTRUSCOP

In this section, the technical details and the most important hardware and software components to introduce the working principle are listed and described. A more detailed description can be found in the work of Schäffner [2012].

- Resolution down to (0.47 x 0.47 x 1) μm^3

Three different lenses can be selected (see Table 3).

Table 3: Available lenses (µSTRUSCOP)

Magnification	10x	20x	50x
Pixel Size [µm]	0,618	0,309	0,124

- Two light sources available: UV-light source and visible light source
- Four different filter cubes: BF, A, GFP, GFP/mCherry (dual filter)
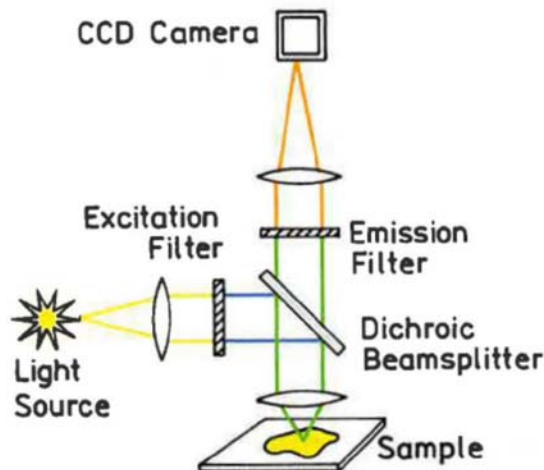
Figure 37: Principle of filter systems [Lakowicz 2006]

For fluorescence microscopy filter cubes, consisting of three different components, are used: excitation filter, emission filter and dichroic beam splitter (see Figure 37). The beam of the light source hits the excitation filter which performs a selection of wavelength to excite the sample. The dichroic beam splitter has two functions: reflection of the excitation wavelength (see green lines in Figure 37) and transmission to the emission filter (see green lines up in

Figure 37). The transmission filter reflects the excitation wavelength and light passes through to the detector or camera [Lakowicz 2006].

The principle of the three different components of a filter cube are shown in Figure 38. There the transmission in % over the wavelength in nm is illustrated.
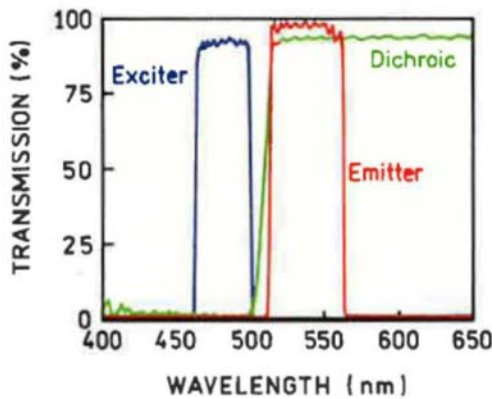
Figure 38: Filter cubes with three components [Lakowicz 2006]

In Table 4 the available filters at μSTRUCSCOP are listed. The selection of the filter is based on the excitation wavelength of the fluorophore.

Table 4: Specification of filter cubes

Filter cubes	A	GFP	GFP/mCherry
Company	Leica	Leica	AHF (www.ahf.de)
Number	11513873	11513890	#250597, #250719, #250586
Excitation wavelength	360/40	470/40	470/30 + 520/40

- Hardware and software stitching and aligning
  Hardware aligning is performed using a position sensor. Software stitching and aligning in two directions is available: in ZD and CD (see Figure 39).
- Typical slice thickness (Microtome Leica RM2255): from 1 to 5 μm
- Paper sample sizes (embedded samples): maximum 6 mm (CD) and 2 mm (ZD) (directions see Figure 39)
- Paper sample size (sandwich method): maximum 9 mm (CD) and 2 mm (ZD)
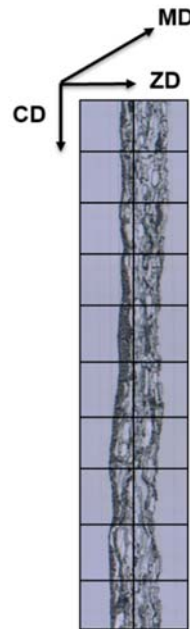
Figure 39: 2D stitching and aligning

5.2 WORKFLOW FOR SSFM

In this chapter the work flow to obtain a calculated penetration depth of binders into the base paper is described. The single steps are illustrated in Figure 40 and further described below.

Figure 40: Workflow of SSFM

5.2.1 Staining the binder

The first step was the classification of binders into groups of intrinsic and extrinsic fluorophores (see Section 3.2) to decide whether a fluorescent dye was necessary or not. Several staining mechanisms and dyes were tested including physio-chemical staining (working via charge differences and differences in hydrophobicity) and chemical staining (reactive staining). The result was that reactive stains are most applicable. The reason for preference of reactive dyes was the formation of irreversible covalent bonds between the dye molecule and the substrate. Due to differences in chemical structure of the coating binders (or additives) the staining procedure needed to be established for every single substrate and dye.

5.2.1.1 Lignin Binders

In the FLIPPR-project a new bio-based binder to substitute oil-based binders, like latex, is developed. These binders are based on industrial lignins (lignosulfonates and kraft lignins) and can be classified into the group of intrinsic fluorophores. So no further staining was necessary.

5.2.1.2 Starch

Water soluble starch (cold dissolving) from AGRANA Research and Innovation Center was fluorescent labeled using 1 wt% 5-([4,6-Dichlorotriazin-2-yl]amino)fluorescein (5-DTAF) (Sigma Aldrich) as fluorescent marker (see Figure 41) at AGRANA. This is a reactive stain and the triazine group links to the OH-groups of the starch molecule as described in Chapter 3.2.2 (Figure 13). Moran-Mirabel et al. [2008] published the staining procedure, which was used in this work. 20 mg of DTAF were dissolved in 25 ml 0,2M sodium hydroxide. 1 g of starch was added to this solution and stirred at room temperature overnight. Afterwards the solution was added to 200ml of cooled ethanol. The precipitated starch was separated via centrifuge and washed several times with ethanol until no unbound DTAF was remaining. After drying the content of bonded DTAF was determined photometrically to control the target bonded amount of DTAF of 1 wt% based on the amount of starch. The yield of this staining mechanism is approximately 50%.
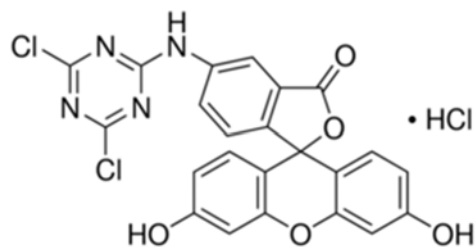
Figure 41: 5-([4,6-Dichlorotriazin-2-yl]amino)fluorescein hydrochloride [Sigma-Aldrich Co. LCC. 2015]

Table 5: Specifications of DTAF [Sigma-Aldrich Co. LCC. 2015]

	DTAF
Formula	$C_{28}H_{12}Cl_2N_4O_5$
CAS Number	21811-74-5
MW	531,73 g/mol
Emissions Maximum	495 nm
Absorption maximum	516 nm

5.2.1.3   Latex

Staining of latex is based on the physio-chemical staining mechanisms. Rhodamine B (see Figure 42) is adsorbed into the latex particle [Golebiowska et al. 2015]. Ozaki et al. [2006] suggested dissolving 0,03 wt% of Rhodamine B in ethanol, to soak the coated paper in that solution and to rinse it afterwards with ethanol. One disadvantage of using ethanol as a solvent is the fact of fiber swelling when dissolving dyes with organic liquids. Wertz et al. [2010] reported a liquid retention value of 21% when soaking cotton with ethanol. The fiber swelling is lower compared to water as solvent which has a liquid retention value of 51% [Wertz et al. 2010]. However, Golebiowska et al. [2015] showed that staining the latex prior to coating color preparation led to better results than staining of coated paper. They found out that staining the dry coating layer is an appropriate method for the determination of the location of latex, but it is not applicable for a double stained system to distinguish between the location of starch and latex. Ozaki et al. [2006] investigated the adsorptivity of Rhodamine B on other coating agents. They determined the fluorescence spectra of Rhodamine B stained components and found out that neither Kaolin, $CaCO_3$, starch nor polyvinylalcolhol showed a fluorescence signal.
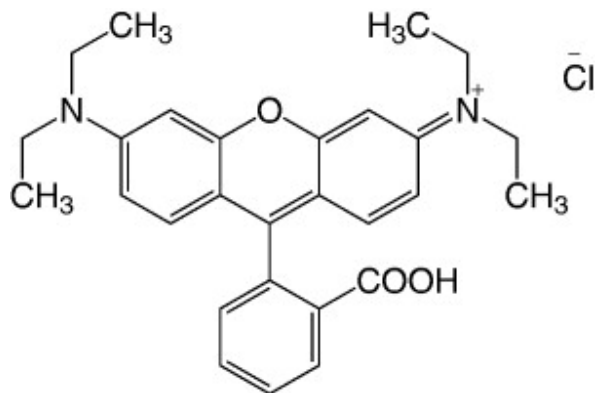
Figure 42: Rhodamine B [Carl Roth GmbH + Co. KG 2015]

In this work, different dissolving concentrations of Rhodamine B were tested and finally, the Rhodamine B concentration was set to 0,01 wt%. When the concentration is too high, this causes out-of-focus light in fluorescence microscopy.

The specification of Rhodamine B can be found in Table 6 including the absorption maximum.

Table 6: Specification of Rhodamine B [Carl Roth GmbH + Co. KG 2015]

	Rhodamine B
Formula	$C_{28}H_{31}ClN_2O_3$
C.I.	45170
MW	479,02 g/mol
Absorption maximum	540 – 560 nm

5.2.2 Coating

Coating colors were prepared using fluorescently stained binders. Coating formulations are listed in detail in the following chapter.

5.2.2.1   Coating material

Coating colors were prepared with $CaCO_3$ (HC 90) as pigment.

Following binders and additives were used:

- Styrene-butadiene latex: Styronal 322 (BASF)
- Starch ZFT 2793 (Agrana Research and Innovation Center)
- Lignosulfonate Binder (LS) (polymerized by the Department of Agrobiotechnology of the University of Natural Resources and Life Sciences)
- Polyvinyl alcohol (PVA): Mowiol 4-98 (Kurary)
- Carboxymethylcellulose (CMC): Finnfix 30 (Noviant)
- Thickener: Sterocoll BL and FS (BASF)
- Sodium hydroxide
- Water

5.2.2.2   Base paper

One important issue, to locate the binder after the coating process, was the use of a paper free of fluorescence.
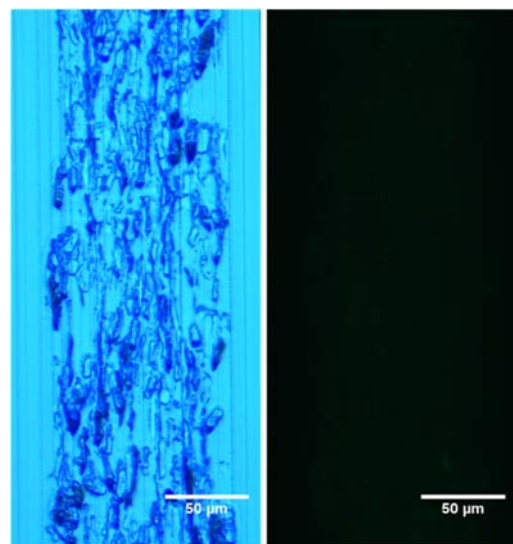
Figure 43: Base paper (BF image left; GFP image right)

Industrial papers are not free of fluorescence because of the recycled coated broke containing optical brightening agents. Those brightening agents are emitting fluorescent light at similar wavelength like lignosulfonate or DTAF. Mechanical pulps and chemical pulps with a high Kappa number cannot be used, because of the auto-fluorescence of lignins (see Chapter 3.2.1.1).

In Figure 43 the base paper used in this work is illustrated. On the left side the BF filtered UV-image and on the right side the GFP filtered UV-image is shown. If the base paper emits fluorescent light, a green color will appear in the right image. Therefore, coating trials were performed with laboratory handsheets made out of bleached eucalyptus fibers (Santa Fe).

5.2.2.3 Coating process

The coating process was performed on three different coating units and the influence of the application method on binder penetration was studied:

- Manual Rod Coater (RK Print-Coat Instruments Ltd., England) (see Figure 44)
  5 ml of coating color is applied and equalized with a rod. Rods with different grooves are available. The speed of the rod movement can be adjusted. However, it is a challenge to control the applied coat weight with the available settings. Afterwards the sheets are dried with a hot air drying unit at 160°C.

Figure 44: Manual Rod Coater

- Laboratory Blade Coater (ENZ Technik AG) (see Figure 45)

  The laboratory blade coater (see Figure 45) was run with a 0,4 mm or 0,5 mm blade with a blade pressure of 1,2 to 1,5 bar. Blade type, blade pressure and coating speed was varied to apply the required coat weight. The coating was dried using two IR-drying units and an air drying section.

Figure 45: Laboratory blade coater

Laboratory made paper was cut into two halves and those halves were fixed with adhesive tape on the paper web (see Figure 46).
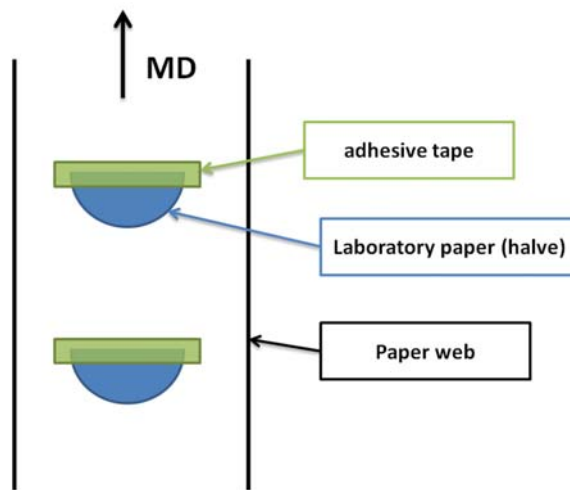
Figure 46: Coating application via laboratory blade coater onto laboratory paper sheets

- SUMET Coating Unit CU5 (see Figure 47)

  The SUMET Coating Unit CU5 was used for single sheet coating. This coating unit is a film press with a coating color pan. Via rod pressure, speed and rod type the coat weight application can be adjusted accurately, compared to the manual rod coater and the laboratory blade coater. Sheets are dried with IR and hot air afterwards.

Figure 47: SUMET Coating Unit CU5

5.2.3 Embedding

Coated paper samples are cut into 25 mm (MD) x 8 mm (CD) strips and infiltrated in a plastic exsiccator with a vacuum pump to remove air from the pores. The vacuum pump was switched on and off in 15 minutes intervals over 4 hours. As infiltration solution Technovit 7100 (Heraus Kulzer GmbH), a cold curing resin based on hydroxyethylmethacrylate, was used. This resin was stained with 0.03 w% Sudan Black (Carl Roth GmbH + Co. KG) to minimize the out-of-focus light especially in fluorescence microscopy. Stirring for 45 minutes with a magnetic stirrer is necessary to get a homogenous solution and dissolve the dye. ,

Infiltrated samples were then embedded in a gelatin capsule (see Figure 48) with a resin mixed of 15 ml Technovit 7100 (stained with Sudan Black) and 1 ml of hardener. After curing overnight samples were polished and are ready for SSFM.

Coating colors containing stained latex were not embedded. Rhodamine B is adsorbed into the latex particle and when adding the embedding resin, the stain gets removed again.
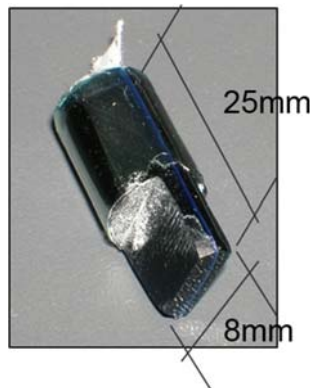
Figure 48: Paper sample embedded with stained resin into a gelatin capsule (after polishing)

5.2.4 Serial Sectioning

5.2.4.1 Embedded samples

Polished samples are first precut with a glass knife (8 mm width) with a slice thickness of 4 μm to obtain a smooth surface and increase durability of the diamond knife. Then they are precut with a diamond knife (Diatome histo cryo 4 mm) with a slice thickness of 4 μm. The settings for the SSFM are fixed. The slice thickness is set to 4 μm and the filter cube is selected regarding the excitation wavelength of the fluorophore. The output of the SSFM is an image stack of 100 images with a distance of 12 μm (see Figure 49).
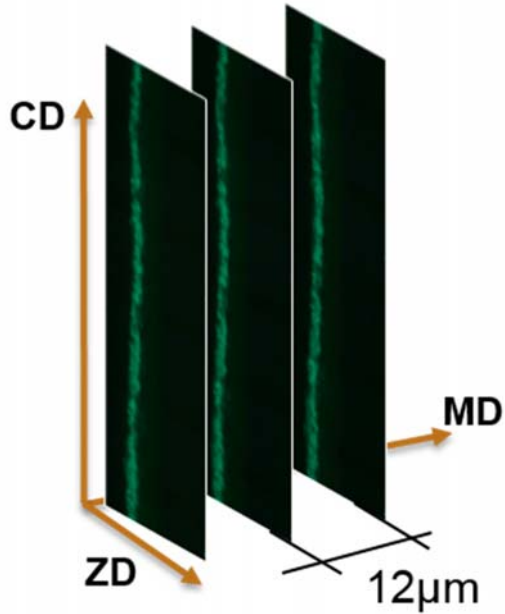
Figure 49: Output of the SSFM

5.2.4.2   Sandwich method

Samples for the sandwich method had a size of 1 cm (CD) x 2 cm (MD). The plastic strip and the paper has not been cut in vertical direction as described in the work of Voura [2008]. The sample holder and the sandwich, consisting of two plastic strips with the sample in between, are illustrated in Figure 50.

Figure 50: Method presented of Voura [2008]

Voura [2008] just analyzed one single cut with a length of up to 2 cm in CD. To be able to analyze a larger area of interest in MD and perform serial sectioning, the plastic strip has been cut horizontally, in this work. The main advantage of this cutting mode is the smoother surface and therefore an observation in three dimensions is possible. This improvement allows a region of interest of 100 µm in MD (20 images and 5 slices of 1 µm for each image). In CD, sample sizes of about 6,5 mm can be

realized compared to maximum 5,5 mm with embedded samples. The samples size in CD with the sandwich method is limited because of fluorescence quenching. After cutting, single images are created which are then stitched and aligned. This process takes some time while the sample is exposed to UV-light. During that time period the sample loses fluorescence intensity. Therefore the sample dimension in CD is limited, because the more single images need to be stitched and aligned the more time is needed. There is also a limitation in MD for the same reason. The sample is exposed to UV-light, over the whole cross-section, penetrating into the sample and this causes fluorescence quenching.

5.2.4.3 Filters

In Chapter 5.2.1 the staining procedure for each binder was described. The fluorescent dyes have different emission spectra and there is the need to use filters. The list of the filters used for each type of binder can be found in Table 7.

Table 7: Filter systems used for different binders and modes

Type	Filter
Coating layer analysis	BF
Starch	GFP
Lignosulfonate	GFP
Latex	GFP/mCherry
Starch/Latex	GFP and GFP/mCherry

5.2.5 Image Processing

The output of the SSFM using the µSTRUCSCOP is an image stack of 100 RGB-images. These images are trimmed with IrfanView to eliminate black borders resulting from the stitching and aligning process. The next step is the segmentation – the transformation from a RGB- to a binary image. ImageJ (free image software: image.nih.gov/ij/) was used for further image processing. Image stacks can be loaded with the "Import" – function.

Segmentation of the image stacks is performed via "Color Threshold" (see Figure 51). Then the window illustrated in Figure 52 is opened. There the algorithm to find the threshold can be selected (highlighted orange in Figure 52). The method of Otsu was indicated to be most feasible for these kind of images. Brightness can be adjusted (highlighted green in Figure 52) to get the best segmentation result. By switching between the selections "Original" and "Filtered" (see blue

highlighted section in Figure 52) the RGB image and binarized image can be compared to evaluate the segmentation result.
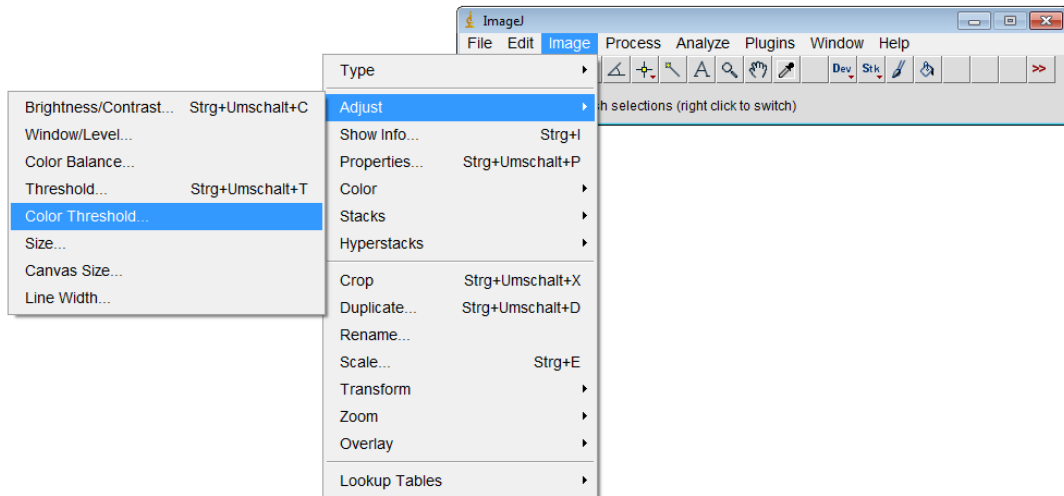
Figure 51: Color Threshold
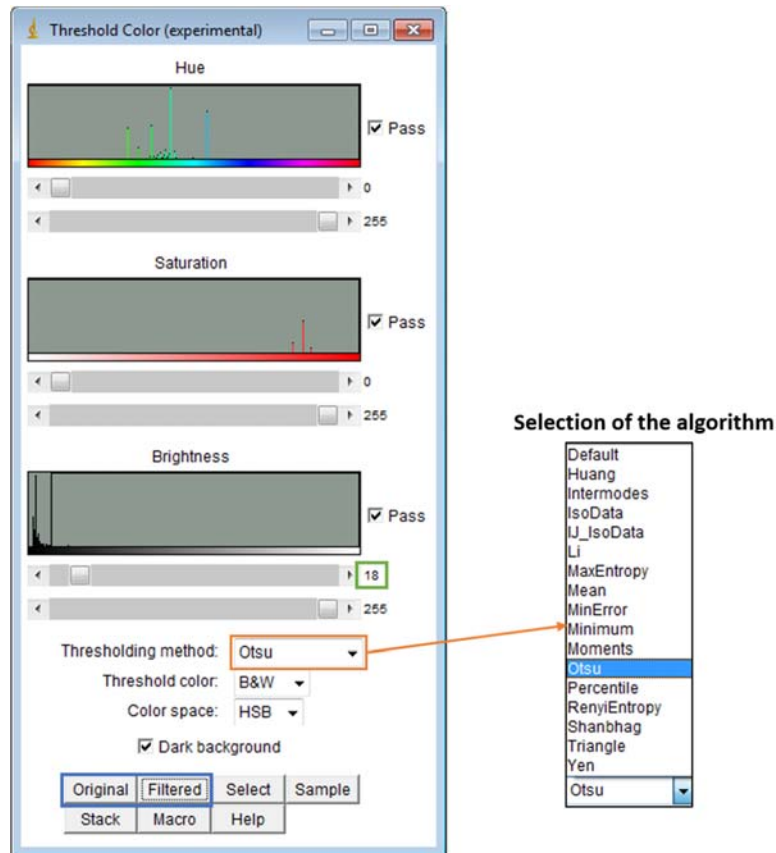
Figure 52: Color threshold – explanation of selections

The whole image stack has to be segmented with the adjusted settings by pressing the button "Stack" (see Figure 52). Images are then saved via "Image Sequence".

The Otsu method iterates thresholds (see Figure 53) and classifies them. Then the foreground (classes 3, 4, 5 in Figure 53) is separated from background (classes 0, 1, 2 in Figure 53).
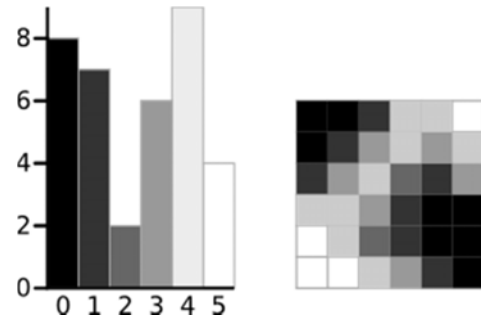
Figure 53: Otsu method for a 6-level greyscale image and histogram [Greensted 2010]

To evaluate the segmentation via the described method above, images were segmented manually to be compared to the automatically binarized images. The manual segmentation is a subjective method.
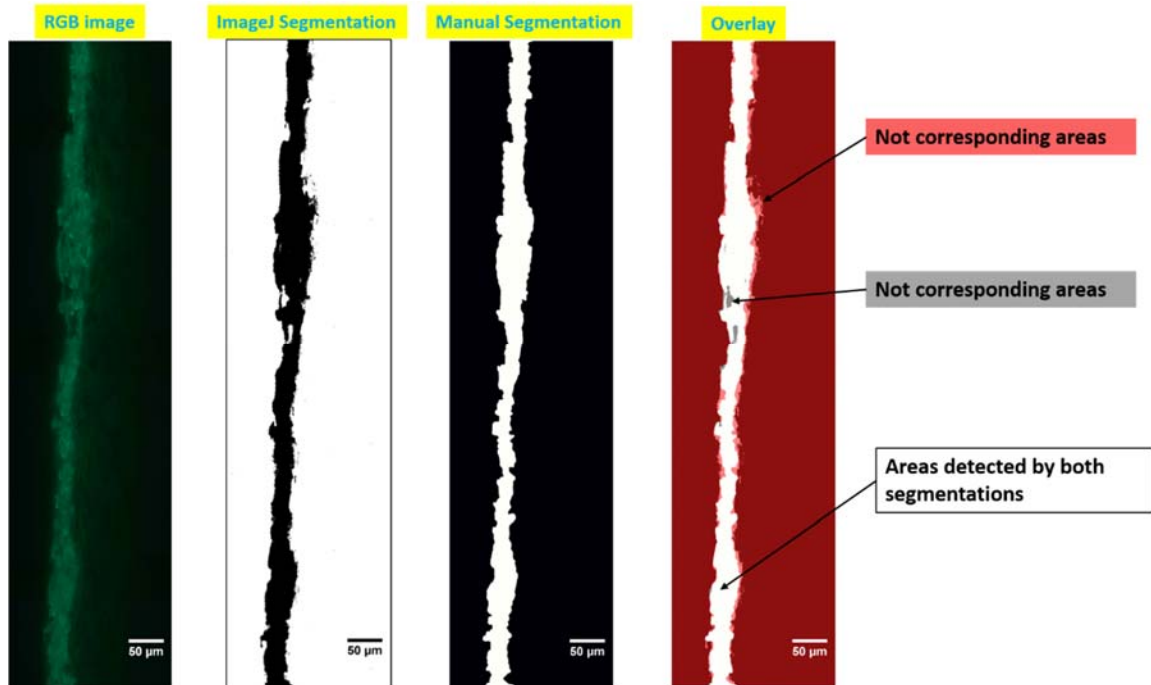
Figure 54: Correlation of ImageJ segmentation and Manual segmentation

In Figure 54, the segmentation results are presented. The first image on the left in Figure 54 is the RGB image. The second image is the binary image segmented by ImageJ as described above. The

third image in Figure 54 shows the manual segmented version. On the right of Figure 54 the overlay of the segmentation is illustrated. The white areas represent the regions detected by both segmentation modes. The light grey and red areas are not corresponding regions. However, the segmentation results correlate well.

5.2.6 3D-Data Calculations

Based on the 3D-data calculations, coating layer properties and penetration behavior of different binders were observed.

5.2.6.1 Coating layer properties

Coating layer thicknesses of all samples, based on the method described by Wiltsche et al. [2012], were determined to control the applied coat weight. Segmentation of the images was developed by Donoser et al. [2006]. Figure 55 on the left shows the cross section image of the coated paper sample (visual light) and the segmentation result in the middle. On the right side of Figure 55, the principle of topography data (τ) and thickness data (t) calculations are shown. Key component is the center line (blue chain dotted line in Figure 55) which is calculated as the curved line between the two borders of both coating layers (see Figure 55 – right image). There different distances from the centerline at defined measuring positions orientated rectangular to the center line can be determined.
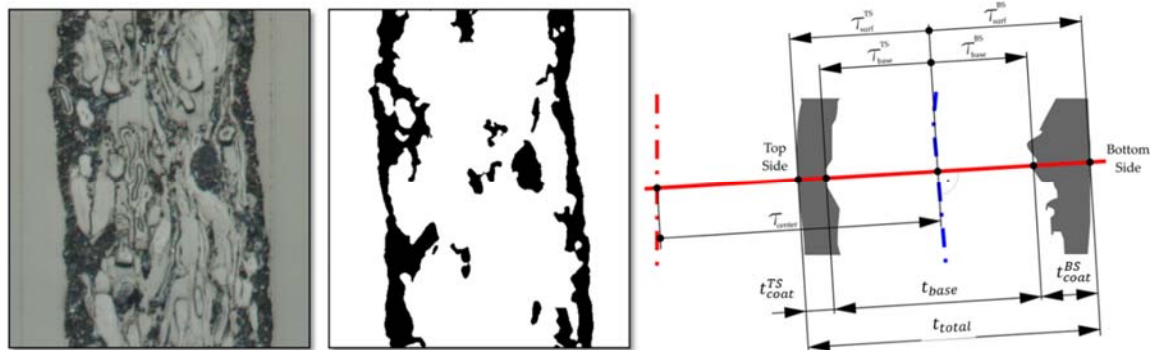
Figure 55: Determination of Coating Layer Properties adapted from [Donoser et al. 2006; Wiltsche et al. 2005]

Regarding this work two values are important for penetration depth calculations of the binder into the base paper: the coating layer thickness (t_{Coat}) and the standard deviation (σ_{Coat}).

5.2.6.2 Penetration behavior of binders

To observe the penetration behavior of binders, the method described in Section 5.2.6.1 was used to calculate the penetration depth of binder into the base paper. Figure 56 schematically shows the calculation of the thickness of the fluorescent layer.

A center line (black chain dotted line in Figure 56) of the fluorescent layer (green area in Figure 56) was calculated. In the case of penetration analysis, the center line in reality is different to this one shown in Figure 56. In general, it is a curved line in the middle of the boarders of the fluorescent layer along the whole cross section.
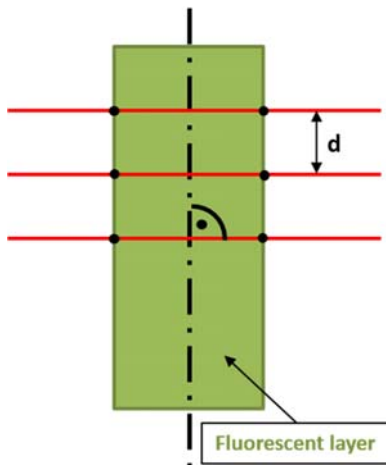
Figure 56: Principle of the thickness calculation of the fluorescent layer

Distances to this centerline at measuring lines (red lines in Figure 56) perpendicular to it were determined and result in a mean thickness value of the segmented fluorescent layer. The distances between the images in MD are listed in Table 8. In the case of embedded samples, 3 cuts with a slice thickness of 4 µm were performed leading to 12 µm of distance between the images in MD. For the sandwich method, the distance between the single images was 5 µm (5 cuts with 1 µm slice thickness). To analyze the same region of interest in MD and CD, the resolution in MD, calculated via MD distance and pixel size, was used as the distance between the measuring lines (d in Figure 56). The resolution in MD is presented in Table 8.

Table 8: Specification of resolution in MD and d

Mode	MD distance [µm]	Pixel Size [µm] (20x magnification)	Resolution MD = d [Pixel]
Embedded	12	0,309	38,83
Sandwich method	5	0,309	16,18

Two cases of binder penetration depth mode can appear – total penetration and partial penetration. The two cases can be distinguished by comparison of the UV-light and the VIS-light image. The

location of the coating layer in the VIS-image and the location of fluorescent binder in the UV-light image need to be determined to decide which case is present.

- Partial penetration: There the binder is localized within the coating layer, but also within the base paper. Therefore, the different layers occurring in the images need to be defined. The fluorescent layer consists of the coating layer (dark red layer in Figure 57) of the VIS-light images and the layer of penetrated binder (light red layer in Figure 57) of the UV-light image. To obtain the penetration depth of binder into the base paper, the mean coating layer thickness (t_{Coat}) (dark red layer in Figure 57) is subtracted from the mean thickness of the fluorescent layer. The result is the mean penetration depth into the base paper (t_{Pen}). In case of depletion of binder at the coating surface, a slight mistake in the calculation of penetration depth into the base paper is made, that needs to be kept in mind.
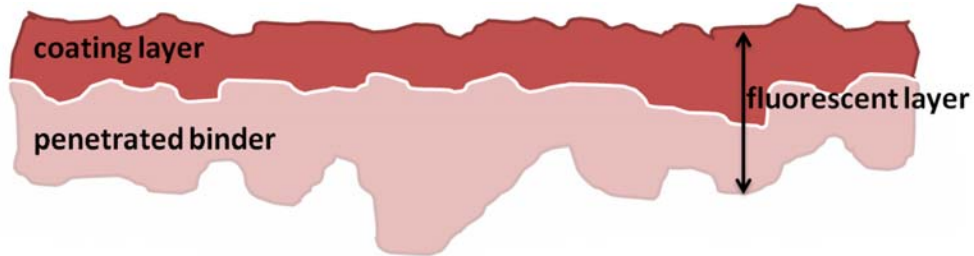
Figure 57: Partial penetration – the different layers

- Total penetration: The binder penetrates totally into the base paper. This means that no binder is remaining within the coating layer (see dark red layer in Figure 58). The calculated mean thickness of the fluorescent layer results in the mean penetration depth of binder into the base paper (t_{Pen}) (see light red layer in Figure 58).
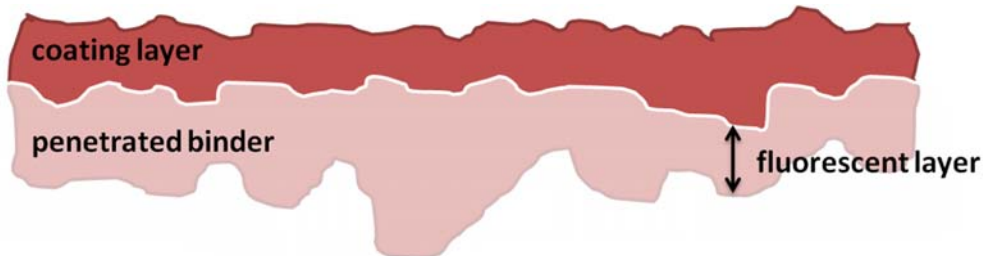
Figure 58: Total penetration – the different layers

The same principle can be applied to determine penetration of optical brightening agents used in coatings.

5.3 EVALUATION OF SSFM WITH CLSM AS REFERENCE METHOD

To evaluate the presented SSFM method, CLSM was performed as reference method. A Leica TCS SPE laser scanning confocal microscope was used.

Samples were not analyzed as proposed in the paper of Ozaki et al. [2006, 2008] or Hirai and Bousfield [2006] in the XZY mode because this method is limited in light penetration depth. Ozaki et al. [2008] applied 22 g/m^2 of coating per side. The stained coating layer thickness calculated by using CLSM in XZY mode were around 10 μm. The limits in light penetration depth may cause this low coating layer thicknesses of the work of Ozaki et al. [2008] compared to the results of Wiltsche et al. [2006] and Vyörykkä et al. [2004]. Wiltsche et al. [2006] applied a coat weight of 12 g/m^2 per side and calculated coating layer thicknesses of 8,4 μm (top side with blade coater). Vyörykkä et al. [2004] calculated 8 μm of a double coated paper with 9 g/m^2 of coating applied. Because of the fact of the limitations in light penetration depth, the cross-sections of the embedded samples were analyzed by CLSM.

Embedded samples were cut with the microtome (diamond knife) and the block was fixed on a glass sample holder with glue. Then the cross section was analyzed with CLSM with a lens of 10 times magnification. As the CLSM method is non-destructive, the same block was then analyzed with SSFM. As the block needed to be precut again to get a smooth surface, not the same region of interest could be analyzed. CLSM creates a pseudo-3D view of the sample, while SSFM leads to a stitched and aligned 3D-image stack. Images of CLSM where 10 times magnified compared to 20 times magnified images of SSFM.
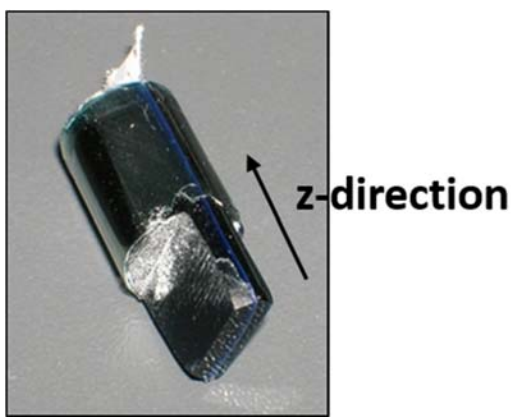
Figure 59: Sample for CLSM and z-direction

The step size in z-direction at the CLSM (see Figure 59) was set to 1 μm. One important issue is the light penetration and therefore, the distance in z-direction (see Figure 59), also called Z-Size, being

analyzed. Z-size varied between 50 and 60 μm depending on the sample analyzed. Four different lasers are available at wavelength of 405, 488, 532 and 635 nm. To control brightness and contrast and to reduce artefacts, two parameters need to be set: the offset (-0,57%) and the gain. The gain of the laser controlling the intensity of light for each sample is presented in Table 9.

Table 9: Gains for CLSM laser

Type	Gain [V]
LS 1	836
LS 2	760
LS 3	911
ST	1069
ST	1128

Table 10: Coating formulation with lignosulfonates as binder

Recipe [%]	LS 1	LS 2	LS 3
CaCO$_3$	100	100	100
Binder LS 1	13		
Binder LS 2		13	
Binder LS 3			13
NaOH	set pH to 8,5	set pH to 8,5	set pH to 8,5
Target solids content	60	60	60

Table 11: Coating formulation with stained starch

Recipe [%]	ST 1	ST 2
CaCO$_3$	100	100
Latex	6	6
Starch	3,75	3,75
Starch stained	0,25	0,25
Thickener		0,1
NaOH	set pH to 8,5	set pH to 8,5
Target solids content	70	60

Coated papers with two different kinds of binders were analyzed: lignosulfonate (LS) and starch (ST). The formulations are listed in Table 10 (LS-coatings) and Table 11 (ST-coatings).

Figure 60 illustrates the images of SSFM (left) and CLSM (right). The same region could not be observed because of necessary precutting of the sample before SSFM. Another issue was the different magnification (SSFM 20 times and CLSM 10 times).
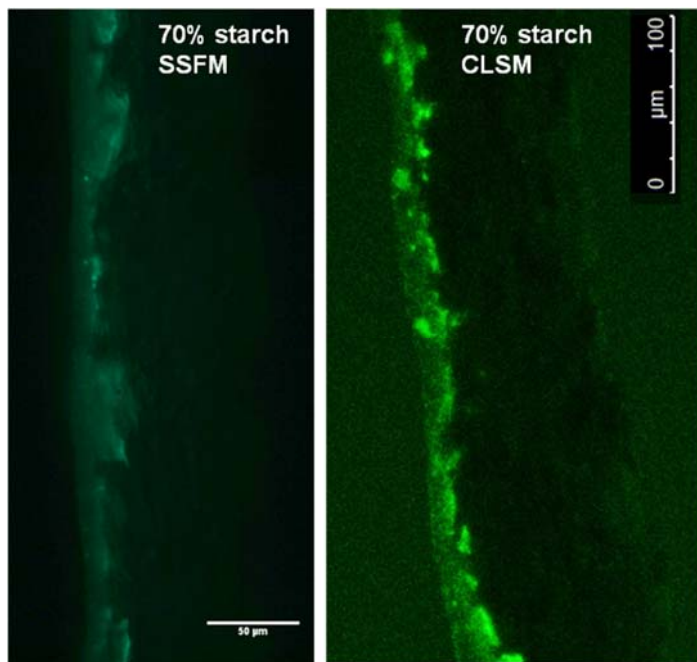
Figure 60: Images of SSFM and CLSM

Areas of higher concentration of starch can be detected at the interface between the coating and the base paper with both methods (see Figure 60). The areas at the coating/base paper interface appear brighter. This effect can be especially observed at 60% solids and there depletion of starch at the coating surface is present.

The images of the CLSM were merged to a pseudo-3D image. The same algorithm to segment the images and to calculate the penetration depth was used as for SSFM. As base paper with a low degree of refining was used, the formation of the sheets was irregular. It was not possible to analyze the same area of interest with both methods because of the need to precut for SSFM to get a smooth surface. Another fact was the fluorescent bleaching effect. The exposure time for SSFM evaluation after the CLSM analysis needed to be higher than before it. The reason for that effect could be bleaching. If the sample is exposed to light the fluorescent light intensity decreases [Lakowicz 2006].

In Figure 61, the correlation of the mean penetration depth of binder into the base paper for the 5 different coatings, determined via SSFM and CLSM, is shown. The CLSM values are a slightly higher than the SSFM values for four of the five formulations presumably, because of the merged pseudo-3D image creation. The coefficient of determination (R^2) of 0,8755 indicates a high correlation between the two methods.
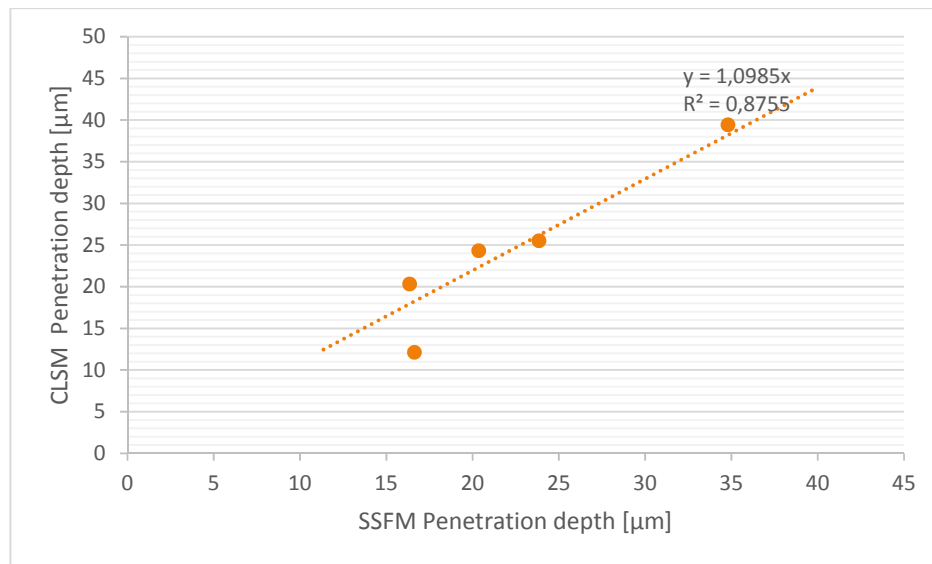
Figure 61: Correlation of SSFM and CLSM

It was attempted to compare the results of binder penetration depth in Figure 61 to values found in the literature. Unfortunately there were hardly any penetration depth presented in the literature. Most of the methods were used to localize the binder, but no penetration depth into the base paper was determined. The use of lignosulfonate binder, however, is not yet presented in the literature. There are different publications regarding latex penetration available, but no concrete penetration depth values into the base paper of starch could be found. The method used for the determination of binder penetration depth into the base paper was CRS. Kugge et al. [2008] and Vyörykkä et al. [2004] presented the difficulties working with starch, because of the similarity in structure of cellulose and starch. Therefore, no penetration depth values for starch are available.

In general, it is difficult to compare the results of SSFM of this work to results from the literature. The reason is the differences in base paper characteristics, in coating formulations and in coating application methods and unknown coat weights.

6 RESULTS AND DISCUSSION

In this chapter, the results of the investigation of different coating binders on binder penetration into the base paper are presented and discussed. The binders are divided into groups of water-soluble and water insoluble binders. Different influences on binder penetration, as described in Chapter 4.3, were investigated.

6.1 WATER – SOLUBLE BINDERS

As described in 2.1, different types of binders exist. In this work two water-soluble binders were tested: starch and lignosulfonate binders. Various effects on binder penetration were investigated, including the degree of polymerization of the binder, the type of the binder and the influence of application, metering and drying on binder penetration.

6.1.1 Influence of the degree of polymerization (DP) of the binder

Lignosulfonate binder was polymerized until different DPs were reached. Coating colors having 60% solids content were applied with the laboratory blade coater (see Table 12). Base paper of eucalyptus pulp, refined with 2000 rpm PFI, was used.

Table 12: Coating formulation with lignosulfonates as binder

Recipe [%]	LS 1	LS 2	LS 3	Ref 1
CaCO$_3$	100	100	100	100
Binder LS 1	13			
Binder LS 2		13		
Binder LS 3			13	
Latex				8
Sterocoll BL				0,18
NaOH	set pH to 8,5	set pH to 8,5	set pH to 8,5	set pH to 8,5
Target solids content	60	60	60	60

In Figure 62 the BF-VIS images (on left for each LS) and the GFP-UV image (on right for each LS) are illustrated. To visualize the binder penetration depth into the base paper the contour of the coating layer of the BF-VIS image was superimposed to the GFP-UV image (white line). The green colored

areas in the GFP images indicate the location of the binder after the coating and drying process. Figure 62 shows the influence of the degree of polymerization on the penetration depth of the binder. LS1 with the lowest degree of polymerization totally penetrated into the base paper with almost no binder remaining in the coating layer to glue the pigments. This fact leads to inacceptable printing results. Ink penetration test could not be performed because of picking off the whole coating layer.
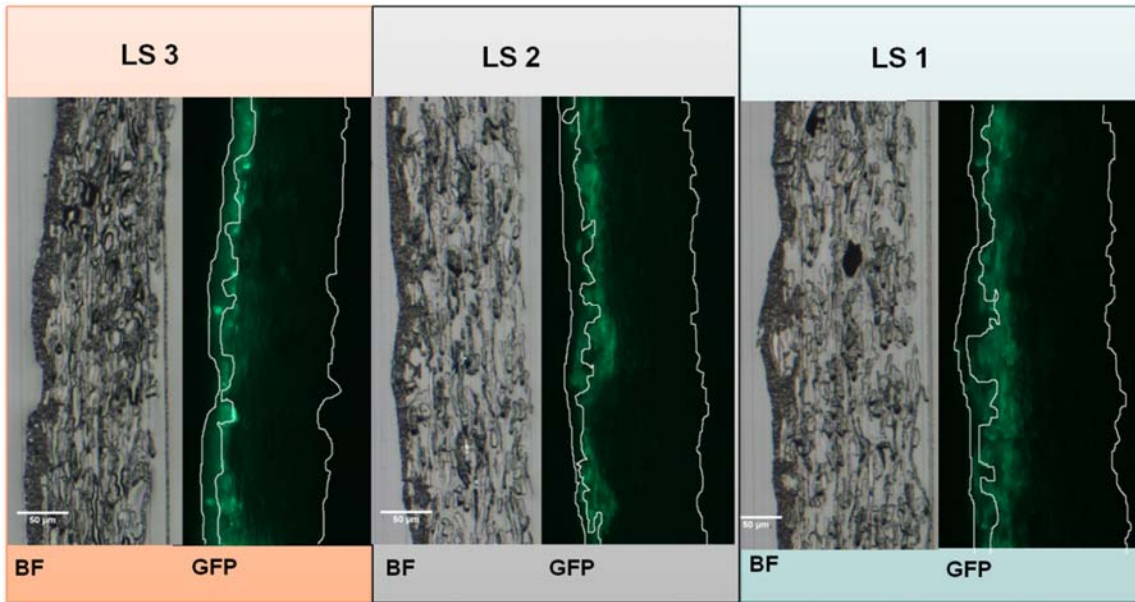
Figure 62: Cross-sections of coated papers (BF – VIS light microscope image, GFP – UV light microscope image) using three different LS – binders

While Figure 62 only shows one part of a single one cross-section, Figure 63 represents the results of the 3D data calculations. With increasing molecular weight the penetration depth of LS-binder into the base paper is decreasing.

Table 13: Coating properties of the LS-coatings

Type	t_{Coat} [µm]	σ_{Coat} [µm]	t_{Pen} [µm]	σ_{Pen} [µm]	BF 20 [mPas]	BF 100 [mPas]	MW of the binder[g/mol]	AA-GWR [g/m²]
LS 1	7,6	5,1	34,8	8,0	9450	2658	5738	1146
LS 2	8,3	5,2	23,9	7,6	10815	2765	43164	871
LS 3	7,1	4,6	16,4	6,5	12690	3215	66170	401

The AA-GWR (Abo Akademi Gravimetric Water Retention) values were determined and they decrease with increasing molecular weight (see Figure 63 and Table 13). The coating layer

thicknesses (t_{Coat}) of the three samples were comparable with values between 7,1 µm and 8,3 µm (see Table 13).
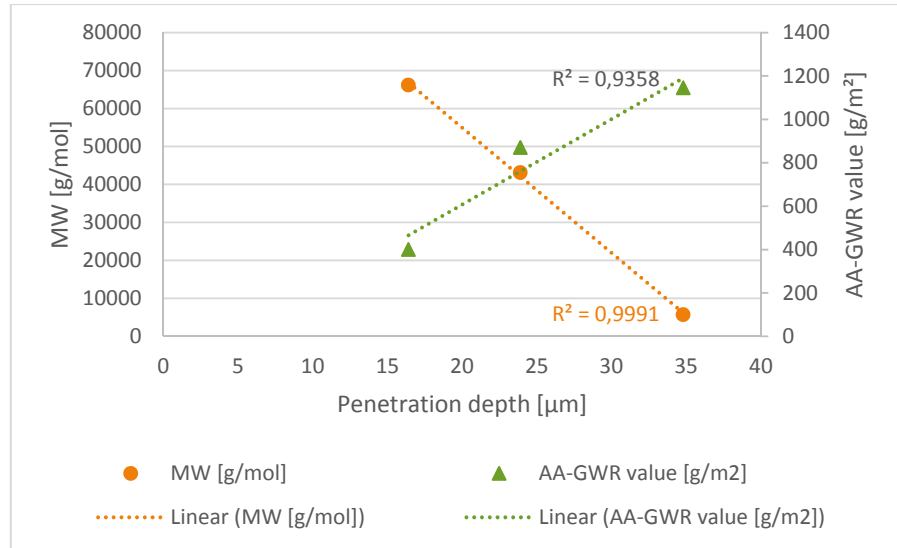
Figure 63: The influence of molecular weight and AA-GWR value on penetration depth
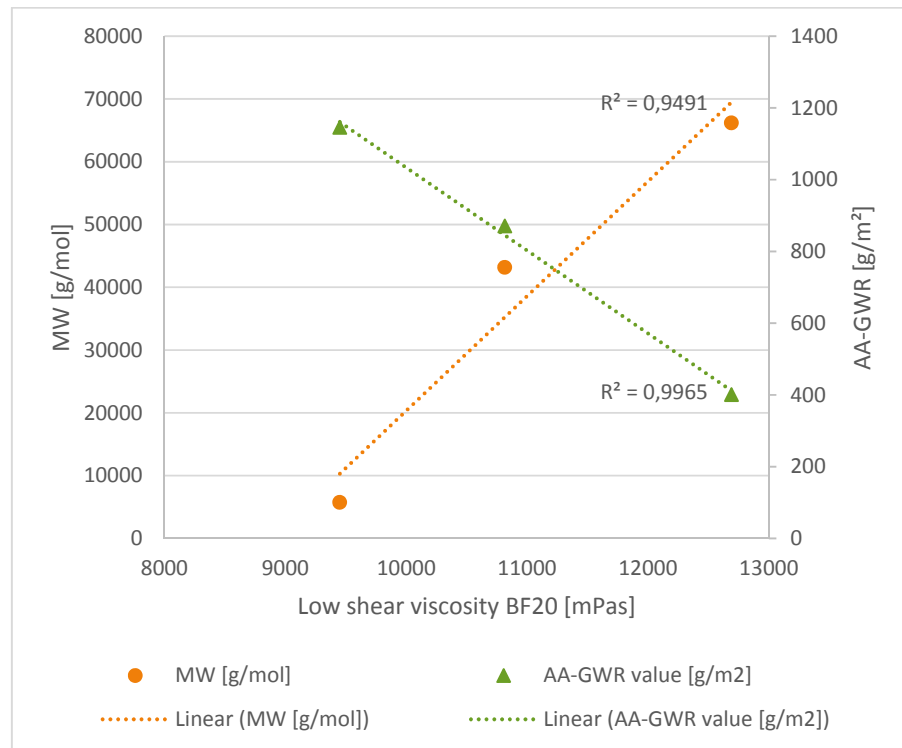
Figure 64: The correlation of MW/AA-GWR value and the low shear viscosity BF20

One observation was the increase in low shear viscosity with increasing molecular weight of the binder and the simultaneous improvement of water retention (see Figure 64). Sandas and Salminen [1991] used different additives to increase the viscosity of the coating color and as a result, the dewatering decreased. Kenttä et al. [2006] and Bitla et al. [2003] reported that the addition of CMC caused an increase in viscosity and lowers binder penetration. Also regarding the lignosulfonate binders the low shear viscosity increased, while the water retention improved and the binder penetration depth decreased.
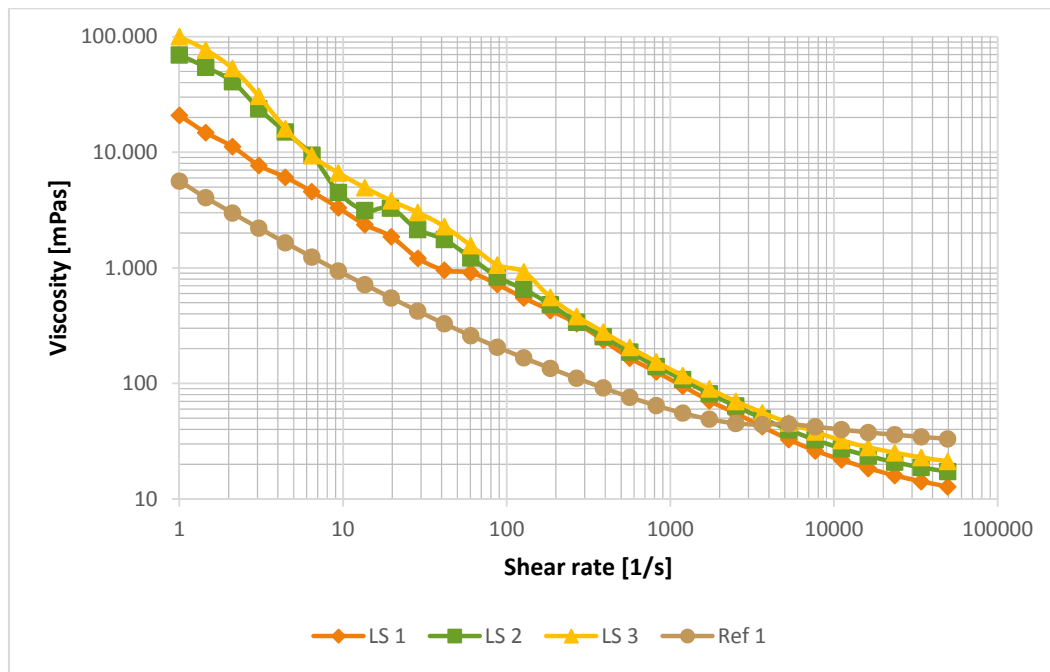
Figure 65: Viscosity over shear rate of the three LS-coatings in comparison with a latex-coating (Ref 1)

As high shear rates are applied in blade coating the coating colors were tested with a Paar Physica rotary rheometer to measure the viscosity under high shear conditions. The results are illustrated in Figure 65 where the three LS-coatings are compared to a latex coating (Ref 1). At higher shear rates the LS-coatings showed a lower viscosity compared to the latex reference. An explanation for this difference could be the use of thickener in latex-coating formulation.

In Figure 66, the correlation of the high shear viscosity at 49.500 rps and penetration depth of LS-binder into the base paper is shown. Lower high shear viscosity leads to increasing penetration depth into the base paper.
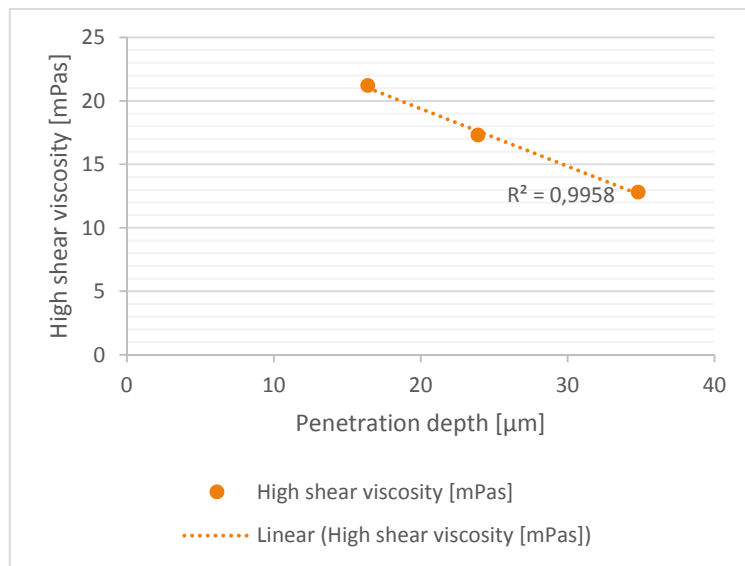
Figure 66: Correlation of high shear viscosity and penetration depth

6.1.2 Influence of the type of binder

The second issue that was investigated was the type of binder. Lignosulfonate-binder (LS) was compared to a conventional starch binder (ST) in coating formulations having 60% solids content (see Table 14). Coating colors were applied with the laboratory blade coater. Base paper of eucalyptus pulp, refined with 2000 rpm PFI, was used.

Table 14: Coating formulations (ST and LS)

Recipe [%]	LS 1	LS 2	LS 3	ST
CaCO$_3$	100	100	100	100
Binder LS 1	13			
Binder LS 2		13		
Binder LS 3			13	
Latex				6
Starch				4
Sterocoll BL				0,1
NaOH	set pH to 8,5	set pH to 8,5	set pH to 8,5	set pH to 8,5
Target solids content	60	60	60	60

The coating layer thicknesses (t_{Coat}) were comparable (see Table 15). Coating color properties and coating layer thickness and penetration depth values are listed in Table 15.

Table 15: Comparison of LS and starch formulations

Type	t_{Coat} [μm]	σ_{Coat} [μm]	t_{Pen} [μm]	σ_{Pen} [μm]	BF 20 [mPas]	BF 100 [mPas]	AA-GWR [g/m²]
LS 1	7,6	5,1	34,8	8,0	9450	2658	1146
LS 2	8,3	5,2	23,9	7,6	10815	2765	871
LS 3	7,1	4,6	16,4	6,5	12690	3215	401
ST	6,8	4,8	24,3	12,5	1425	519	117

The viscosity over shear rate is illustrated in Figure 67. This figure shows the effect of starch coatings having a lower viscosity at low shear and a higher viscosity at high shear rates compared to lignosulfonate coatings. The more pronounced shear thinning effect at high shear rates of LS-coating compared to the ST-coating could again be explained with the addition of thickener.
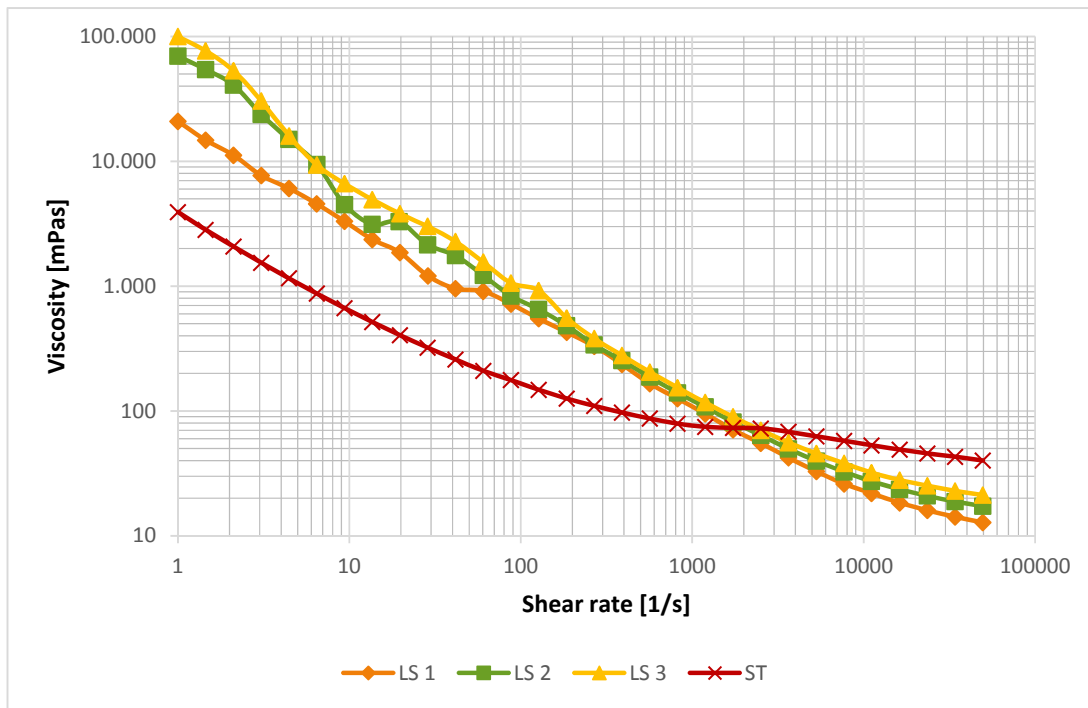
Figure 67: Viscosity over shear rate of the LS 1 and ST formulation

Starch behaves differently compared to lignosulfonates regarding penetration into the base paper (see Figure 68). Starch coatings have a far lower AA-GWR value than lignosulfonate coatings, as can be seen in Figure 68. Although ST-coatings had a higher high shear viscosity and a lower AA-GWR value, binder penetration was relatively high compared to LS-coating. Also Engström et al. [1991]

and Chattopadhyay et al. [2014] observed the effect of promoted starch penetration into the base paper in a formulation with latex-starch mixtures.
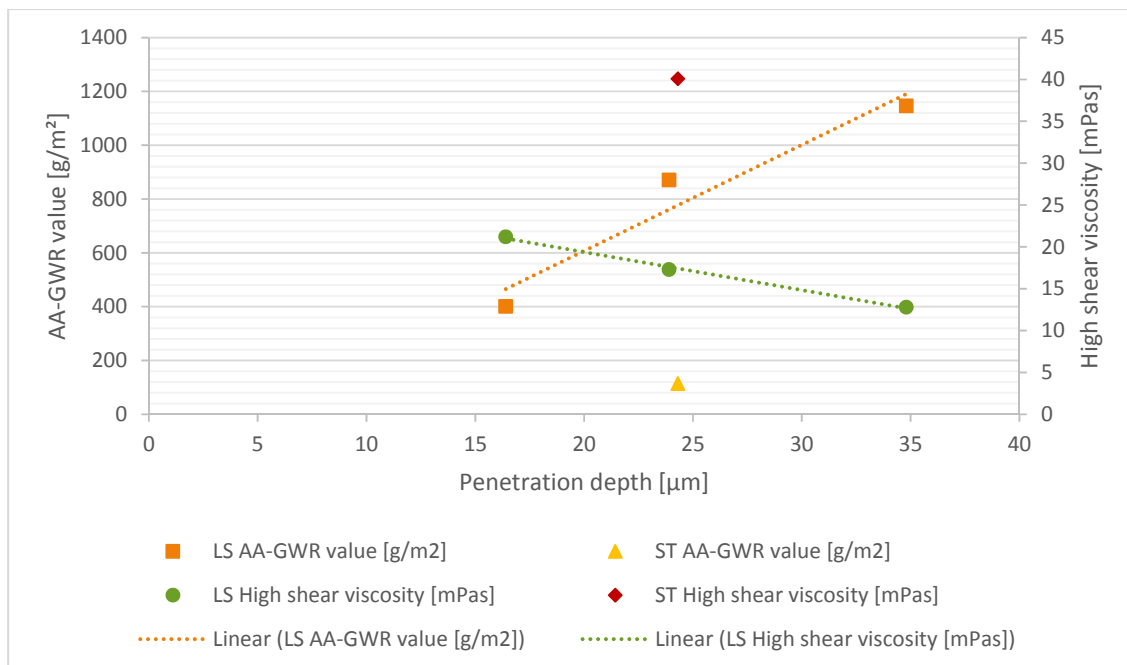
Figure 68: Correlation of AA-GWR values/high shear viscosity and binder penetration depth (LS and ST)
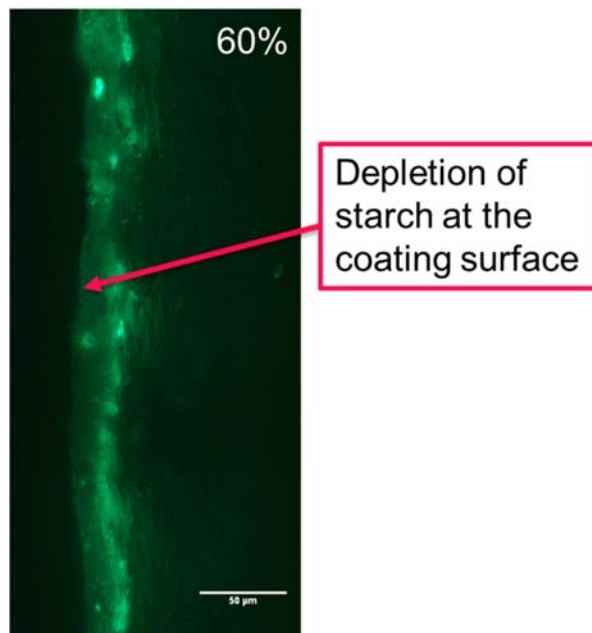
Figure 69: Effect of depletion of starch at the coating surface

One effect observed for ST-coating was the depletion of binder at the coating surface, especially at low solids content of 60% as illustrated in Figure 69. A possible explanation for this depletion of starch at the surface could be the use of a latex-starch mixture (6/4). Chattopadhyay et al. [2014] and Du et al. [2011] saw the same effect when latex was added to a starch coating. Then the amount of starch at the coating surface decreased significantly, compared to a coating applied at the same conditions without latex. Another fact is the low solids content of 60% which causes an increase in penetration as also observed by Clark et al. [1969].

6.1.3 Influence of solids content

The solids content is one major known effect influencing the binder penetration into the base paper. Coating formulations with 70% and 60% solids content were realized (see Table 16). Both the SUMET and the laboratory blade coating unit were used to investigate the influence of solids content. Base paper, made of eucalyptus bleached pulp refined with 2000 rpm PFI, was used.

Table 16: Coating formulations with starch

Recipe [%]	ST 70	ST 60
CaCO$_3$	100	100
Latex	6	6
Starch	4	4
Sterocoll BL	0,1	0,1
NaOH	set pH to 8,5	set pH to 8,5
Target solids content	70	60

Table 17: Coating layer thickness of colors having different solids content

Type	Coater	t$_{Coat}$ [µm]	σ$_{Coat}$ [µm]	t$_{Pen}$ [µm]	σ$_{Pen}$ [µm]	BF 20 [mPas]	BF 100 [mPas]	AA-GWR [g/m²]
ST 70	SUMET	11	5,2	20,1	11,4	4935	1632	95
ST 60	SUMET	8,5	5,1	29,3	15,1	1425	519	117
ST 70	Blade	13,1	5,8	12,1	9,4	4935	1632	95
ST 60	Blade	6,8	4,8	24,3	12,5	1425	519	117

There were difficulties in reaching the same coat weight with 60% and 70% solids (see Table 17). Coating layer thickness with 60% solids content was significantly lower with both coating methods.

Coating color properties and coating layer thickness and penetration depth values are listed in Table 17.
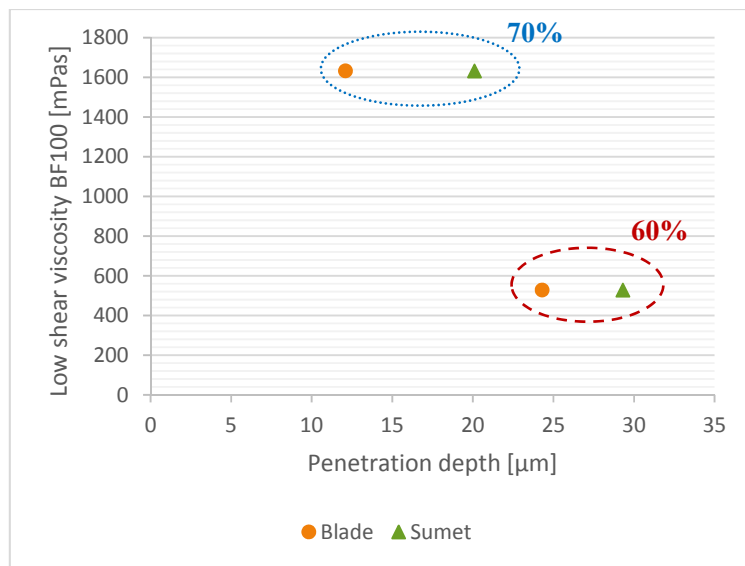
Figure 70: Comparison of penetration depth correlated to BF100 viscosity at different solids contents

In Figure 70, BF100 low shear viscosity over the starch penetration into the base paper is illustrated. Coatings having 60% and 70% solids content are compared. The BF100 viscosity was lower at coatings having 60% solids content and starch penetration into the base paper was higher despite the lower coat weights achieved (see Table 17). Regarding coatings having 60% solids, a depletion of starch at the coating surface was observed.

An interesting fact is the lower starch penetration into the base paper with coatings applied at the laboratory blade coater compared to the SUMET Coater. A possible explanation could be different conditions at the metering element. At the blade coater pressure penetration and at the SUMET Coater capillary penetration seems to be the driving force for binder penetration. Clark et al. [1969] investigated pressure and capillary migration of different types of latex and starch. Pressure penetration did not vary a lot with solids content. But lower solids content led to more capillary penetration both of latex and starch. This could be an explanation for the lower observed penetration depth of blade coatings in comparison to SUMET coatings.

In Figure 71 the distribution curves of the fluorescent layer of the ST-coatings applied with the SUMET and the blade coater are illustrated. Although the coat weights of coatings having 60% solids content were lower, the mean thicknesses of the fluorescent layers were higher. All distribution

curves show a positive skewness. The skewness of the coatings having 60% solids content was higher compared to coatings having 70% solids content.
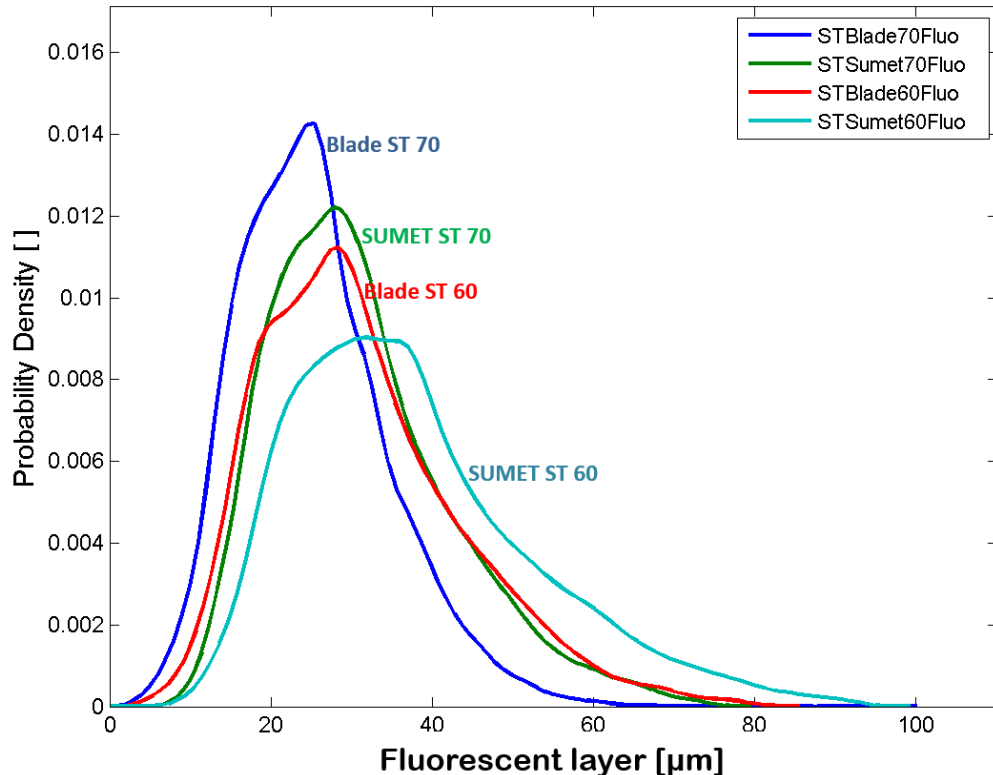
Figure 71: Distribution curves of the starch coatings (SUMET and Blade)

6.1.4 Influence of application, metering and drying method

The influence of drying is more important regarding binder migration towards the coating surface. Kline [1991] observed the influence of different drying mechanisms (hot air, cold air and IR) on binder migration. Zang et al. [2010] and Yamazaki et al. [1993] mentioned the delay time between application and drying as one impact on binder motion. Clark et al. [1991] focused on capillary and pressure penetration, which can be correlated with different application and metering methods.

To investigate the influence of coating application, metering and drying method, the same coating colors were applied using the three available coating units (manual rod coater, blade coater and SUMET Coating Unit CU5). Coating formulations can be found in the chapters above.

Manual rod coated sheets were dried with hot air and the delay time between application and drying was between 15 and 30 seconds. Delay time of SUMET coater is a little bit lower than delay time of the laboratory blade coater, but both are far lower compared to manual rod coater.

Coating layer thicknesses of the colors applied with the manual rod coater were higher compared to blade and SUMET coater (see Table 18). This is caused by the lack of control units at manual rod coater.

Table 18: Coating layer thickness of the different coating colors

Type	Solids content [%]	Coater	t_{Coat} [μm]	σ_{Coat} [μm]	t_{Pen} [μm]	σ_{Pen} [μm]	BF20 [mPas]	BF100 [mPas]	AA-GWR [g/m²]
LS 1	60	Manual	14,2	6,6	36,4	8,6	9450	2658	1146
LS 1	60	Blade	7,6	5,1	34,8	8,0	9450	2658	1146
LS 1	60	SUMET	7,6	5,6	22,0	7,4	9450	2658	1146
LS 3	60	Manual	9,9	5,7	22,7	7,1	12690	3215	401
LS 3	60	Blade	7,1	4,6	16,4	6,5	12690	3215	401
LS 3	60	SUMET	7,4	5,5	21,2	8,5	12690	3215	401
ST 70	70	Manual	11,9	6,1	16,9	10,2	4935	1632	93,7
ST 70	70	Blade	13,1	5,8	12,1	9,4	4935	1632	93,7
ST 70	70	SUMET	11	5,2	20,1	11,4	4935	1632	93,7
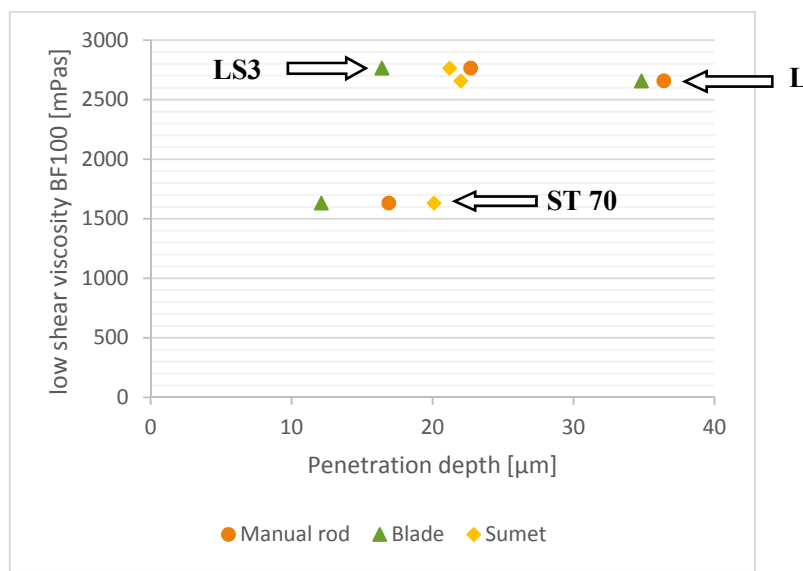
Figure 72: Penetration depth of coatings applied with three coating units

The results of penetration depth analysis are illustrated in Figure 72. Regarding lignosulfonate-binder the manual rod coated samples showed the highest penetration depths into the base paper. This could

be the effect of higher coat weights applied with manual rod coater and the high delay time between application and drying.

Regarding starch-binder, the SUMET coated samples showed the highest penetration values, which was not expected. These findings contradict to the work of Dappen [1951] showing differences in starch concentration at the coating and fiber interface. The longer the time period for coating fixation, the deeper the binder penetrates into the base paper.

Blade coatings (LS and ST) showed a lower penetration depth into the base paper (see Figure 72) than manual rod coatings. SUMET coating penetration depths were independent from the type of binder. All coatings had relative high viscosities which are not usual for SUMET coating application. The coating layers were uneven and showed stripes resulting from the rod, which probably also influence the coating and fluorescent layer analysis.

Although the ST-coatings had a solids content of 70% the coating penetration depth was relative high compared to LS-coatings with higher AA-GWR values. Yamazaki et al. [1993] observed the affinity of starch to penetrate into the base paper. With longer delay times starch penetration increased even more compared to latex [Yamazaki et al. 1993].

6.2   CONCLUSIONS OF THE INVESTIGATION OF WATER-SOLUBLE BINDERS

Four influences on penetration behavior of water-soluble binders were investigated. Results showed that binder penetration is decreasing with higher molecular weight of a lignosulfonate binder. Furthermore, the comparison of lignosulfonate and starch showed, that starch coatings having a lower AA-GWR value, show less starch penetration into the base paper than lignosulfonate based coatings. One interesting effect of lignosulfonate coatings were the increase of high shear viscosity with decreasing AA-GWR values.

Coating formulations having a lower solids content showed increased binder penetration compared to high solids coatings.

The comparison of the penetration results of the different coating units was difficult. Manual rod coater was hard to handle in adjusting the coat weight. The coat weights and the penetration depths were higher compared to SUMET and blade coater. The comparison of SUMET and blade coater led to interesting results. Blade coated paper samples showed less binder penetration into the base paper than SUMET coated paper samples. This may be an effect in difference of capillary and pressure penetration.

6.3   WATER – INSOLUBLE BINDERS

Water-insoluble binders are most common in coating application. SB-latices, varying in their T_g, are used in pre- and top-coatings of different paper grades. Three different coating colors were realized (see Table 21). The idea was to test two different amounts of latex (8 pph, 16 pph) and a starch-latex coating. In chapter 6.3.1 the focus is on the influence of base paper. In chapter 6.5 the different coatings are discussed in detail and the influence of the binder composition and the amount of binder on penetration into the base paper is observed.
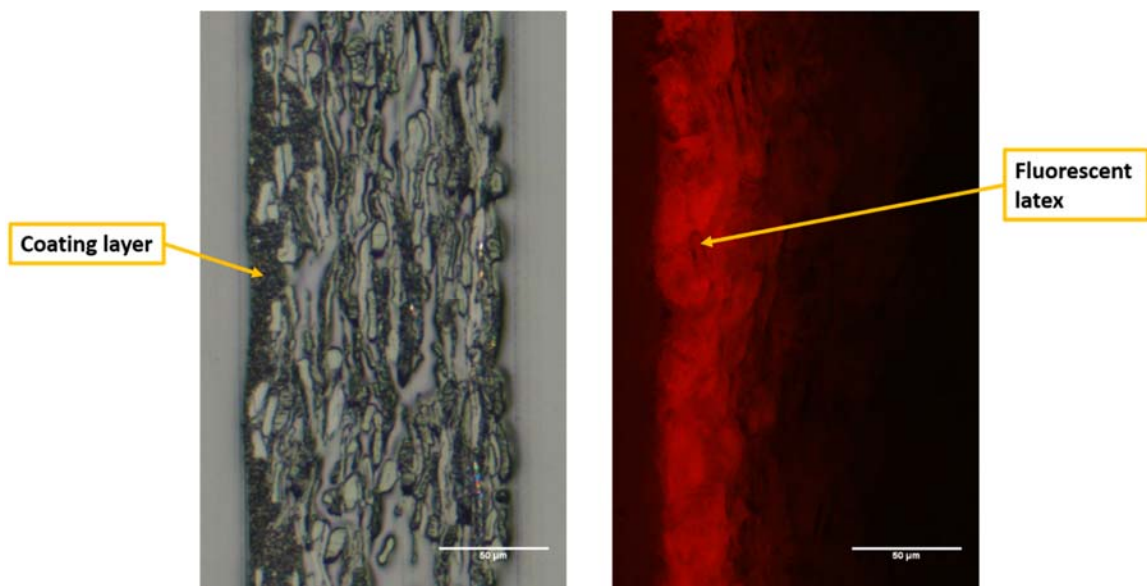
Figure 73: Coated paper with VIS (left) and fluorescent coating layer with stained latex (right)

The determination of the thickness of the fluorescent layer was performed by the sandwich method of SSFM. The fluorescent layer containing the stained latex is illustrated in Figure 73 (right image). Embedding of the samples containing stained latex was not possible because the resin removed the dye from the latex film. Image quality of the sandwich method is not as good as it is cutting embedded samples. The cutting method does not lead to such low surface roughness as it does when sectioning embedded samples. Therefore, objects of the images are not as sharp. However, the quality is sufficient for performing the segmentation and the 3D-data evaluation. The coating layer thickness was analyzed by the presented method of Wiltsche et al. [2011] based on the VIS images illustrated in Figure 73 (left image). Samples were embedded previous to sectioning for the determination of the mean coating layer thickness.

6.3.1 Influence of base paper

Previous works name the influence of the substrate the coating is applied to as the key factor regarding motion of the binder [Huang and Lepoutre 1998; Clark et al. 1969; Al-Turaif and Bousfield 2005; Engström et al. 1991].

For the investigation of the base paper influence on binder penetration four different base papers (see Table 19) were tested. Base paper A and B differed in degree of refining. Filler was added to base paper C. Base Paper D is calendered to modify the pore structure and the roughness.

The coatings were applied with SUMET Coating Unit CU5. The reason for choosing the SUMET Coating Unit was the single sheet mode and the possibility to adjust the coat weight. The coat weight of each single sheet was determined immediately after coating to realize the same coat weight for all types of formulations.

Table 19: Specification of base paper for coating trials

Base paper type	Pulp	Refining	Additive
A	Eucalyptus bleached	2000 PFI	-
B	Eucalyptus bleached	6000 PFI	-
C	Eucalyptus bleached	2000 PFI	20% filler ($CaCO_3$) + Retention agent (Percol 8383)
D	Eucalyptus bleached	2000 PFI	Calendering – once each side per sheet (2000daN, room temperature)

The basic paper properties of the four different base papers are shown in Table 20.

Table 20: Paper properties of base paper A, B, C and D

Base paper type	Schopper Riegler [°SR]	Basis weight [g/m^2]	Thickness [µm]	Air permeability [ml/min]
A	27,4	81,4	117,72	1176,2
B	49,1	82,1	105,96	103,6
C		83,1	119,44	1637,8
D		81,7	90,24	443

6.3.1.1 Influence of fillers

Fillers modify the paper structure and pore system of a paper sheet. Therefore, base paper A was compared to base paper C regarding latex penetration into the base paper. Figure 74 shows the latex penetration depth into the two different types of base paper over the coat weight. The target was to apply the same amount of coating on the different base papers. All coatings showed a significant lower latex penetration depth when coated on base paper C.
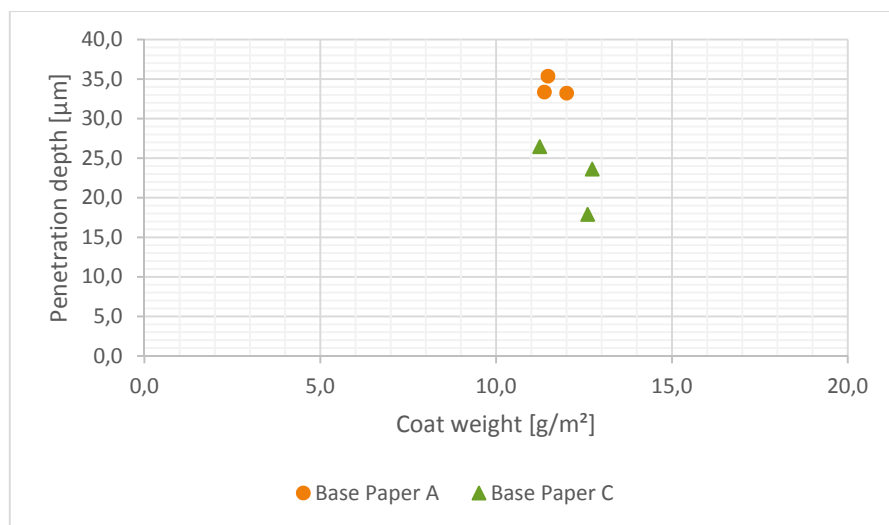
Figure 74: The influence of fillers in the base paper on latex penetration
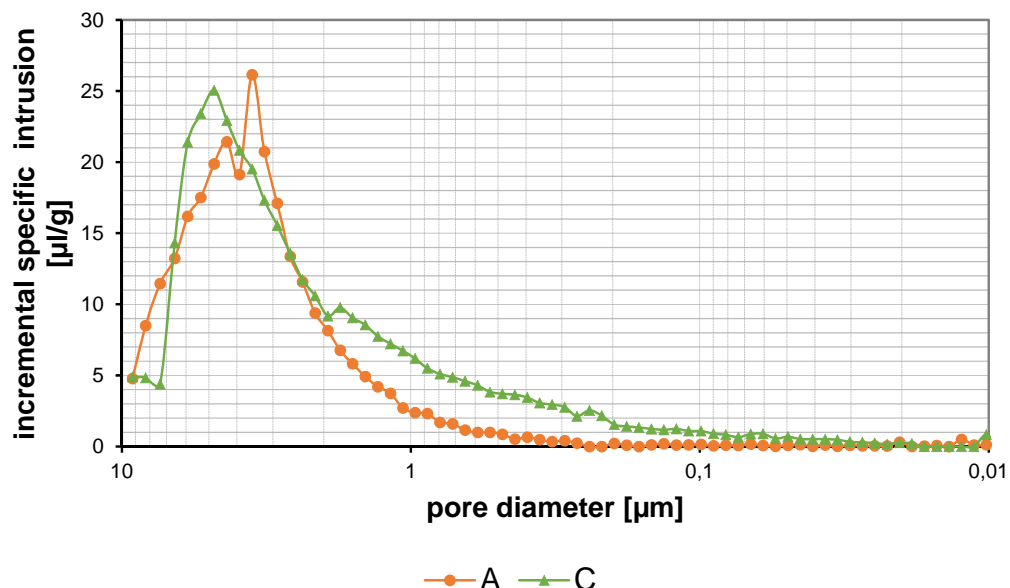
Figure 75: mercury porosimetry of base paper A and C

As filler, CaCO$_3$ (60% > 2 μm) was used. Air permeability of base paper C was higher than that of base paper A (see Table 20). This may be caused by fillers disturbing the bonding of fibers and leading to lower amount of bonded areas. This theory contradicts with the lower latex penetration values into base paper C. Therefore, mercury porosimetry to compare the pore structure of base paper A and C was performed. In Figure 75, the incremental specific intrusion over pore diameter is illustrated. Base paper C shows more large pores but a significantly higher amount of smaller pores than base paper A. Mercury porosimetry determines the pore structure of the whole paper sheet and does not distinguish between surface and structure pores.

6.3.1.2   Influence of refining

To investigate the influence on refining, the bleached eucalyptus pulp was refined once with 2000 rpm PFI (base paper A) and once with 6000 rpm PFI (base paper B). Schopper Riegler of base paper A was 27,4 compared to 49,1 of base paper B. The higher degree of refining caused a mean decrease of sheet thickness of 10% and air permeability was 91% lower.

Figure 76 shows the latex penetration depth into the two different base paper grades. The latex penetration into base paper B was lower compared to base paper A. The difference was expected to be higher because of the large differences in air permeability.
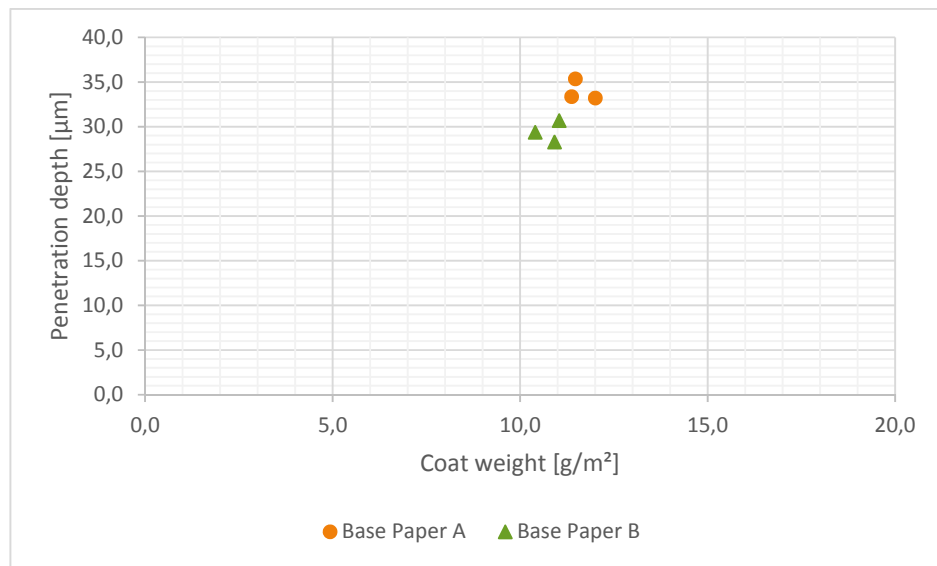
Figure 76: The influence of the degree of refining on latex penetration

Mercury porosimetry was performed to get more information about the pore structure of the paper sheets in comparison. In Figure 77, the resulting pore size distributions are shown. The pores of base

paper B are smaller compared to those of base paper A. So, the latex penetration depth decreased, less than expected, with higher amount of smaller pores (see Figure 76 and Figure 77).
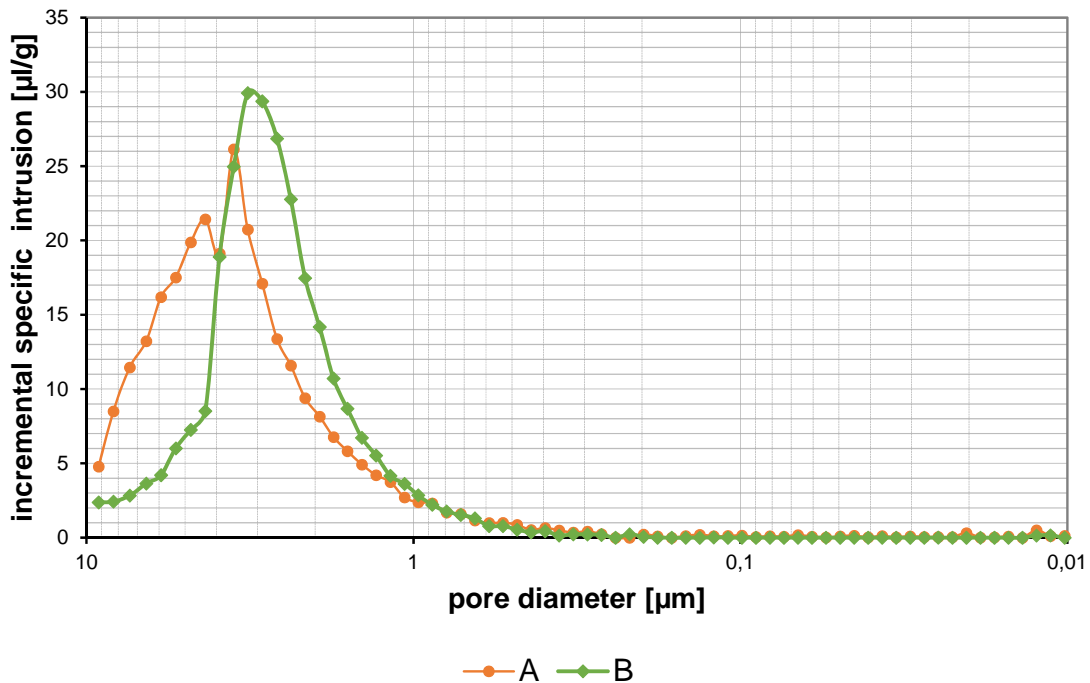
Figure 77: Mercury porosimetry of base paper A and B

In the Lucas-Washburn equation the capillary penetration of a fluid without external pressure is discussed. As pore radii and penetration lengths are direct proportional, the larger the pores are, the deeper the fluid would penetrate into the substrate. Therefore, a bigger difference of penetration into base paper A compared to B was expected. In contrast to that, Schölkopf et al. [2010] found out that a fluid flow is accelerated in small pores in contrast to large pores, based on the Bosanquet equation. Probably a combination of both theories are present in this case and therefore, the small difference of penetration into the base paper A compared to B appears.

6.3.1.3 Influence of calendering

The influence of calendering the sheets previous to coating application was investigated. Therefore, base paper of type A was calendered once at each side with 2000 daN at room temperature. Calendered sheets are named base paper D. The calendering caused a decrease in sheet thickness of 23% and air permeability of 62%.
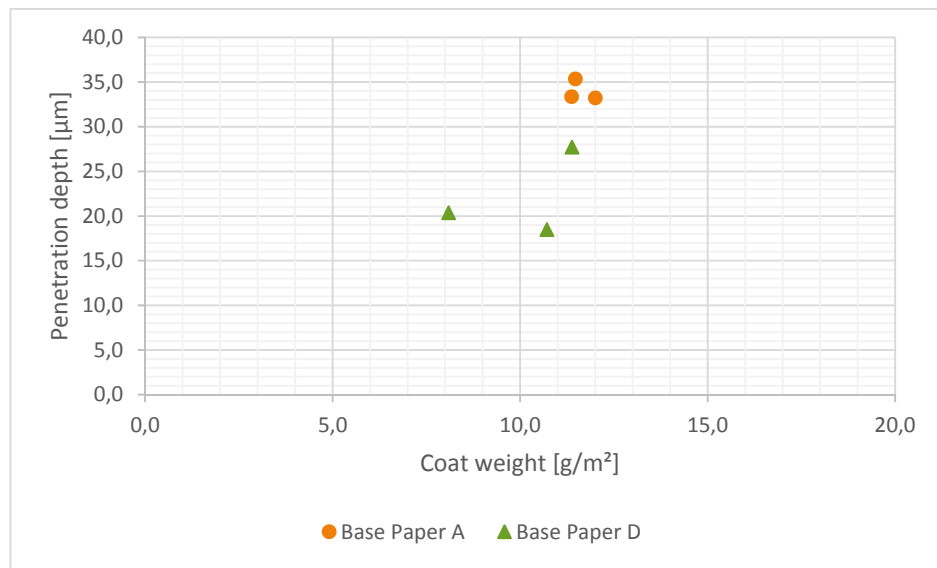
Figure 78: The influence of the calendering on latex penetration
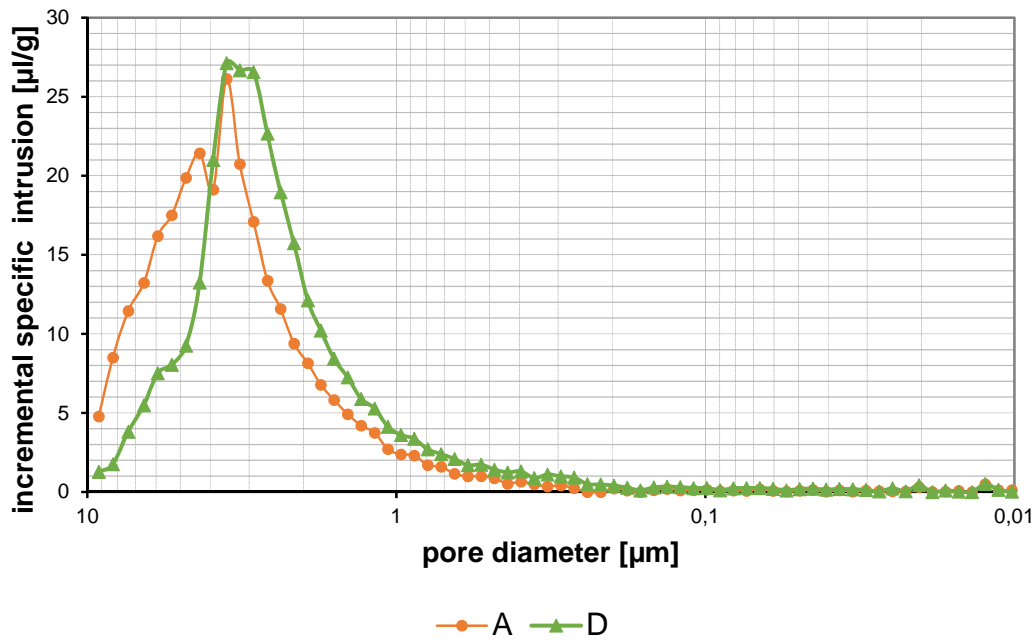
Figure 79: Mercury porosimetry of base paper A and D

In Figure 78, the latex penetration depth into both types of base papers are shown. Penetration values for base paper D were significantly lower, as expected. Mercury porosimetry shows smaller pores of base paper D compared to base paper A (see Figure 79). Smaller pores lead to a lower latex penetration into the base paper. Huang and Lepoutre [1998] saw the same effect. They observed the coating hold-out properties of a dense and a porous sheet. The dense sheet had a mean pore size of

87

2,1 µm and the porous sheet of 6,2 µm, determined by mercury porosimetry. The coating pick up of the porous sheets was 1 g/m^2 higher, compared to dense sheets. The effect of the higher amount of pores and as a consequence the higher surface roughness overwhelmed effects of surface chemistry, like sizing. Also Al-Turaif and Bousfield [2005] saw a difference in location of latex, when applying the coating on a porous and a non-porous substrate. Latex followed the water phase into the substrate [Al-Turaif and Bousfield, 2005].

6.3.2   Influence of coating color formulation on binder penetration

In the literature, the influences of coating formulation were investigated. Al-Turaif and Bousfield [2005] and Bitla et al. [2003] observed the binder motion varying the level of binder used. Ström et al. [2010] focused on measuring the pore volume at different latex levels in coating colors. Furthermore, the behavior of binder was investigated in coatings consisting of mixtures of latex and starch [Du et al. 2011, Chattopadhyay et al. 2014, Engström et al. 1991 and Yamazaki et al. 1993].

To investigate the influence of coating formulation and additives on binder penetration, three different coating colors, listed in Table 21, were prepared. In this chapter coating I and II are compared having different binder levels. Coating III was realized to test the behavior of a coating color regarding latex penetration, when starch is present beside latex as binder.

Table 21: Coating formulations with stained latex

Recipe [%]	I	II	III
CaCO$_3$	100	100	100
Latex stained	8	16	6
Starch			4
NaOH	set pH to 8,5	set pH to 8,5	set pH to 8,5
Target solids content	65	65	65

The measured properties of the prepared coating colors are shown in Table 22. Brookfield viscosity of coating I was significant lower than those of coating II and III.

Table 22: Specification of the stained latex formulations

Type	Binder	Solids content [%]	AA-GWR [g/m²]	BF 20 [mPas]	BF 100 [mPas]
I	8 pph latex	65	394,4	300	172
II	16 pph latex	64,9	302	1500	590
III	6 pph latex/4 pph starch	65,2	144,8	1490	600
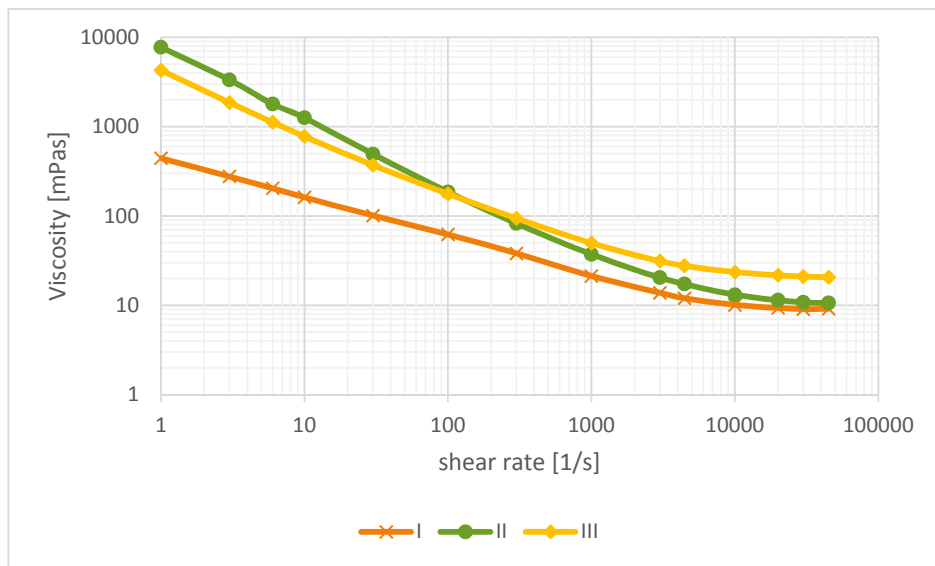
Figure 80: Rheology of the coatings

Table 23: Solids contents before and after coating

Type	Solids content before coating [%]	Solids content after coating [%]	Increase solid content [%]	AA-GWR [g/m²]
I	65	68,95	3,95	394,4
II	64,9	67,91	3,01	302
III	65,2	67,85	2,65	144,8

Water retention values (see Table 22) was lowered with the addition of starch to the coating formulation. This effect was observed by Bartell [1976], Kenttä et al. [2006], Bitla et al. [2003], Bushhouse [1992] and Sandas and Salminen [1991]. In Figure 80, the rheograms of the coatings are illustrated. Coating I has the lowest low and high shear viscosity. Coating II has a higher low shear

viscosity than Coating I, but the high shear viscosities are almost the same. Color III shows the highest high shear viscosity.

Solids content of the coating colors were determined before and after the coating process. The solids content after coating process was measured by analyzing the remaining coating in the pan. Table 23 shows a correlation of the increase in solids content and the AA-GWR values.

6.3.2.1   Influence of binder level

To investigate the influence of binder level on penetration behavior, color I and II containing 8pph and 16pph of latex were compared regarding latex penetration depth into the base paper. The results are shown in Figure 81. Just coatings on two base papers (C and D) showed a difference in latex penetration.
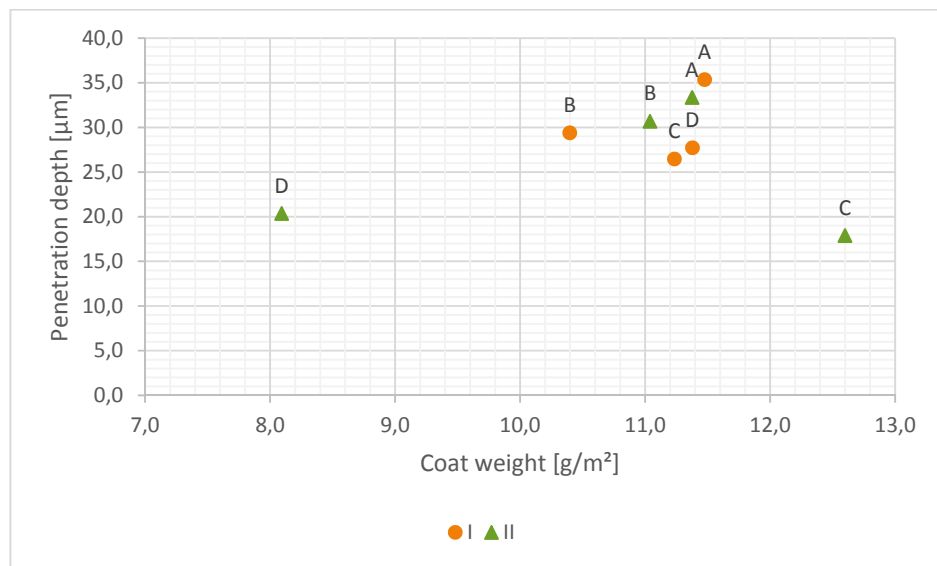
Figure 81: Latex penetration of coating I and II

The formulation with 16pph of latex showed a higher low shear viscosity (see Figure 82). The shear rates at the SUMET Coater are rather low and in case of coating II the penetration depth was expected to be lower compared to coating I, because of the far higher low shear viscosity. On the other hand the penetration of latex may be higher, when more latex is present in a coating formulation.

Al-Turaif and Bousfield [2005] focused on latex migration towards the surface and did find a higher latex content, when more latex was present in the formulation. In contrast to that Bitla et al. [2003] did not find an influence of level of binder on latex movement.
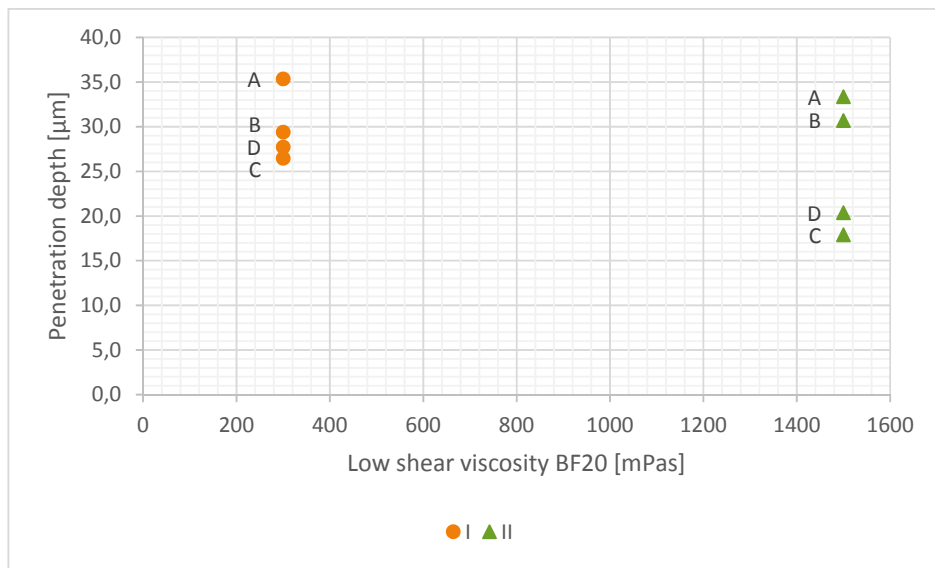
Figure 82: Latex penetration of coating I and II correlated to low shear viscosity

6.3.2.2 Behavior of starch-latex mixtures

Latex penetration into the base paper was investigated by comparing coating I and III. Those two coatings contain the same ingredients but in coating III two parts of latex were substituted with four parts of starch.
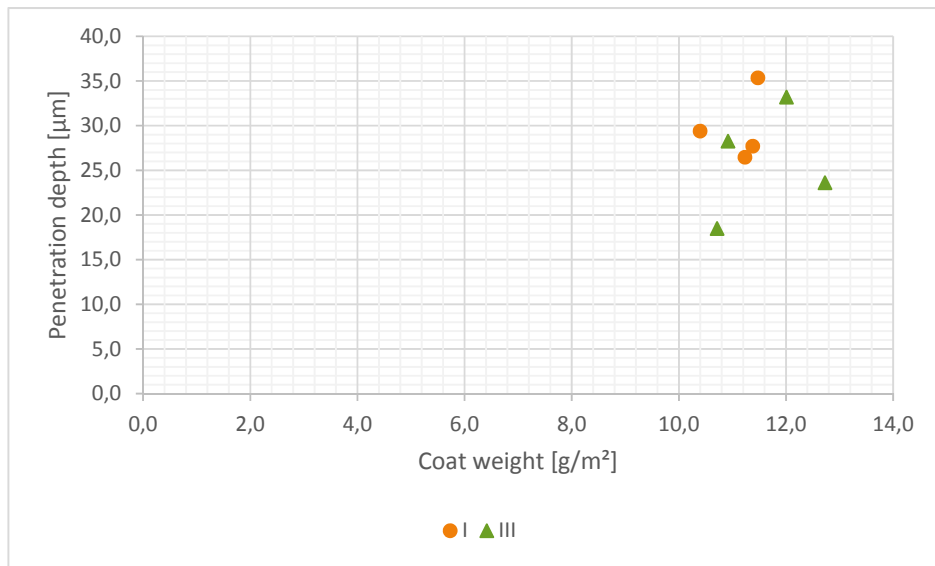
Figure 83: Latex penetration of coating I and III

The results of the latex penetration are shown in Figure 83. The differences between the two colors were not significant. Again base paper C and D showed a lower latex penetration depth in starch-

latex coating compared to coating I. Starch lowers the AA-GWR value as reported by Sandas and Salminen [1991]. This effect can be observed in Figure 84. The coating III shows a far lower AA-GWR value. Therefore, the penetration of latex was expected to be lower in presence of starch, because the latex tends to follow the water phase into the base paper. When the water retention of the coating is getting better with the addition of starch, the penetration of latex into the base paper was expected to decrease. But the latex penetration did not decrease significantly, as can be seen in Figure 84. Chattopadhyay et al. [2014] observed the behavior latex and starch motion, when using coatings with both binders. They found out that latex forms a barrier on the surface and starch cannot move towards the surface. Starch and also some latex was moving into the base paper during coating application [Chattopadhyay et al. 2014]. This could be a reason, why the penetration of latex of coating III did not decrease, although the water retention was better.

Figure 84: AA-GWR values correlated with latex penetration depth of coating I and III

6.4 Conclusions of the investigation of water-insoluble binders

The results of the study show a significant influence of the base paper on latex penetration. Porous structure of the paper sheets is the key factor to control binder penetration.

Figure 85 shows a comparison of all tested base papers in comparison. In conclusion, the use of fillers (base paper C) and calendering (base paper D) show lower latex penetration depths compared to the reference (base paper A). An increase of the degree of refining (base paper B) does not lower the latex penetration significantly.
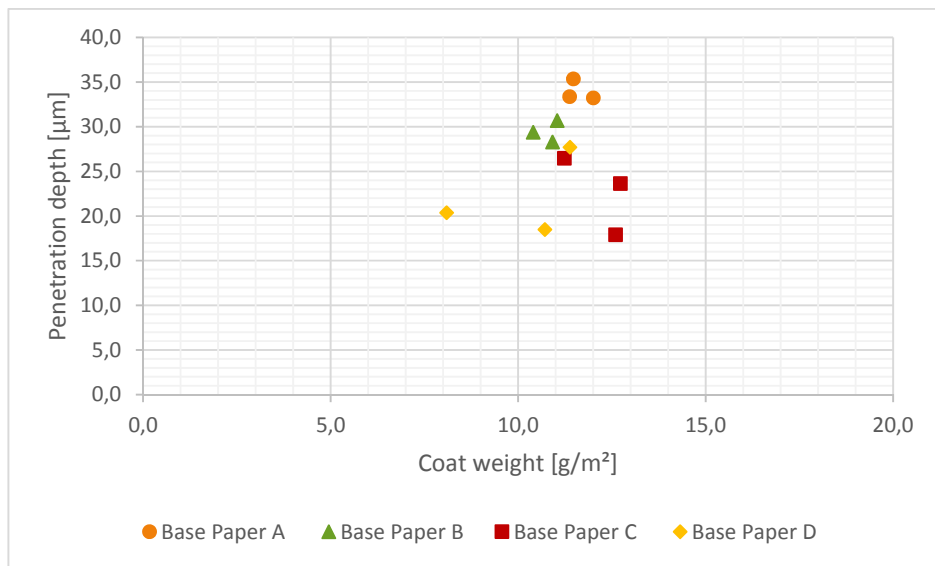
Figure 85: Comparison of the tested base papers regarding latex penetration depth
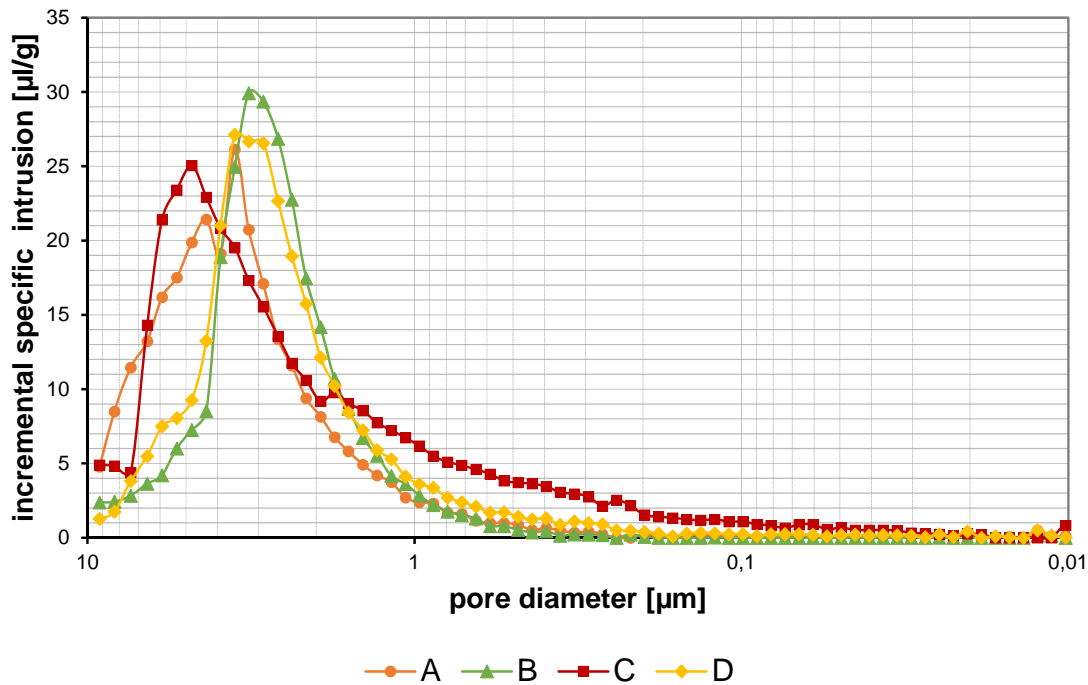
Figure 86: Mercury porosimetry of the different base papers

Figure 86 shows the pore size distribution of the different base paper grades. In Figure 87, pore sizes were classified into 5 classes. The idea was to compare the penetration behavior at different pore sizes of the four base papers.

Base paper A has the largest pore structure and therefore latex penetration is high. Base paper B and D are similar regarding pore structure. Figure 87 shows a higher amount of smaller pores in sheet structure regarding base paper D compared to base paper B. This correlates to the observations of latex penetration, which is lower at base paper D. Base Paper C has the highest amount of small pores. There seems to be a correlation of pore size and penetration depth as described by Lucas-Washburn equation. As mercury porosimetry just determines the pore structure of the whole paper sheet, there probably are differences in surface and structure pores regarding base paper C, explaining the lower penetration depth values.
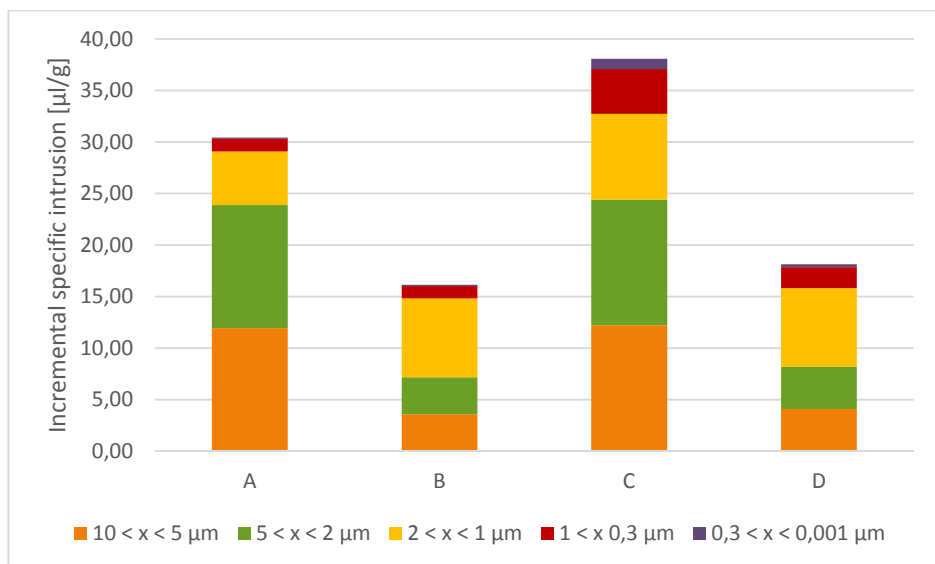
Figure 87: Mean incremental specific intrusion values classified by pore size

In conclusion, the investigation of coating composition on latex penetration into the base paper did not show a significant difference by varying binder level and adding starch.

Regarding the comparison of low and higher latex level in coatings, the effect of higher low shear viscosity could overwhelm the presence of more binder available.

The starch-latex mixture also does not show a significant difference in latex penetration compared to a pure latex coating. There the effect of lower AA-GWR value could overwhelm the theory of latex barrier at the surface presented by Chattopadhyay et al. [2014].

Furthermore, the influence of base paper could be larger than the variance by different coating formulations as reported by Engström et al. [1991].

6.5 MIXTURES OF WATER − SOLUBLE AND WATER − INSOLUBLE BINDERS

The addition of starch to a latex coating color showed influences on binder penetration and migration (see Chapter 4.3.3.1). In this work, the idea was to use dual staining, labeling of starch and latex, and localize them after the coating process. Coating formulations are shown in Table 24. Starch was stained with DTAF and latex with Rhodamine B. Those two dyes emit fluorescent light at different wavelength.

Table 24: Coating formulation of double staining

Recipe [%]	IV
CaCO$_3$	100
Latex stained	6
Starch stained	4
NaOH	set pH to 8,5
Target solids content	65
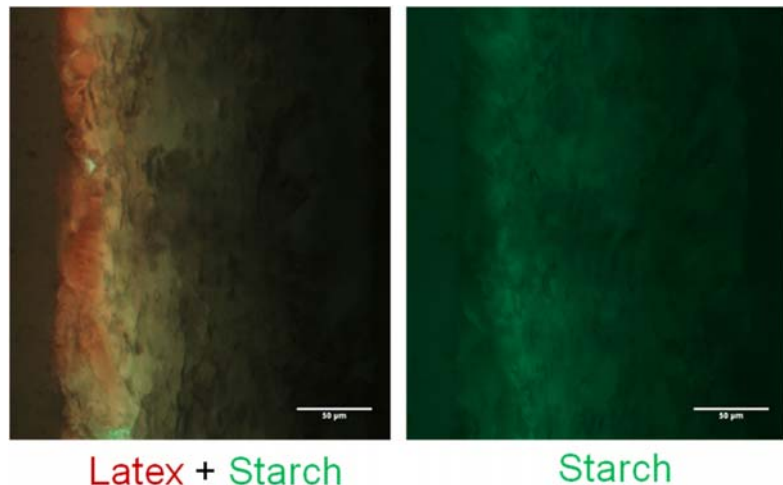
Figure 88: Images of stained starch (green) and latex (red) coating

In Figure 88 the images of starch-latex mixtures in coatings on Paper B (6000 rpm PFI) are shown in principle. The left image of Figure 88 localizes both binders using the dual filter (GFP/mCherry). The latex appears red and the starch green. The issue of the optimization of dual staining was to find the ideal concentrations to label the binders. If the concentration of one binder is too high, it emits a large amount of light and outshines the emission of the second binder at the used light exposure. Figure 88 (left image) shows that latex migrates towards the surface of the coating surface and starch

penetrates into the base paper. In Figure 88, the right image shows the same cross-section filtered with the GFP (single) filter. There just starch is detected and this image confirms the statement that starch tends to penetrate into the base paper, while latex stays in the coating layer and migrates towards the surface. There is hardly any starch remaining at the coating layer surface (see Figure 88 right image). Engström et al. [1991] and Chattopadhyay et al. [2014] observed the same effect of depletion of starch at the coating surface in latex-starch mixtures.

Figure 89 shows the coating color IV (see Table 24) on base paper C (2000 rpm PFI with 20% of filler). Images were evaluated optically. Regarding base paper C the starch depletion at the coating surface seems to be lower. There is more starch remaining in the coating layer and less penetration into the base paper. Here, the influence of the base paper the coating is applied to, is visible again. The work of Du et al. [2011], Dappen [1951] and Chattopadhyay et al. [2014] show the effect of different surface starch and latex contents, when applying the coating onto a porous and a non-porous substrate.
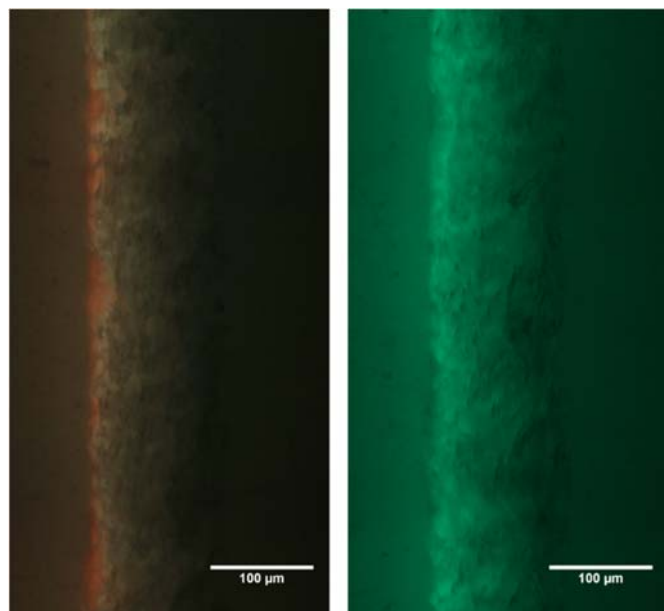
Figure 89: Dual staining on Paper C

Regarding double-stained samples, penetration depth values could not be calculated. The segmentation having two different colors in one image complicates the segmentation. On that point of research a segmentation was not possible.

7   FURTHER FIELDS FOR THE APPLICATION OF SSFM

The beginning of the research with fluorescence microscopy and serial sectioning started with investigations focusing on the base paper with fiber staining as the target. The procedure of labeling fibers was established to form covalent bonds between the cellulose and the dye molecule. In this chapter some investigations on base paper and fibers are presented.

Another issue being investigated via fluorescence microscopy was the localization of optical brightening agents. OBAs absorb UV light and emit fluorescent light. The idea was to localize the OBA after the coating process and determine the penetration depth into the base paper. Another issue was the investigation of the influence of two types of carrier for OBA on penetration depth.

7.1   INVESTIGATION OF BASE PAPERS CONTAINING STAINED FIBERS

SSFM has been applied to investigate fiber and base paper properties. The target was to simplify the segmentation process of fibers and to allow 3D analysis of fiber structures in paper sheets. Images of fluorescence microscopy contain color information and the idea was to identify black regions as background and colored regions as fibers. A staining mechanism to label the fibers was developed. 5-DTAF was used to stain the cellulose fibers. This dye forms covalent bonds with the OH-groups of the cellulose. On the one hand fibers were stained before sheet forming and on the other hand industrial produced papers were stained too (paper staining).

7.1.1   Paper staining

Paper staining has one main advantage. Different industrial papers can be analyzed and the influence of laboratory sheet forming can be avoided.

Regarding the staining of paper samples there is the need to use water-free solvents to avoid fiber swelling. Therefore 5-DTAF was dissolved in DMSO (100 mg per 1 ml). This solution was added to 3 ml water-free toluene to reach a DTAF concentration of 10 mg per 100 mg air dry fibers. Paper samples were kept in that solution for 20 hours, washed with toluene afterwards and embedded and sectioned.

Unbleached long fiber sulfate pulp was used for laboratory sheet forming. The sheet was air dried to obtain a sheet with big pores and unbound fiber cross sections. Paper was stained with DTAF as

described above. Figure 90 illustrates one part of the sheet (left). The magnification can be seen in the second image. This image is GFP filtered.
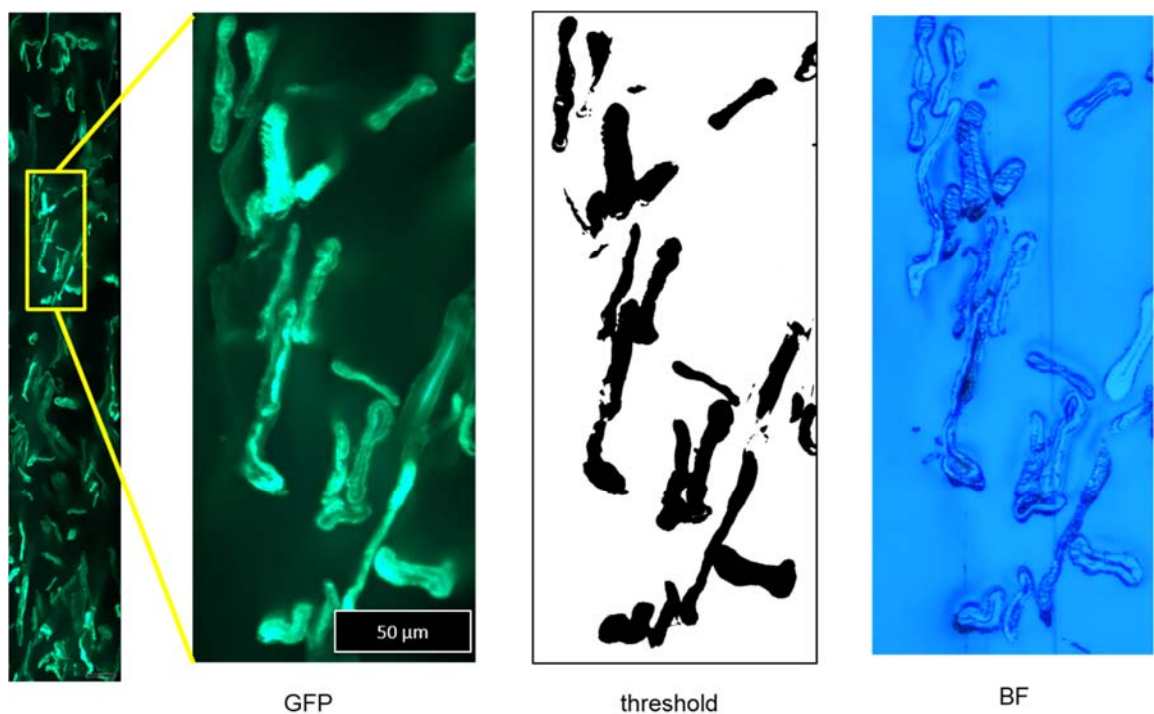
Figure 90: Images of long fiber sulphate pulp of an air dried sheet

One big issue regarding the characterization of fibers and paper sheets was the out of focus light. There is a shadow appearing next to the fibers (see Figure 90 – second image). This light shines through from areas below the surface and creates a kind of 3D effect. Embedding resin was contrasted with different colors and particles but the out of focus light could not be extinguished. The higher the degree of refining or the more chemically treated a fiber is, the more out of focus light appears. The reason could be the increase of light refraction areas. Furthermore not all fibers are fully labeled by the fluorophore. In Figure 90 the fourth image shows the BF filtered section. When the BF and the GFP image is compared there are fibers detected which are not fully stained. When the threshold of the GFP-image is calculated (see Figure 90 third image), these fibers are not detected as fibers.

Also laboratory handsheets made out of different types of pulp were stained. Short fiber pulp showed more out of focus light than long fiber pulp. Furthermore, stained thermomechanical pulp (TMP) was observed via SSFM. A better image quality was observed compared to chemical pulp. The reason for that could be the lignin content of TMP. The lignin is auto-fluorescent and the spectrum of lignin has an overlap with the spectrum of DTAF. This effect leads to intensified fluorescence emission and

sharper fiber contours (see Figure 91 – SSFM (GFP)). In Figure 91, the comparison of the BF-filtered UV-light image (top), the GFP-filtered UV-light image (middle) and the CLSM-image (bottom) as evaluation is shown. More out of focus light can be observed at GFP-filtered UV-light image in contrast to CLSM-image. The fluorescent stain was not absorbed uniformly by the different fibers, as can be seen in Figure 91, focusing on the brighter and darker fiber cross-sections. All in all the evaluation of SSFM with CLSM regarding paper staining led to comparable results.
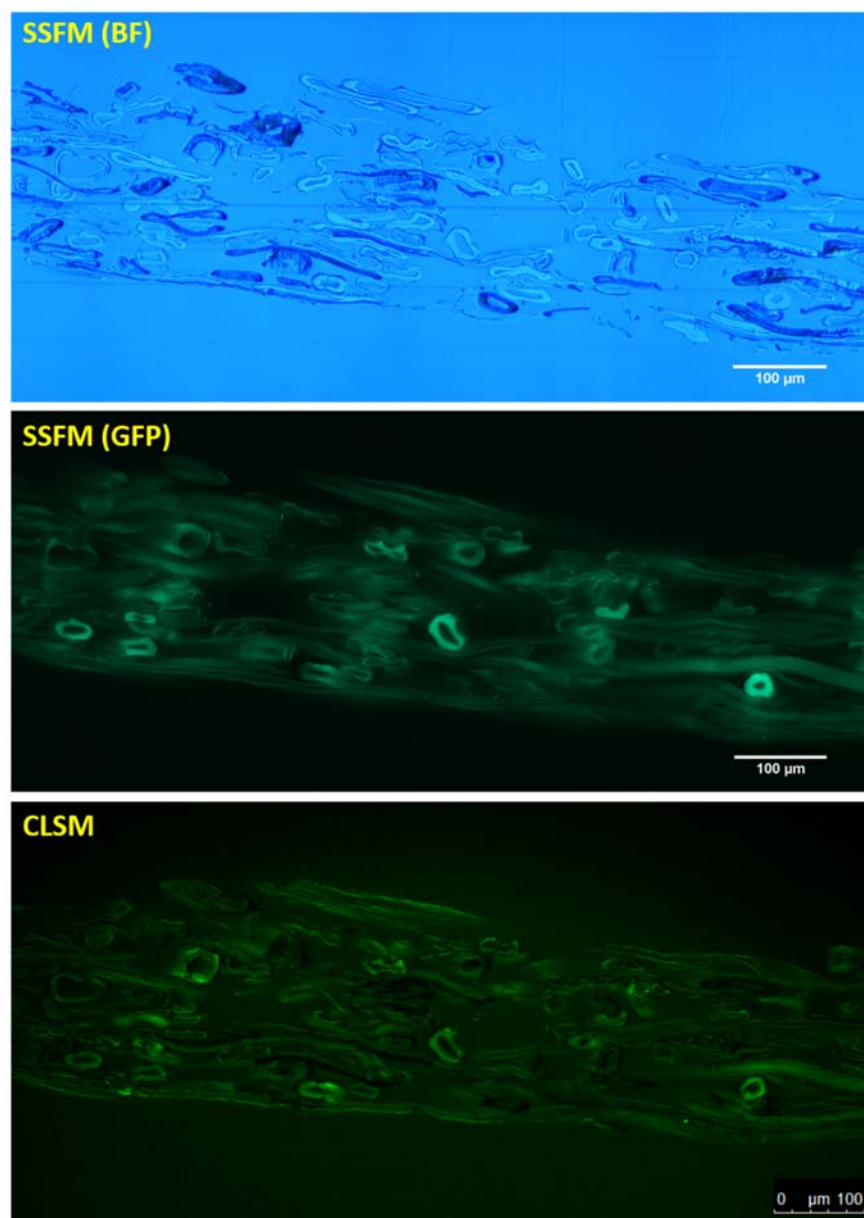
Figure 91: Laboratory handsheets of TMP pulp (stained with DTAF) – comparison of SSFM and CLSM

7.1.2   Fiber staining

For fiber staining 100 mg of DTAF was dissolved in 1ml DMSO. The concentration of DTAF was 20 mg per 1 g oven dry fibers. Long fiber sulphate pulp was used. Reaction time was set to 18 hours. Washing with water for several times afterwards is necessary to separate the unbonded dye molecules from the fibers. The sheet was formed on a suction filter to keep the amount of fibers low, to facilitate the detection. Figure 92 shows the GFP-filtered cross-section on the left and the BF-filtered UV-light image on the right. In Figure 92 the out of focus light effect is visible again. Fibers from cross sections below the observed surface shine through and create a pseudo 3D-image.
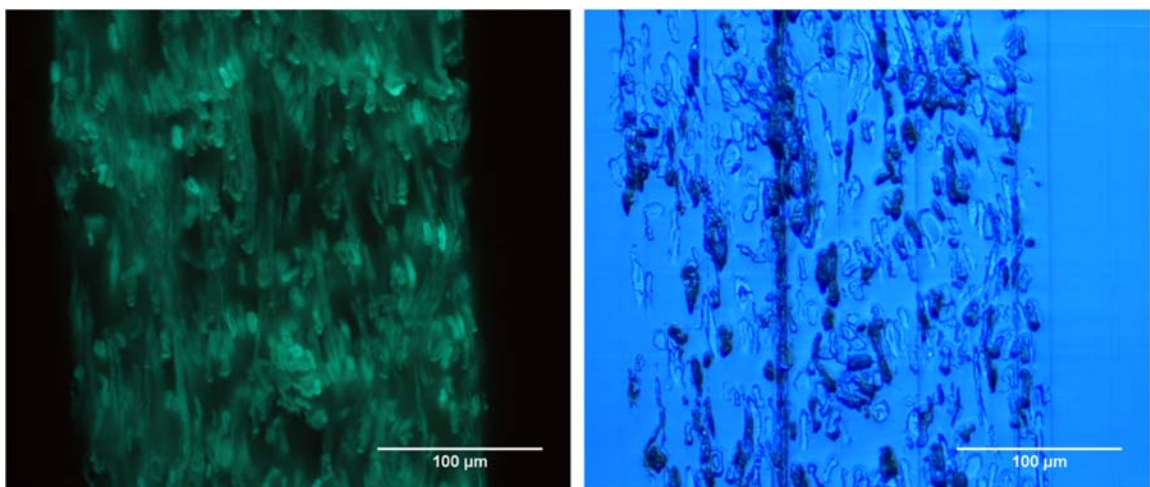
Figure 92: Fiber staining and sheet forming with suction filter
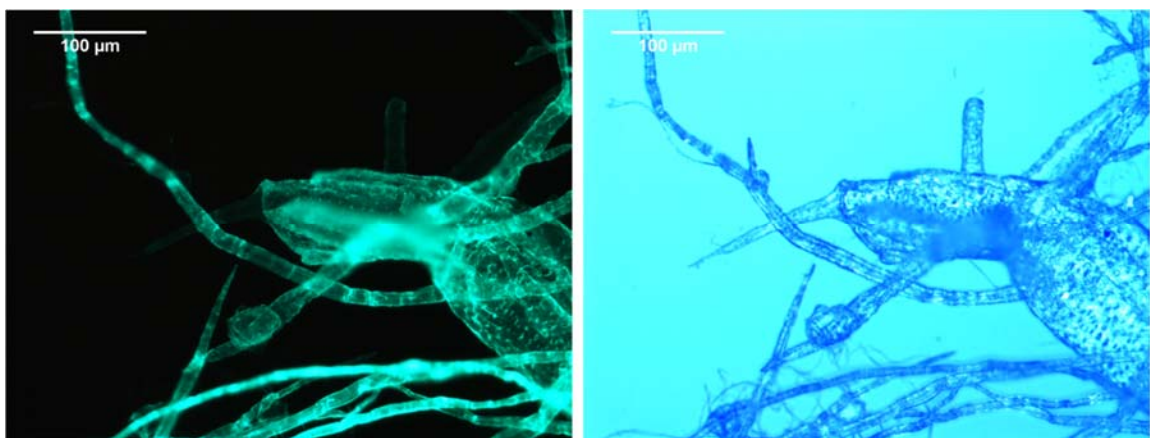
Figure 93: Stained fibers (fluorescence microscopy)

Stained fibers were observed via fluorescence microscopy. The images are shown in Figure 93. Again GFP on the left and BF on the right. The application of UV-light and GFP filter show more details of the vessel illustrated in Figure 93. Fibrils of the fibers were not stained well, because they are not visible in GFP-filtered UV-light image (Figure 93 – left).

In conclusion, fibers and paper can be stained with the developed procedure with DTAF and analyzed via SSFM. Not every fiber or fibril is labeled well. Paper staining is favored because of the possibility to analyze industrially produced paper, but the selection of solvent of the DTAF is important to prevent fiber swelling. 3D-data cannot be provided because out of focus light does not allow a segmentation with sufficient quality. Single fiber details, like properties of vessel cells, can be observed with fluorescence microscopy of DTAF-stained pulp.

7.2 LOCALIZATION OF OPTICAL BRIGHTENING AGENTS AFTER THE COATING PROCESS

SSFM was applied to localize the optical brightening agents in precoatings. The recipes of the coating colors containing optical brighteners are presented in Table 25. Two different PVAs were tested as carrier of the OBA. Mowiol 4-98 has a lower viscosity than Mowiol 10-98.

Table 25: Coating recipes for the localization of optical brightener after the coating process

Recipe [%]	OBA 1	OBA 2
$CaCO_3$	100	100
Latex	8	8
Blankophor PT	0,2	0,2
Mowiol 4-98	0,5	
Mowiol 10-98		0,5
Sterocoll BL	0,1	0,02
NaOH	set pH to 8,5	set pH to 8,5
Target solids content	70	70

In Figure 94 the distribution of the optical brightener of Color OBA 1 is illustrated (left image/ A filtered). The UV-light image (BF filtered) is shown on the right side of Figure 94 to show the coating layer thickness on the left border. The optical brightener can be localized at the interface of coating and base paper (see Figure 94).
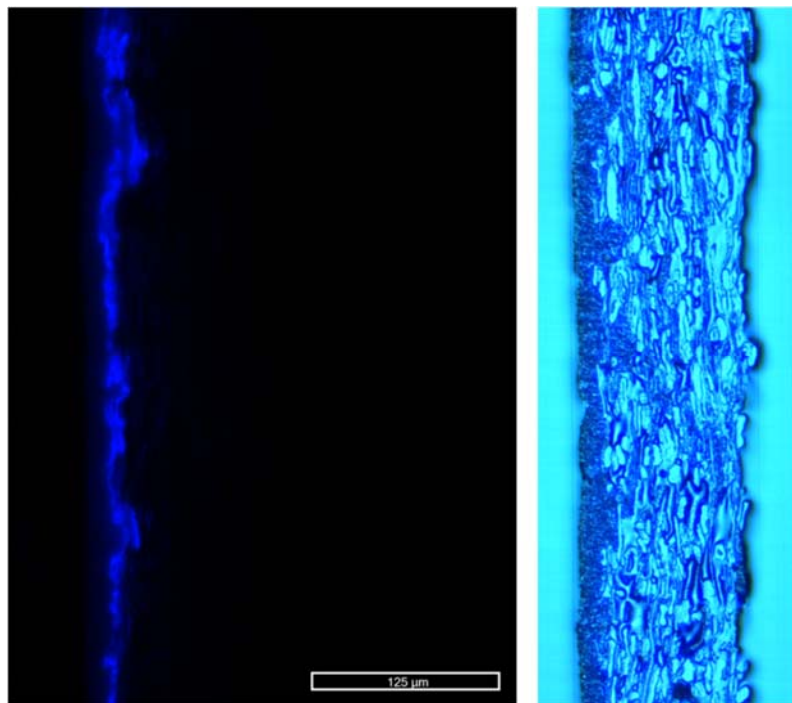
Figure 94: Distribution of optical brightener in paper coatings

The penetration depth of OBA into the base paper was measured. Brightness (with and without UV) was determined with Color Touch 2. Rheologies of the coating colors are similar (see Figure 96).

Table 26: Coating layer thickness of OBA1 and OBA 2 and penetration depth into the base paper

Type	Solids content [%]	Coater	t_{Coat} [μm]	σ_{Coat} [μm]	t_{Pen} [μm]	σ_{Pen} [μm]
OBA 1	70	SUMET	9,7	5,7	12,6	4,8
OBA 2	70	SUMET	11,7	6,0	12,9	4,9

As illustrated in Table 26 there was no difference in penetration depth into the base paper detectable between the two formulations with different types of PVA. The distribution curves of OBA 1 and OBA 2 were similar, as shown in Figure 95.

Brightness measurement of the coated surface did also not show any significant difference. This trial shows that different PVA-grades, varying in their viscosity, do not have an effect on the OBA penetration. One interesting fact observed was that the OBA is not located within the coating layer. During application, the OBA moves with the water phase into the first layers of the base paper.

In fact, SSFM is an appropriate method to detect OBAs of coated paper but the base paper used for coating containing OBA needs to be free of fluorescence. Therefore, papers from industrial paper machines usually cannot be analyzed.
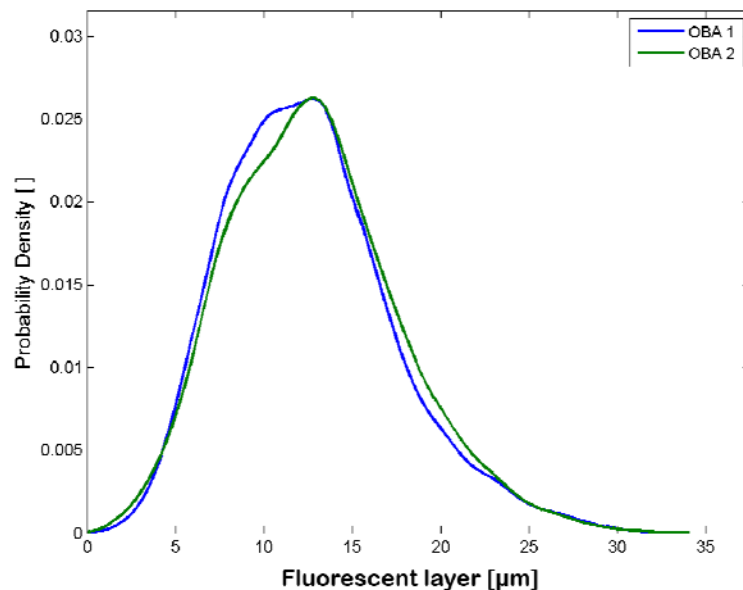
Figure 95: Distribution curve of fluorescent layer
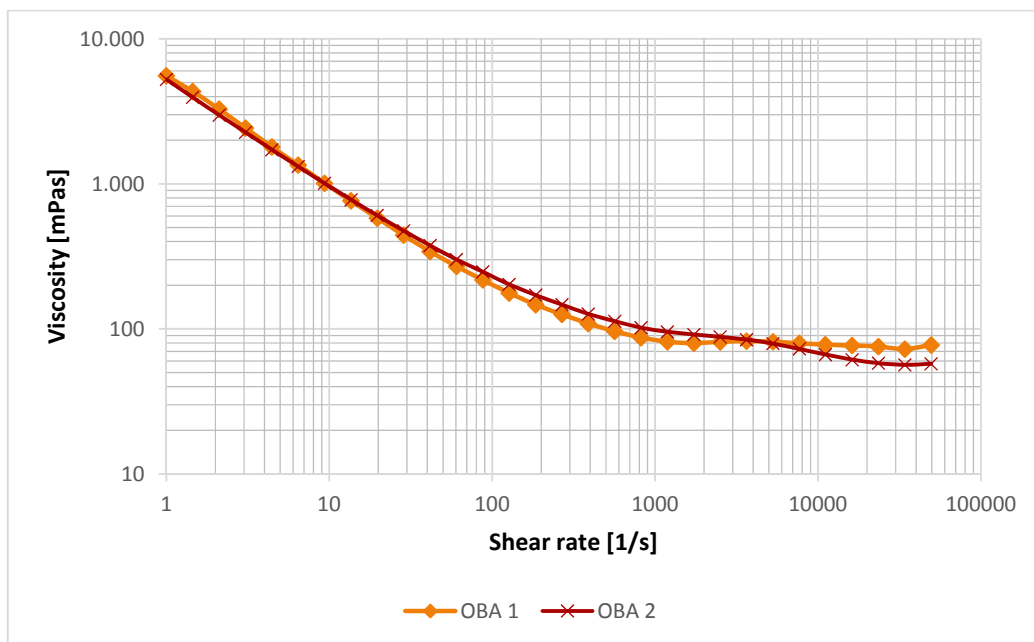
Figure 96: Rheology of the coating colors containing optical brightener

103

8 SUMMARY AND OUTLOOK

A new method to analyze binder penetration into the base paper has been developed. This method called SSFM is based on serial sectioning in combination with fluorescence microscopy. The necessary working steps were presented.

Furthermore, this thesis contains basic information about binder penetration, the mechanisms behind binder penetration, the influencing factors on binder penetration and a summary of methods to determine binder penetration.

This thesis shows that SSFM is an appropriate method to localize the binder after the coating process. Several staining methods were tested to label the most common binders used in coating application. Water-soluble and water-insoluble binders were tested regarding penetration behavior into the base paper.

Following influences on binder penetration were investigated:

- Degree of polymerization of the binder
- Type of binder
- Solids content of the coating color
- Application, metering and drying method
- Base paper
    - o Fillers
    - o Degree of refining
    - o Calendering
- Coating formulation and additives

Investigations on water-soluble binders showed the degree of polymerization of lignosulfonate-based binders played a main role. Solids content of starch coatings also had a big influence on penetration depth into the base paper. Regarding water-insoluble binders, the latex penetration depth varied a lot by using different base paper grades.

Furthermore, double stained samples were analyzed, meaning that the coating color consists of two binders labeled with stains emitting light at different wavelength. Therefore, the location of each binder can be determined individually.

This work also shows further application fields of SSFM. Sheet structure via stained fibers and the localization of optical brightening agents in coating colors can be analyzed.

In this thesis, all trials were performed in laboratory scale and with laboratory handsheets. Latex penetration could also be investigated on industrial papers including OBA of coated broke, because Rhodamine B emits light at higher wavelength than OBA does. Furthermore paper made out of fibers with higher Kappa number can be used for the same reason. Therefore, influences of industrial papers having different properties could be studied using SSFM. Latex penetration could also be observed in pilot scale, because Rhodamine B is a rather inexpensive dye.

Further influences, especially variations of coating formulations regarding co-binders and thickeners could be realized in the future.

In this work, just one type of starch had been used for the penetration depth analysis. SSFM could be applied to compare penetration depth of different starch grades.

One main issue for the future could be the investigation of binder movement between different coating layers. Coatings of industrial paper usually consist of two to three layers. With SSFM the ability of the binder to move after being dried and rewetted when another layer is applied, could be studied.

9 LITERATURE

AAT Bioquest, 2014, http://aatbio.com/gen4prst.pl?Cid=200, 05.10.2015

Ahmed M., Stal L.J., Hasnain S., *DTAF: An efficient probe to study cyanobacterial-plant interaction using confocal laser scanning microscopy (CLSM)*, Journal of Industrial Microbiology and Biotechnology, Vol. 38, Iss. 1, 2011, pp. 249 – 255

Albinsson B., Li.S., Lundquist K., Stomerg R., *The origin of lignin fluorescence*, Journal of Molecular Structure, Vol. 508, Iss. 1-3, 1999, pp. 19 – 27

Al-Turaif H.A., Bousfield D.W., *The influence of pigment size distribution and morphology on coating binder migration*, Nordic Pulp and Paper Research Journal, Vol. 20, Iss. 3, 2005, pp. 335 – 339+344

Bartell D.G., *The role of water retention agents and flow modifiers in paper coatings*, Pulp and Paper Canada, Vol. 77, Iss. 9, 1976, pp. 65 – 68

Bitla S., Tripp C.P., Bousfield D.W., *A Raman Spectroscopic Study of Migration in Paper Coatings*, Journal of Pulp and Paper Science, Vol. 29, Iss. 11, 2003, pp. 382 – 385

Bushhouse S.G., *The effect of coating viscosity on surface latex concentration*, Tappi Journal, Vol. 75, Iss. 3, 1992, pp. 231 – 237

Carl Roth GmbH + Co. KG., 2015, https://www.carlroth.com/de/de/Chemikalien/A-Z-Chemikalien/R/Rhodamin-B-%28C-I-45170%29/Rhodamin-B-%28C-I-45170%29/p/0000000100002e8d00020023_de, 12.10.2015

Chattopadhyay R., Bousfield D., Tripp C., *Dynamic binder migration characterized by IR measurements*, 13th TAPPI Advanced Coating Fundamentals Symposium, October 2014, pp. 124 – 133

Chern C.-S., *Principles and applications of emulsion polymerization*, Wiley, 2008, ISBN: 978-0-470-12431-4, Chapter 1

Chinga G., Helle T., *Structure characterization of pigment coating layer on paper by scanning electron microscopy and image analysis*, Nordic Pulp and Paper Research Journal, Vol. 17, Iss. 3, 2002a, pp. 307 – 312

Chinga G., Helle T., *Quantification of structure details of LWC paper coating layers*, Nordic Pulp and Paper Research Journal, Vol. 17, Iss. 3, 2002b, pp. 313 – 318

Chinga G., Helle T., *Staining with OsO_4 in the study of coated paper structure*, Paperi ja Puu – Paper and Timber, Vol. 85, Iss. 1, 2003, pp. 44 – 48

Clark N. O., Windle W., Beazley K.M., *Liquid Migration in Blade Coating*, Tappi, Vol. 52, Iss. 11, 1969, pp. 2191 – 2202

Crain E.R., 2015, https://www.spec2000.net/09-coreperm.htm, 05.10.2015

Dahlström C., Uesaka T, *Microstructure Variations in Paper Coating: Direct Observations*, Industrial and Engineering Chemistry Research, Vol. 51, Iss. 24, 2012a, pp. 8246 – 8252

Dahlström C., Uesaka T, *Coating microstructures: binder distributions*, Proceedings of TAPPI Advanced Coating Fundamentals Symposium, Atlanta, 2012b, pp. 250 – 257

Dahlström C., Uesaka T., Norgren M., *Base sheet structures that control coating uniformity: Effects of length scale*, Proceedings of TAPPI Advanced Coating Fundamentals Symposium, 2008, pp. 124 – 133

Dahlström C., Allem R., Uesaka T., *New method for characterizing paper coating structures using argon ion beam milling and field emission scanning electron microscopy*, Journal of Microscopy, Vol. 241, Iss. 2, 2011, pp. 179 – 187

Dappen W.J., *Distribution of starch in clay coatings*, Tappi Journal, Vol. 34, Iss. 7, 1951, pp. 324 – 335

Di Risio S., Yan N., *Characterizing coating layer z-directional binder distribution in paper using atomic force microscopy*, Colloids and Surfaces A: Physiochem. Eng. Aspects, Vol. 289, Iss. 1-3, 2006, pp. 65 – 74

Donoser M., Bischof H., Wiltsche M., *Color blob segmentation by MSER analysis*, ICIP, Atlanta (US), 2006, pp. 757 – 760

Donoser M., Mauthner T., Bischof H., Kritzinger J., *A probabilistic approach for tracking fibers*, Proceedings – International Conference on Pattern Recognition, ICPR 2008, Tampa (US), 2008, Article number 4764560

Drnovšek T., Perdih A., *Selective staining as a tool for wood fiber characterization*, Dyes and Pigments, Vol. 67, Iss. 3, 2005, pp. 197 – 206

Du Y., Zang Y.-H., Du J., *Effects of starch on latex migration and on paper coating properties*, Industrial and Engineering Chemistry Research, Vol. 50, Iss. 16, 2011, pp. 9781 – 9786

Engström G., Rigdahl M., Kline J., Ahlroos J., *Binder distribution and mass distribution of the coating layer – cause and consequence*, Tappi Journal, Vol. 74, Iss. 5, 1991, pp. 171 – 179

Engström G., Morin V., Song L.B., *Analysis of porosity distribution in coating layers*, Tappi Journal, Vol. 80, Iss. 5, 1997, pp. 203 – 209

Fardim P., Holmbom B., *ToF-SIMS imaging: A valuable chemical microscopy technique for paper and paper coatings*, Applied Surface Science, Vol. 249, Iss. 1-4, 2005, pp. 393 – 407

Golebiowska E, Blakeley A., Bousfield D., Gramlich W., *Tagging Starch and Latex in Paper Coatings*, PaperCon, Atlanta, 2015

Greensted A., 2010, http://www.labbookpages.co.uk/software/imgProc/otsuThreshold.html, 18.10.2015

Groves R., Matthews P.G., Heap J., Malcolm M.D., Penson J. E., Righway C.J., *Binder migration in paper coatings – a new perspective*, The Science of Papermaking, Vol. 2, 12th Fundamental Research Symposium, Oxford, 2001, pp. 1149 – 1181

Hattula T.,Aschan P-J., *A comparison of double coatings of board based upon styrene-butadiene- and polyvinylacetate latex,* Paperi ja Puu, Vol. 5, 1981, pp. 387 – 396

Harapanhalli R.S., Schafranek W., Ong G.L., Mattes M.J., *Lysine-directed radioiodination of proteins with a cyanuric chloride derivate of aminofluorescein*, Analytical Biochemistry, Vol. 231, Iss. 1, 1995, pp. 50- 56

Heitner C., Dimmel D.R., Schmidt J.A., *Lignin and Lignans: Advances in Chemistry*, Taylor and Francis Group LCC, ISBN 978-1-57444-486-5, 2010, Chapter 1 and 3

Helbert W., Chanzy H., Husum T.L., Schülein M., Ernst S., *Fluorescent cellulose microfibrils as substrate for the detection of cellulase activity*, Biomacromolecules, Vol. 4, Iss. 3, 2003, pp. 481 – 487

Hendershot R.E., Klun R.T., *Fundamentals of emulsion polymer technology*, Coating Binder Short Course, Tappi Press, ISBN: 0-89852-771-6, 1990, pp. 81 – 91

Hirai K., Bousfield D.W., *Characterization of paper coating penetration by laser scanning microscopy*, Proceedings of Tappi Advanced Coating Fundamentals Symposium, 2006, pp. 90 – 105

Ho A., Yan N., *Comparative study of coating structural characteristics of lightweight coated papers by spray and MSP coating methods*, Proceedings of Tappi Advanced Coating Fundamentals Symposium, 2012, pp. 99 – 112

Huang T., Lepoutre P., *Effect of basestock surface structure and chemistry on coating holdout and coated paper properties*, Tappi Journal, Vol. 81, Iss. 8, 1998, pp. 145 – 152

Kappel L., Hirn U., Bauer W., Schennach R., *A novel method for the determination of bonded area of individual fiber-fiber bonds*, Nordic Pulp and Paper Research Journal, Vol. 24, Iss. 2, 2009, pp. 199 – 205

Kappel L., Hirn U., Gilli E., Bauer W., Schennach R., *Revisiting polarized microscopy for fiber-fiber bind area measurement – Part I: Theoretical fundamentals*, Nordic Pulp and Paper Research Journal, Vol. 25, Iss. 1, 2010, pp. 65 – 70

Kappel L., Hirn U., Gilli E., Bauer W., Schennach R., *Revisiting polarized microscopy for fiber-fiber bind area measurement – Part II: Proving the applicability*, Nordic Pulp and Paper Research Journal, Vol. 25, Iss. 1, 2010, pp. 71 – 75

Kearney R.L., Maurer H.W., *Starch and Starch Products in Paper Coating*, Tappi Press, ISBN 0-89852-050-9, 1990, Chapter 2

Kenttä E., Pöhler T., Juvonen K., *Latex uniformity in the coating layer of paper*, Nordic Pulp and Paper Research Journal, Vol. 21, Iss. 5, 2006, pp. 665 – 669

Kim B.Y., Bousfield D.W., *Characterization of base paper properties on coating penetration*, Journal of Korea TAPPI, Vol. 35, Iss. 5, 2003, pp. 17 – 25

Kline J., *Measuring binder migration with ultraviolet analysis*, Tappi Journal, Vol. 74, Iss. 4, 1991, pp. 177 – 182

Kontschieder P., Donoser M., Bischof H., Kritzinger J., Bauer W., *Detecting paper fiber cross sections in microtomy images*, Proceedings – International Conference on Pattern Recognition, ICPR 2010, Istanbul (Turkey), Article number 5597795, pp. 316 - 319

Kritzinger J., Hirn U., Donoser M., Bauer W., *Characterization of spatial coating layer formation – definition of a representative sample size*, Proceedings of TAPPI Advanced Coating Fundamentals Symposium, Montreal, 2008, pp. 340 – 351

Kritzinger J., Bauer W., Hunziker P., Kässberger M., *Quantification of the penetration of coating pigments into the base paper determined by automated serial sectioning*, Paper Conference Trade Show 2011, PaperCon 2011, Covington (US), 2011, pp. 292 – 300

Kritzinger J., Bauer W., *A study of the influence of pre- and post-calendering on the structural parameters of a coating layer applied with a curtain coater*, Paper Conference and Trade Show 2012: Growing the Future, PaperCon 2012, New Orleans, Code 96216

Kritzinger J., Bauer W., Salminen P., Preston J., *A Novel approach to quantify spatial coating-layer formation*, Tappi Journal, Vol. 9, Iss. 11, 2010, pp. 7 – 13

Kugge C., *An AFM Study of Local Film Formation of Latex in Paper Coatings*, Journal of Pulp and Paper Science, Col. 30, Iss. 4, 2004, pp. 105 – 111

Kugge C., Greaves M., Hands K., Scholes F.H., Vanderhoek N., Ward J., *Paper coating analysis by confocal Raman spectroscopy*, Appita Journal, Vol. 61, Iss. 1, 2008, pp. 11 – 16

Lakowicz J.R., *Principles of Fluorescence Spectroscopy*, Springer, ISBN 978-0-387-31278-1, Third edition: 2006, Chapter 1, pp. 1 – 25

Lepoutre P., *Paper coatings – substrate absorbency and coating structure*, Tappi Journal, Vol. 61, Iss. 5, 1978, pp. 51 – 55

Lepoutre P., *The structure of paper coatings: an update*, Progress in Organic Coatings, Vol. 17, Iss. 2, 1989, pp. 89 – 106

Lin S.Y., Dence C.W., *Methods in Lignin Chemistry*, Springer, ISBN 3-540-50295-5, 1992, pp. 113 – 115

Lorbach C., Hirn U., Kritzinger J., Bauer W., *Automated 3D measurements of fiber cross section morphology in handsheets*, Nordic Pulp and Paper Research Journal, Vol. 27, Iss. 2, 2012, pp. 264 – 269

Matthews G.P., *Computer modelling of fluid permeation in porous coatings and paper – an overview*, Nordic Pulp and Paper Research Journal, Vol. 15, Iss.5, 2000, pp. 476 – 485

Moran-Mirabel, J. M., Santhanam, N., Corgie, S. C., Craighead, H. G. and Walker, L. P. *Immobilization of Cellulose Fibrils on Solid Substrates for Cellulose-Binding Studies through Quantitative Fluorescence Microscopy*, Biotechnology and Bioengineering, Vol. 101, 2008, pp. 1129 – 1141

Mulisch M., Welsch U., *Romeis Mikroskopische Technik*, Spektrum Akademischer Verlag Heidelberg, ISBN 978-3-8274-1676-6, 2010, Chapter 3

Openstax CNX, 1999-2015, http://cnx.org/contents/a4293fc2-4de2-4506-b890-a7abdeb70c16@5/Viscosity-and-Laminar-Flow-Poi, 05.10.2015

Ozaki Y., Bousfield D.W., Shaler S.M., *Three-dimensional Characterization of Ink Vehicle Penetration by Laser Scanning Confocal Microscopy*, Journal of Pulp and Paper Science, Vol. 31, Iss. 1, 2005, pp. 48 – 52

Ozaki Y., Bousfield D.W., Shaler S.M., *Three-dimensional observation of coated paper by confocal laser scanning microscope*, Tappi Journal, Vo. 5, Iss. 2, 2006, pp. 3 – 8

Ozaki Y., Bousfield D.W., Shaler S.M., *Characterization of coating layer structural and chemical uniformity for samples with backtrap mottle*, Nordic Pulp and Paper Research Journal, Vol. 23, Iss. 1, 2008, pp. 8 - 13

Paltakari J., *Papermaking Science and Technology*, Pigment Coating and Surface Sizing of Paper, Paperi ja Puu Oy, Book 11, ISBN 978-952-5216-27-1, 2009, Chapter 4

Proctor A.R., Hoover J.F., *Styrene-butadiene latex in paper and paperboard coating application*, Coating Binder Short Course, Tappi Press, 1990, ISBN 0-89852-771-6, pp. 93 – 108

Pöhler T., Juvonen K., Sneck A., *Coating layer microstructure and location of binder – Results from SEM analysis*, Tappi Advanced Coating Fundamentals Symposium, 2006, pp. 79 – 89

Rigdway C.J., Weihs J., Grossmann O., Hunziker P., Gane P.A.C., *Designing nanotechnology coatings for replacement of fibrous white top liner*, Nordic Pulp and Paper Research Journal, Vol. 28, Iss. 4, 2013 pp. 560 – 572

Roberts J.C., *Paper Chemistry*, Blackie & Son Ltd., 1991, ISBN-13: 978-94-011-6476-4, pp.137 - 140

Rosenau T., Renfrew A.H.M., Adelwöhrer C., Potthast A., Kosma P., *Cellulosics modified with slow-release reagents. Part I. Synthesis of triazine-anchored reagents for slow release of active substances from cellulosic materials*, Polymer, Vol. 46, Iss. 5, 2005, pp. 1453 – 1458

Rosenau T., Potthast A., Liebner F., Ebner G., Renfrew A.H.M., Eichhorn S., Fürst-Wiesmann E.-B., *A general approach to cellulosic material with controlled slow release of active substances by derivatization of a cellulosic carrier matrix with trifunctional triazines*, Cellulose, Vol. 16, Iss. 5, 2009, pp. 929 – 942

Sandas S.E., Salminen P.J., *Pigment-cobinder interactions and their impact on coating rheology, dewatering and performance*, Tappi Journal, Vol. 74, Iss. 12, 1991, pp. 179 – 187

Sauer M., Hofkens J., Enderlein J., *Handbook of Fluorescence Spectroscopy and Imaging*, Wiley-VCH, ISBN 978-3-527-316699-4, 2011, Chapter 1, pp. 1 - 30

Schäffner H., *Entwicklung eines fluoreszenzoptischen Verfahrens zur Ermittlung von Materialstrukturen auf Basis eines automatisierten Mikrotomiekonzeptes*, 2012, PhD

Schölkopf J, Gane P.A.C., *The Moment Ink Contacts the Surface: A Fresh Look at the Absorption Dynamic into Coated Papers*, International Paperworld IPW, Iss. 2, 2004, pp. 36 – 42

Schölkopf J., Gane P.A.C., Ridgway C.J., Mattews G.P., *Influence of inertia on liquid absorption into paper coating structures*, Nordic Pulp and Paper Research Journal, Vol. 15, Iss. 5, pp. 422 – 430

Siegler R., Sternson L.A., Stobaugh J.F., *Suitability of DTAF as a fluorescent labelling reagent for direct analysis of primary and secondary amines - spectral and chemical reactivity considerations*, Journal of Pharmaceutical and Biomedical Analysis, Vol7, Iss. 1, 1989, pp. 45 – 55

Sigma-Adrich Co. LCC., 2015, http://www.sigmaaldrich.com/catalog/product/sial/d0531?lang=de&region=AT, 12.10.2015

Skowronski J., Lepoutre P., *Water-paper interaction during paper coating*, Tappi Journal, Vol. 68, Iss. 11, 1985, pp. 98 – 102

Stead C.V., *Halogenated Heterocycles in reactive dyes*, Dyes and Pigments, Vol. 3, Iss. 2-3, 1982, pp. 161 – 171

Ström G., Hornatowska J., Changhong X., Teresaki O., *A novel SEM cross-section analysis of paper coating for separation of latex from void volume*, Nordic Pulp and Paper Research Journal, Vol. 25, Iss. 1, 2010, pp. 107 – 113

Tam K.Y., Smith E.R., Booth J., Compton R.G., Brennan C.M., Atherton J.H., *Kinetics and mechanism of dyeing processes: The dyeing of cotton fabrics with a procion blue dichlorotriazinyl reactive dye*, Journal of Colloid and Interface Science, Vol. 196, Iss. 2, 1997, pp. 387 – 398

Valeur B., *Molecular Fluorescence Principles and Applications*, Wiley-VCH, 2002, ISBN 3-527-29919-X, Chapter 1 – 3, pp. 3 – 71

Vanderhoff J.W., Bradford E.B., *Mechanism of film formation of Latices*, Tappi, Vol. 46, Iss. 4, 1963, pp. 215 – 221

Voura C., *Untersuchung des Penetrationsverhaltens von niedrigviskosen Druckfarben in CaCO$_3$-hältige Papierstrukturen*, PhD thesis, 2008

Vyörykkä J., Vuorinen T., Bousfield D.W., *Confocal Raman microscopy: A non-destructive method to analyze depth profiles of coated and printed papers*, Nordic Pulp and Paper Research Journal, Vol. 19, Iss. 2, 2004, pp. 218 – 223

Vyörkkä J., Fogden A., Daicic J., Ernstsson M., Jääskeläinen A-S., *Characterization of Paper Coatings – Review and Future Possibilities*, Advanced Coating Fundamentals Symposium, 2006, pp. 32 – 57

Walter J.C., *The Coating Process*, Tappi Press, ISBN 0-89852-058-4, 1993, Chapter 2, Section I

Watanabe J., Lepoutre P., *A Mechanism for the Consolidation of the Structure of Clay-Latex Coatings*, Journal of Applied Polymer Science, Vol. 27, Iss. 11, 1982, pp. 4207 – 4219

Wertz J-L., Bédué O., Mercier J.P., *Cellulose Science and Technology*, EPFL Press, ISBN 978-2-940222-41-4, first edition, 2010, pp. 156 – 157

Whalen-Shaw M. J., *Binder Migration: In Paper and Paperboard Coatings*, Tappi Press, ISBN 0-89852-270-6, 1993

Wiltsche M., Donoser M., Bauer W., Bischof H., *A new-slice based concept for 3D paper structure analysis applied to spatial coating layer formation*, Transaction of the 13th FRS, Cambridge (UK), 2005, Vol. 2, pp. 853 – 899

Wiltsche M., Bauer W., Donoser M., *Coating application method and calendaring influence on spatial coating layer formation obtained by an automated serial sectioning method*, Proceedings of 9th Tappi Advanced Coating Fundamentals Symposium, Tappi Press, Turku (Finland), 2006, pp. 413 – 415

Wiltsche M.; Donoser M.; Kritzinger J.; Bauer W., *Automated serial sectioning applied to 3D paper structure analysis*, Journal of Microscopy, Vol. 242, Iss. 2, 2011, pp. 197 – 205

Winnik M.A., *Latex film formation*, Current Opinion in Colloid & Interface Science, Vol. 2, Iss. 2, 1997, pp. 192 – 199

Yamazaki K., Nishioka T., Hattori Y., Fujita K., *Print mottle effect of binder migration and latex film formation during coating consolidation*, Tappi Journal, Vol. 76, Iss. 5, 1993, pp. 79 – 84

Zang Y.-H., Du J., Du Y., Wu Z., Cheng S., Liu Y., *The migration of styrene butadiene latex during the drying of coating suspensions: when and how does migration of colloidal particles occur?*, Langmuir, Vol. 26, Iss. 23, 2010a, pp. 18331 – 18339

Zang Y.-H., Liu Z., Cao Z.L., Mangin P., *An extension of Lepoutre's mechanism for the consolidation of the structure of latex-pigment coatings*, Journal of Pulp and Paper Science, Vol. 36, Iss. 3-4, 2010b, pp. 79 - 84

Zang Y.-H., Fan Q., Lili G., Du Y., Zou X., *Towards a comprehensive understanding of binder migration during drying of coatings*, Proceedings of 13th TAPPI Advanced Coating Fundamentals Symposium, Minneapolis (US), 2014, pp. 5 – 10